Figures and tables

Figures

(Figure 1.1) Simplified geological map of south-west England showing the distribution of magmatic rocks and the approximate location of sites described in the text (modified from Floyd, 1982b). Sites are numbered and grouped as in (Table 1.1).

(Figure 2.1) Distribution of tectonic zones in the Variscan Orogen of Europe (modified from Franke, 1989).

(Figure 2.2) Map of south-west England showing major structural features, together with K/Ar age zones (after Dineley, 1986).

(Figure 2.3) Distribution and correlation of structural units in central south-west England (after Selwood and Thomas, 1986a).

(Figure 2.4) Geological map of south Cornwall showing various allochthonous units, including the Lizard Complex, resting on the northern parautochthon of the Porthtowan Formation and Mylor Slate Formation (after Holder and Leveridge, 1986).

(Figure 2.5) Devonian lithostratigraphical sequences in the parautochthon and allochthon units of south Cornwall (after Holder and Leveridge, 1986).

(Figure 2.6) Correlation of observed Devonian lithostratigraphy across Devon (after Durrance and Laming, 1982).

(Figure 2.7) Generalized facies relationships throughout the Devonian and Carboniferous of central south-west England (after Selwood and Thomas, 1986b). LD = Lower Devonian; MD = Middle Devonian; UD = Upper Devonian; LC = Lower Carboniferous; UC = Upper Carboniferous.

(Figure 2.8) Geological outline map of south-west England, showing the distribution of mica lamprophyres relative to the exposed Cornubian granite batholith (grey) and its geophysically determined margin (after Leat *et al.,* 1987). The Exeter Volcanic 'Series' is shown within the New Red Sandstone outcrop and younger Mesozoic rocks (diagonal ruling). 1 = Land's End Granite; 2 = Carnmenellis Granite; 3 = St Austell Granite; 4 = Bodmin Moor Granite; 5 = Dartmoor Granite.

(Figure 2.9) Distribution of the two main magmatic groups within the Exeter Volcanic 'Series', mid-Devon (after Edmonds *et al.,* 1969).

(Figure 3.1) Outline map of south-west England, showing the location of Group A sites.

(Figure 3.2) (left) Geological map of the Lizard, showing the main lithologies (modified from British Geological Survey Sheet 359; Green, 1964a; Leake *et al.,* 1990); and (above) their division into three tectonic units (after Bromley, 1979).

(Figure 3.3) Distribution of $Al_{2}0_{4}$—CaO and Ni—Cr in Lizard peridotites, dunites and ultramafic cumulates (data from Parker, 1970; Kirby, 1979a; Leake and Styles, 1984) relative to typical ophiolite- and stratiform-related ultramafics (data from Rivalenti *et al.*. (1981) and the literature).

(Figure 3.4) Chondrite-normalized REE data for the different assemblages of the Lizard peridotite (from Frey, 1969; Davies, 1984) and typical Alpine peridotites (data from Frey, 1984).

(Figure 3.5) Incompatible-element and normalized REE patterns for the Lizard basaltic dykes, showing the distinctions between the three chemical groups (data from Davies, 1984; Kirby, 1984).

(Figure 3.6) Lithological borehole logs for the Traboe ultramafic—mafic cumulate complex at Traboe, Lizard area (data from Leake and Styles, 1984).

(Figure 3.7) MORB-normalized multi-element patterns for selected *mélange* metabasalts compared with an example of transitional-type MORB from the Reykjanes Ridge.

(Figure 3.8) Diagram showing the variation in the La/Nb ratio for the Tubbs Mill pillow lavas and some of the *mélange* metabasaltic clasts relative to the Lizard dykes and Upper Devonian—Lower Carboniferous basic volcanics from south-west England.

(Figure 3.9) Geological sketch map of the Kennack Sands site (A2).

(Figure 3.10) Banded gneiss, Kennack Sands. (Photo: M.T. Styles.)

(Figure 3.11) Geological sketch map of the Polbarrow—The Balk site (A3) (after Sandeman, 1988).

(Figure 3.12) Acid-veined gabbro at Parn Voose. (Photo: M.T. Styles.)

(Figure 3.13) Geological sketch map of the Coverack site (A5).

(Figure 3.14) Xenoliths of peridotite enclosed within troctolite, Coverack Beach. (Photo: M.T. Styles.)

(Figure 3.15) Troctolite veining peridotite, Coverack. (Photo: M.T. Styles.)

(Figure 3.16) Sheeted, basic dykes at Porthoustock Point. The dykes locally form about 80% of the outcrop with only thin gabbroic screens separating them. (Photo: M.T. Styles.)

(Figure 3.17) Interlayered basic and ultrabasic cumulate rocks, Traboe-type schists, Porthkerris. (Photo: M.T. Styles.)

(Figure 3.18) Geological sketch map of the Porthallow Cove—Porthkerris Cove site ( )

(Figure 3.19) Folded pyroxenite layers in gabbroic rock, Porthkerris. (Photo: M.T. Styles.)

(Figure 3.20) Geological sketch map of the Lankidden site (A8) showing distribution of outcrops between landward exposures and low-water reefs.

(Figure 3.21) Lenses of peridotite enclosed within later gabbro, Carrick Luz, Lankidden. (Photo: M.T. Styles.)

(Figure 3.22) Flaser gabbro, Carrick Luz, Lankidden. (Photo: M.T. Styles.)

(Figure 3.23) Shear zones developed in gabbro, Carrick Luz, Lankidden. (Photo: M.T. Styles.)

(Figure 3.24) A spectacular development of pillow lavas, of Frasnian age, on Mullion Island. (Photo: P.A. Floyd.)

(Figure 3.25) Photomicrograph of pillow lava from Mullion Island. Primary plagioclase, zoned clinopyroxene and ilmenite are set in a secondary pumpellyite-facies mineral matrix. (Photo: P.A. Floyd.)

(Figure 3.26) The rocky cliffs of Elender Cove expose metavolcanic greenschists of the Start Complex. Elender Cove, near Prawle Point, Devon. (Photo: David Noton Photography.)

(Figure 4.1) Outline map of south-west England showing the location of Group B sites.

(Figure 4.2) Variation of Zr and Nb in Upper Devonian (small dots and crosses) and Lower Carboniferous (large dots) basaltic lavas relative to different geographical regions. Data largely from Floyd *et al.* (1983) and unpublished.

(Figure 4.22) Typical, banded, basic hornfels of volcanic origin, composed of dark layers of hornblende and biotite, with light-coloured, segregation lenses of diopside. Tater-du, Cornwall. (Photo: P.A. Floyd.)

(Figure 4.23) View of Pentire Point cliffs showing Upper Devonian pillow-lava mounds. (Photo: P.A. Floyd.)

(Figure 4.24) Pillow-lava breccia formed by fragmentation on cooling soon after submarine extrusion. Pentire Point, Cornwall. (Photo: P.A. Floyd.)

(Figure 4.25) *In situ* autobrecciation of a lava pillow. Pentire Point, Cornwall. (Photo: P.A. Floyd.)

(Figure 4.26) Upper Devonian pillow lavas of alkali-basalt composition. Chipley Quarries, Devon. (Photo: PA. Floyd.)

(Figure 4.27) Cross-section through two pillows showing the high degree of vesicularity and its concentric disposition. Chipley Quarries, Devon. (Photo: P.A. Floyd.)

(Figure 4.28) (Opposite) Wedge of argillite (pale-coloured cliffs) resting on dark intrusive dolerite near sea-level. Trevose Head, Cornwall. (Photo: P.A. Floyd.)

(Figure 4.29) Photomicrograph of a hydrous dolerite showing large irregular crystal of dark, primary, kaersutitic amphibole replacing colourless clinopyroxene (bottom right); long needle-like apatite crystal traverses the amphibole unaltered (top). Trevone Bay, Cornwall. (Photo: P.A. Floyd.)

(Figure 4.30) Photomicrograph of a hydrous dolerite showing the fan-like growth of secondary Al-rich pumpellyite that replaced the original plagioclase. Trevone Bay, Cornwall. (Photo: P.A. Floyd.)

(Figure 4.31) Geological map of the area to the south of Liskeard showing the location of the Clicker Tor ultramafic body (after Burton and Tanner, 1986).

(Figure 4.32) Photomicrograph of partly altered olivine crystals (with veins) and intercumulus pyroxene in the ultramafic body at Clicker Tor, Cornwall. (Photo: P.A. Floyd.)

(Figure 4.33) Weathering of the Polyphant ultramafic body (hydrous picrite) showing a core boulder of serpentinite within a highly oxidized, degraded matrix. Polyphant, Cornwall. (Photo: P.A. Floyd.)

(Figure 4.34) Photomicrograph of the Polyphant hydrous picrite, showing serpentinized olivine crystals, pyroxene and dark kaersutitic amphibole (top left). Polyphant, Cornwall. (Photo: P.A. Floyd.)

(Figure 4.35) (Opposite) Map and section of north Cornwall, showing the distribution and relationship of the major nappes (after Selwood and Thomas, 1986a). The Tintagel Volcanic Formation occurs in the Tredorn Nappe.

(Figure 4.36) Contorted greenschists belonging to the Tintagel Volcanic Formation at Gullastem, north of Tintagel, Cornwall. (Photo: P.A. Floyd.)

(Figure 4.37) Distribution of the Tintagel Volcanic Formation between Bossiney Bay and Trebarwith Strand, north Cornwall (after Freshney and McKeown, *in* Dearman *et al.,* 1970).

(Figure 4.38) Sketch and section of Tintagel headland, north Cornwall, showing the thin upper slice of the Tintagel Volcanic Formation truncated by thrusts and cut by later normal faults (after McKeown. in Dearman *et al.,* 1970).

(Figure 4.39) The conical knoll of Brent Tor is composed of Lower Carboniferous basaltic pillow lavas and hyaloclastites which formed a near-emergent seamount with a reworked volcaniclastic apron. Brent Tor, Devon. (Photo: P.A. Floyd.)

(Figure 4.40) Map and cross-sections of Greystone Quarry, showing the development of undulating thrust surfaces cutting dolerite and the transportation of Upper Devonian sediments over Lower Carboniferous volcanics by the major Greystone Thrust (after Turner, 1982).

(Figure 4.41) Diagrammatic sketch of intrusive dolerite bodies in the Pitts Cleave Quarry, near Tavistock (after Dearman and Butcher, 1959). A) main face (*c.* 230 m long) and B) southern face (*c.* 85 m long).

(Figure 4.42) Well-developed columnar jointing in dolerite. Pius Cleave Quarry, Tavistock, Devon. (Photo: P.A. Floyd.)

(Figure 4.43) Modal and chemical variation in thu• upper part of the Ryecroft dolerite sill, Teign Valley, east Devon (data from Morton and Smith, 1971).

(Figure 5.1) Outline map of south-west England showing the location of Group C sites.

(Figure 5.2) Normative quartz-albite-orthoclase (Q-Ab-Or) diagram (after Exley and Stone, 1982, Figure 23.2).

(Figure 5.3) Variation diagrams for Zr—K/Rb, Zr/TiO_2—K/Rb, Nb—Y and Zr—TiO_2 in south-west England granite types and different plutons (after Exley *et al.,* 1983).

(Figure 5.4) The St Austell model. Diagram showing the first intrusion of Type-B granite (Table 5.1) cut by multiphase second intrusion of biotite granite, with metasomatic aureole of Type D caused by intrusion of Type E.

(Figure 5.5) Chondrite-normalized REE profiles for Corinthian granites. Data for Land's End, Carnmenellis, Bodmin Moor and Dartmoor from Darbyshire and Shepherd (1985).

(Figure 5.6) The 1980s model. Granitic magma generated in the lower crust (but with mantle components) and evolving both by assimilating upper-crustal constituents and differentiating Li-mica granite magma. Magma becomes increasingly hydrated by drawing in increasing quantities of meteoric water during ascent.

(Figure 5.7) Schematic representation of fluid evolution in the eastern sector of the Cornubian metallogenic province showing the importance of 'immiscibility events' and mixing (after Shepherd et al., 1985).

(Figure 5.8) Diagrammatic representation of water circulation in Cornubian granite. Areas of low heat flow, U and ^{222}Rn concentration are associated with china clay and indicate draw-down; areas of high heat flow, U and ^{222}*R11* concentration indicate uprise (based on Durrance *et al.,* 1982).

(Figure 5.9) Haytor Rocks, exposing the coarse megacrystic granite of Dartmoor. The megacrystic character of the granite is visible in the foreground exposure. (Photo: S. Campbell.)

(Figure 5.10) Map of the St Austell Granite outcrop, showing the chief granite types, localities mentioned in the text (filled circles) and the following sites: C4 = Luxulyan Quarry; C10 = Wheal Martyn; C11 = Cam Grey Rock; C12 = Tregargus Quarries; C13 = St Mewan Beacon; and C14 = Roche Rock.

(Figure 5.11) Contact between Dartmoor Granite and Devonian slates, re-exposed after face cleaning by the Nature Conservancy Council in 1980. (Photo: Mj. Harley.)

(Figure 5.12) Diagrammatic section across the Tregonning Granite, based on coastal exposures, showing the location of sites at Rinsey Cove (C7) and Megiliggar Rocks (C15) (after Exley and Stone, 1982, figure 21.2).

(Figure 5.13) The headland of Cape Cornwall which exposes contacts between Land's End Granite and adjacent metasediments. (Photo: S. Campbell.)

(Figure 5.14) Geological sketch map of the Cape Cornwall area (site (:8).

(Figure 5.15) Small granite cupola emplaced in pelitic hornfelses of the Mylor Slate Formation. Porthmeor Cove, Cornwall. (Photo: K.A. Cottle.)

(Figure 5.16) Later dyke of megacrystic granite cutting and displacing an earlier leucogranite dyke. Porthmeor Cove, Cornwall. (Photo: R.A. Cottle.)

Tables

Boxed values are those belonging to the ferric element association.

[**References**](#)

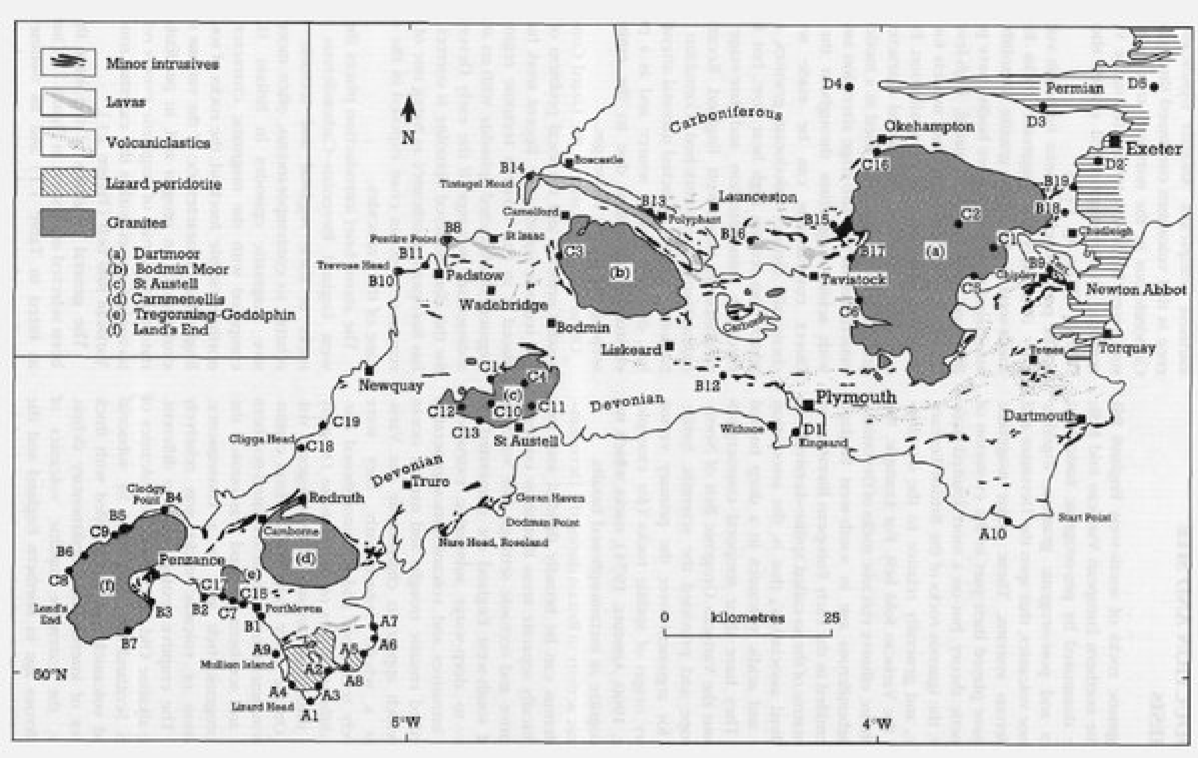

(Figure 1.1) Simplified geological map of south-west England showing the distribution of magmatic rocks and the approximate location of sites described in the text (modified from Floyd, 1982b). Sites are numbered and grouped as in (Table 1.1).

Group A sites: Lizard ophiolite and mélange	Group B sites: Pre-orogenic volcanics	Group C sites: Cornubian granite batholith	Group D sites: Post-orogenic volcanics
A1 Lizard Point (SW 696116 - SW 706115)	B1 Porthleven (SW 628254 - SW 634250)	C1 Haytor Rocks area (SX 758773)	D1 Kingsand Beach (SX 435506)
A2 Kennack Sands (SW 734165)	B2 Cudden Point-Prussia Cove (SW 548275 - SW 555278)	C2 Birch Tor (SX 686814)	D2 Webberton Cross Quarry (SX 875871)
A3 Polbarrow-The Balk (SW 717135 - SW 718128)	B3 Penlee Point (SW 474269)	C3 De Lank Quarries (SX 101755)	D3 Posbury Clump Quarry (SX 815978)
A4 Kynance Cove (SW 684133)	B4 Carrick Du-Clodgy Point (SW 507414 - SW 512410)	C4 Luxulyan (Goldenpoint, Tregarden) Quarry (SW 054591)	D4 Hannaborough Quarry (SS 529029)
A5 Coverack Cove-Dolor Point (SW 784187 - SW 785181)	B5 Gurnards Head (SW 432387)	C5 Leusdon Common (SX 704729)	D5 Killerton Park (SS 971005)
A6 Porthoustock Point (SW 810217)	B6 Botallack Head-Porth Ledden (SW 362339 - SW 365322)	C6 Burrator Quarries (SX 549677)	
A7 Porthallow Cove-Porthkerris Cove (SW 798232 - SW 806226)	B7 Tater-du (SW 440230)	C7 Rinsey Cove (Porthcew) (SW 593269)	
A8 Lankidden (SW 756164)	B8 Pentire Point-Rumps Point (SW 923805 - SW 935812)	C8 Cape Cornwall area (SW 352318)	
A9 Mullion Island (SW 660175)	B9 Chipley Quarries (SX 807712)	C9 Porthmeor Cove (SW 425376)	
A10 Elender Cove-Black Cove, Prawle Point (SX 769353 - SX 769356)	B10 Dinas Head-Trevose Head (SW 847761 - SW 850766)	C10 Wheal Martyn (SW 003556)	
	B11 Trevone Bay (SW 890762)	C11 Carn Grey Rock and Quarry (SX 033551)	
	B12 Clicker Tor Quarry (SX 285614)	C12 Tregargus Quarries (SW 949541)	
	B13 Polyphant (SX 262822)	C13 St Mewan Beacon (SW 985534)	
	B14 Tintagel Head-Bossiney Haven (SX 047892 - SX 066895)	C14 Roche Rock (SW 991596)	
	B15 Brent Tor (SX 471804)	C15 Megiliggar Rocks (SW 609266)	
	B16 Greystone Quarry (SX 364807)	C16 Meldon Aplite Quarries (SX 567921)	
	B17 Pitts Cleave Quarry (SX 501761)	C17 Praa Sands (Folly Rocks) (SW 573280)	
	B18 Trusham Quarry (SX 846807)	C18 Cameron (Beacon) Quarry (SW 704506)	
	B19 Ryecroft Quarry (SX 843847)	C19 Cligga Head area (SW 738536)	

(Table 1.1) List of GCR igneous rock sites in south-west England. See (Figure 1.1) for locations.

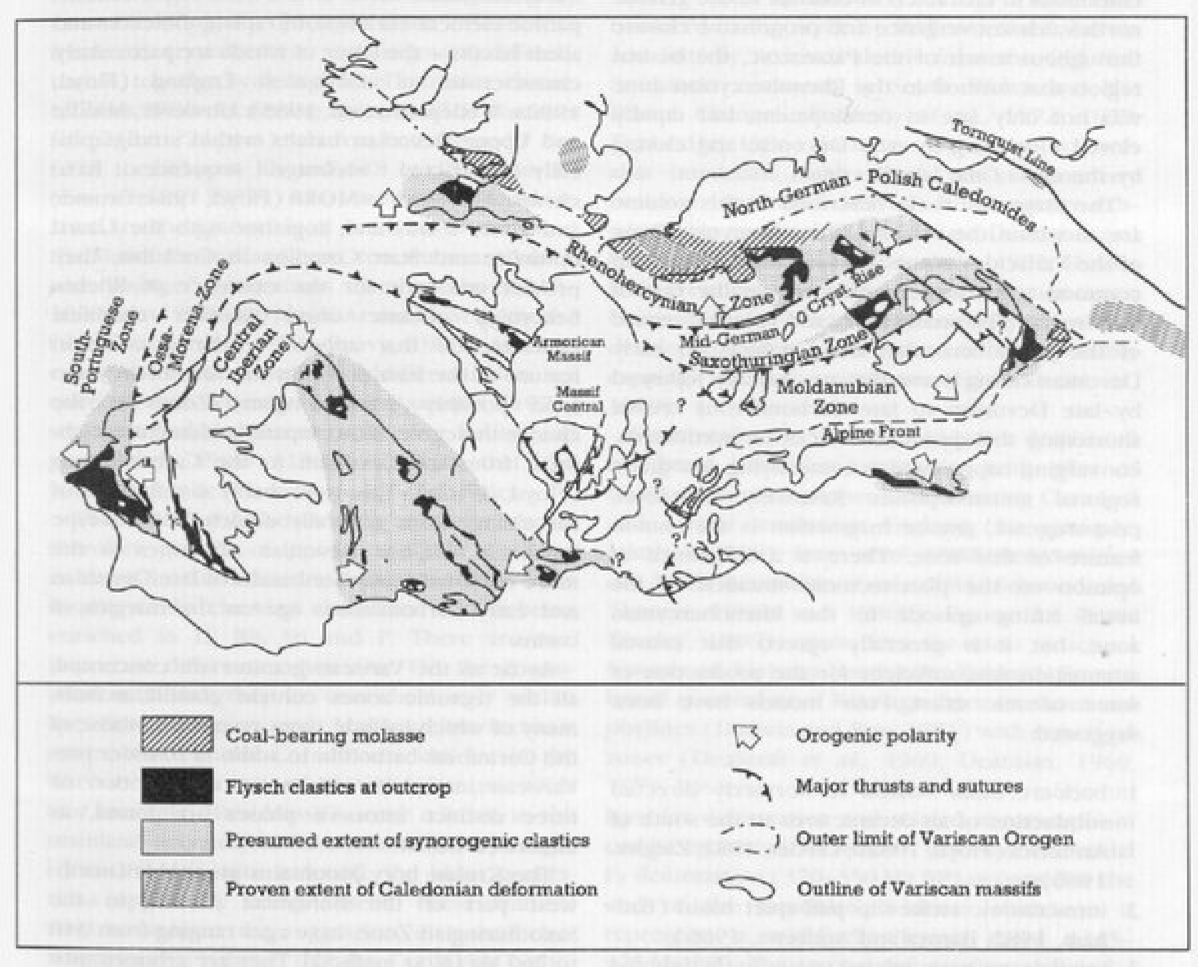

(Figure 2.1) Distribution of tectonic zones in the Variscan Orogen of Europe (modified from Franke, 1989).

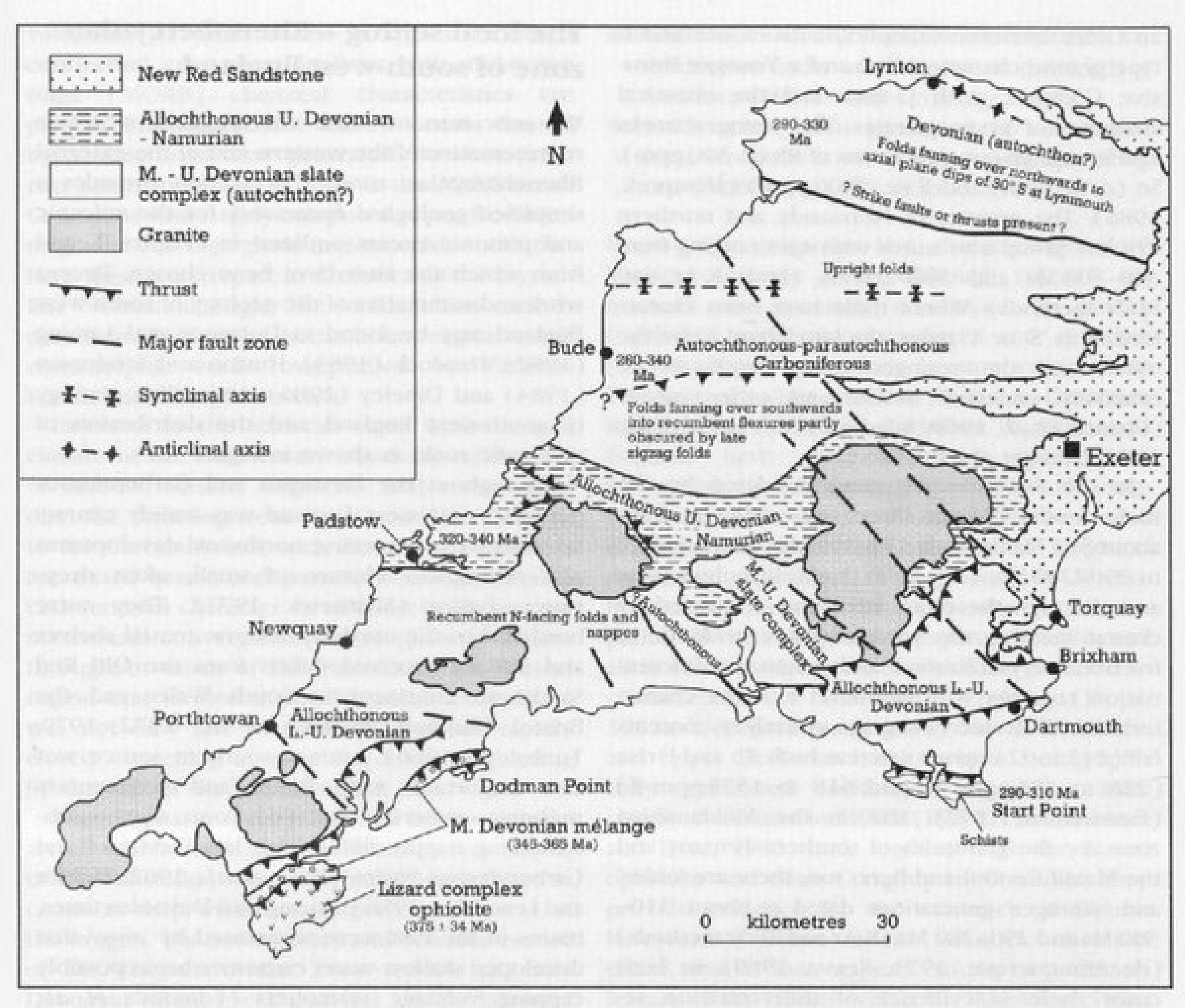

(Figure 2.2) Map of south-west England showing major structural features, together with K/Ar age zones (after Dineley, 1986).

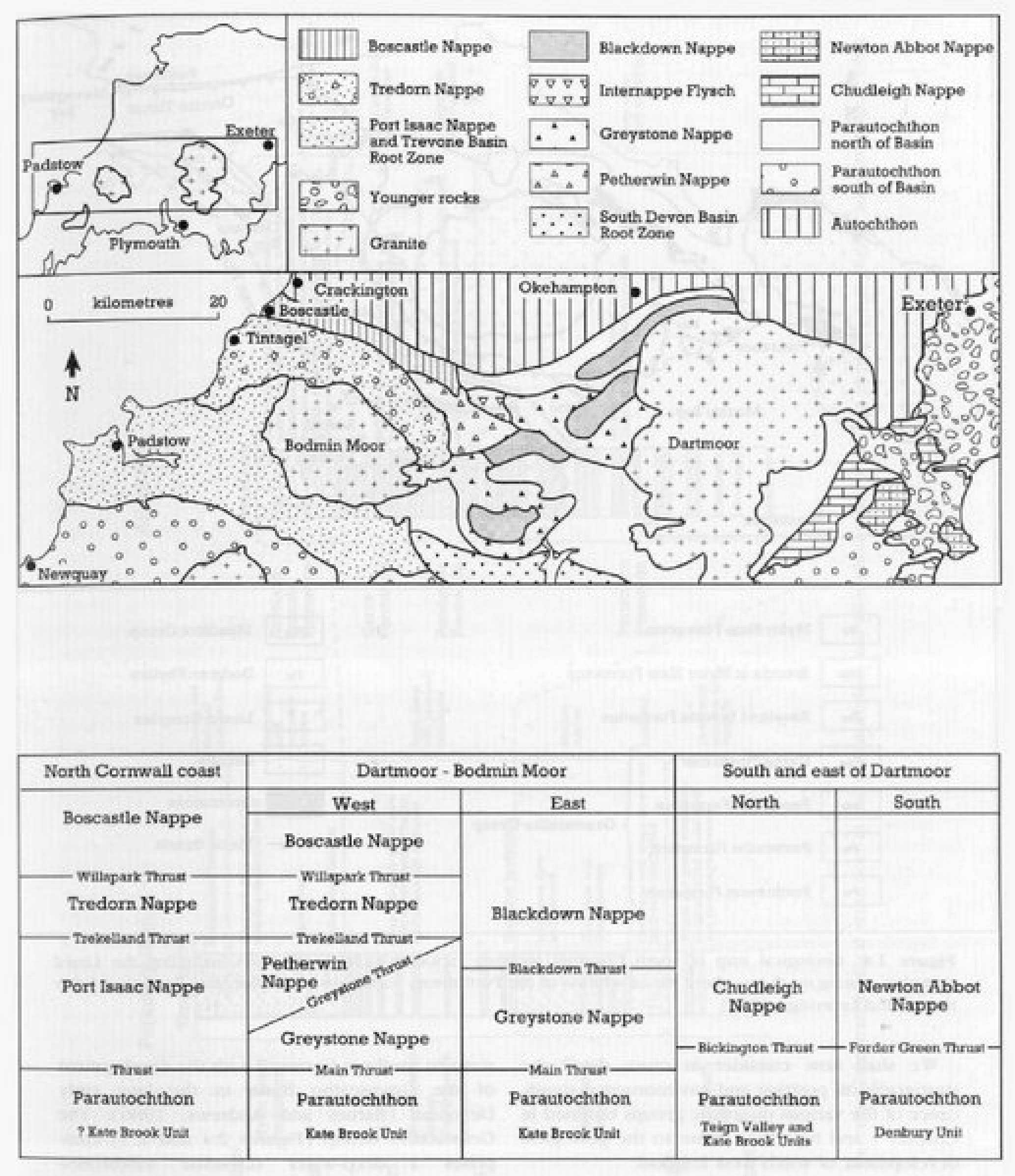

(Figure 2.3) Distribution and correlation of structural units in central south-west England (after Selwood and Thomas, 1986a).

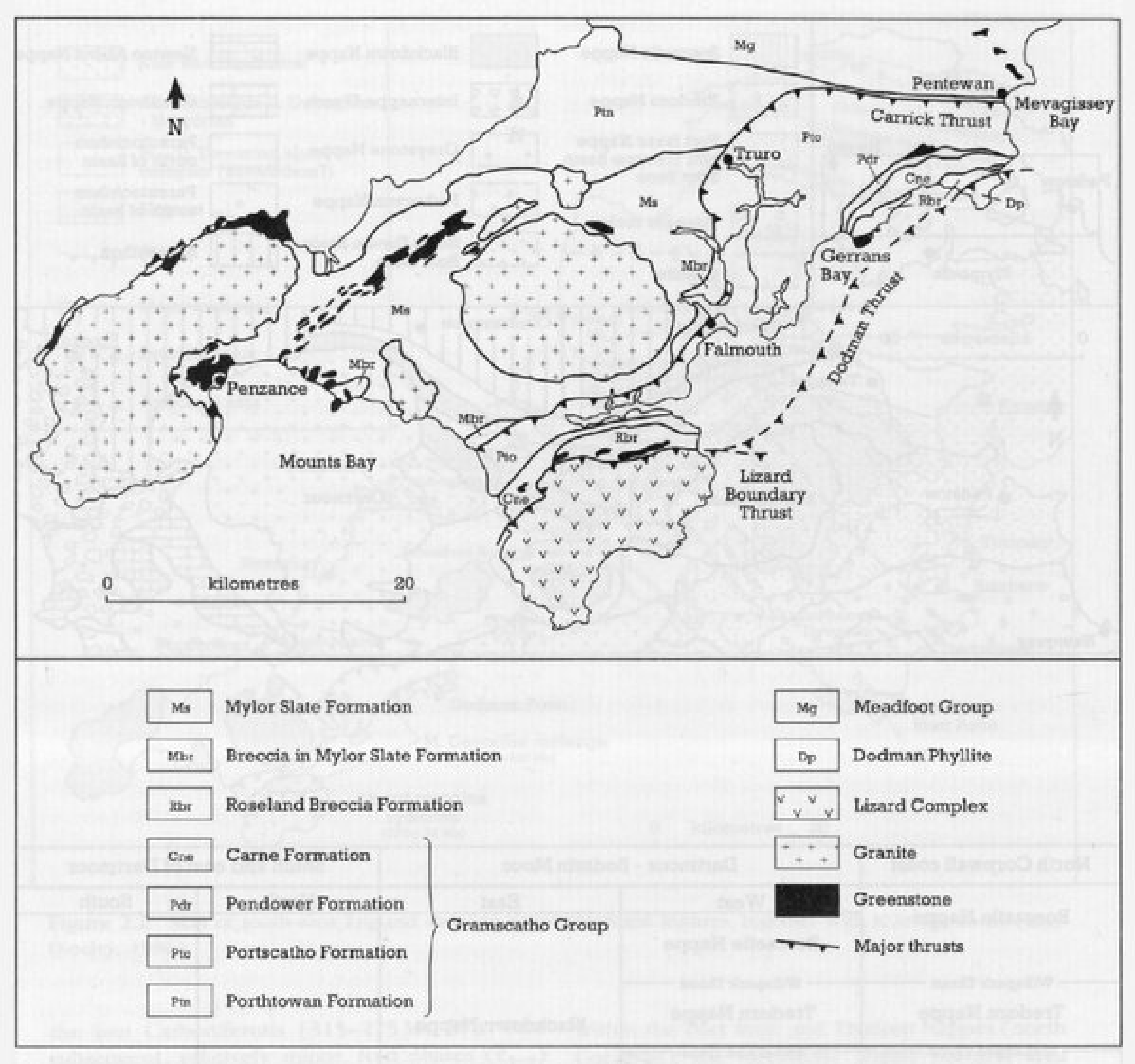

(Figure 2.4) Geological map of south Cornwall showing various allochthonous units, including the Lizard Complex, resting on the northern parautochthon of the Porthtowan Formation and Mylor Slate Formation (after Holder and Leveridge, 1986).

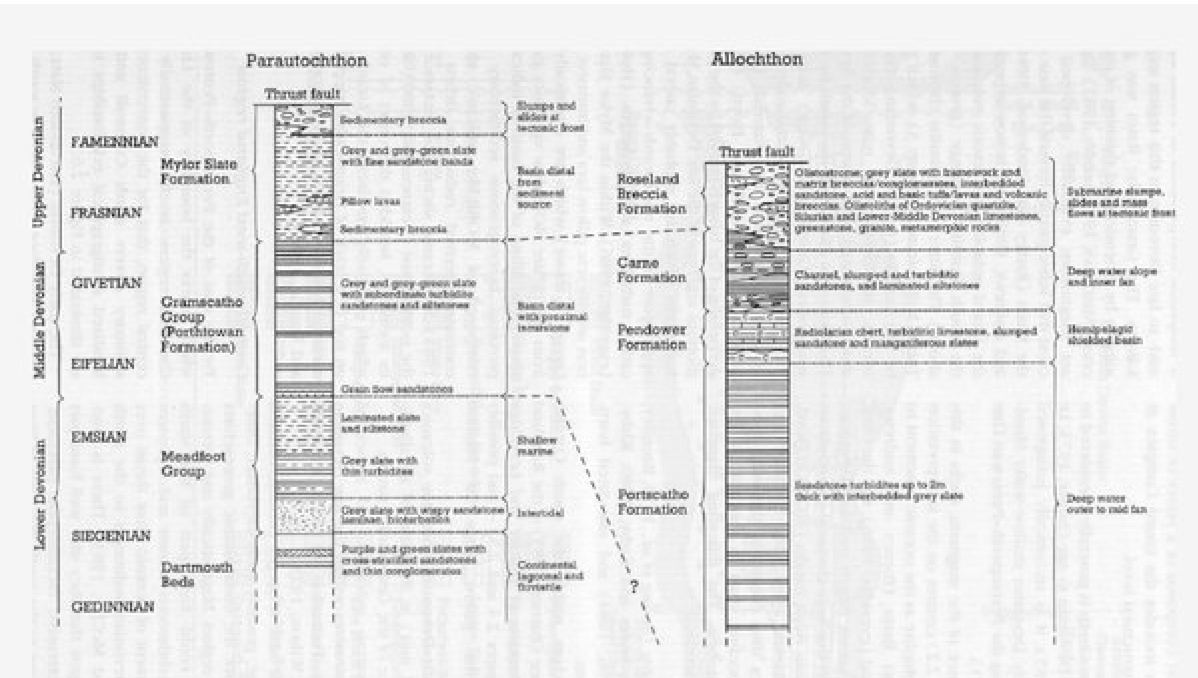

(Figure 2.5) Devonian lithostratigraphical sequences in the parautochthon and allochthon units of south Cornwall (after Holder and Leveridge, 1986).

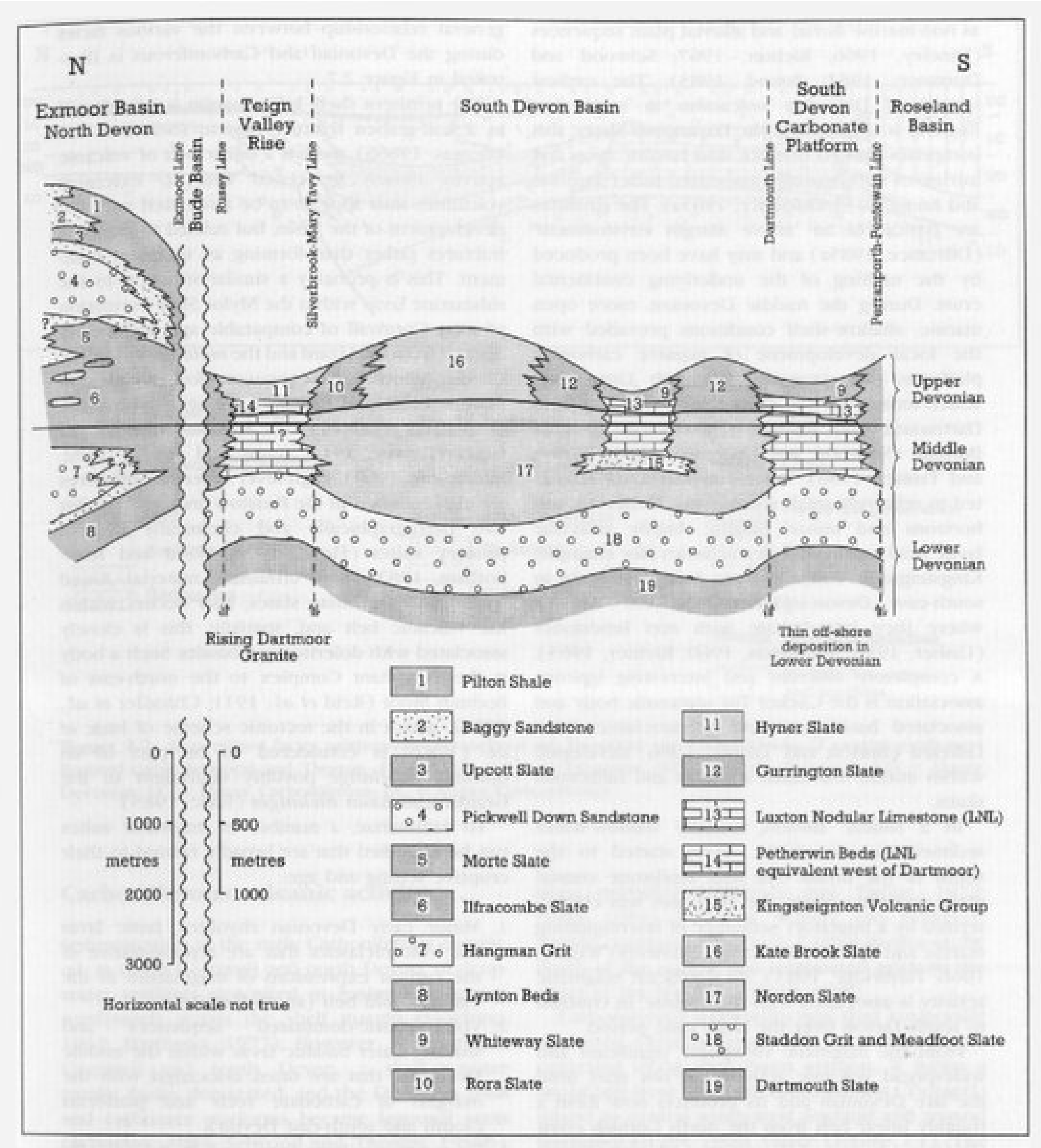

(Figure 2.6) Correlation of observed Devonian lithostratigraphy across Devon (after Durrance and Laming, 1982).

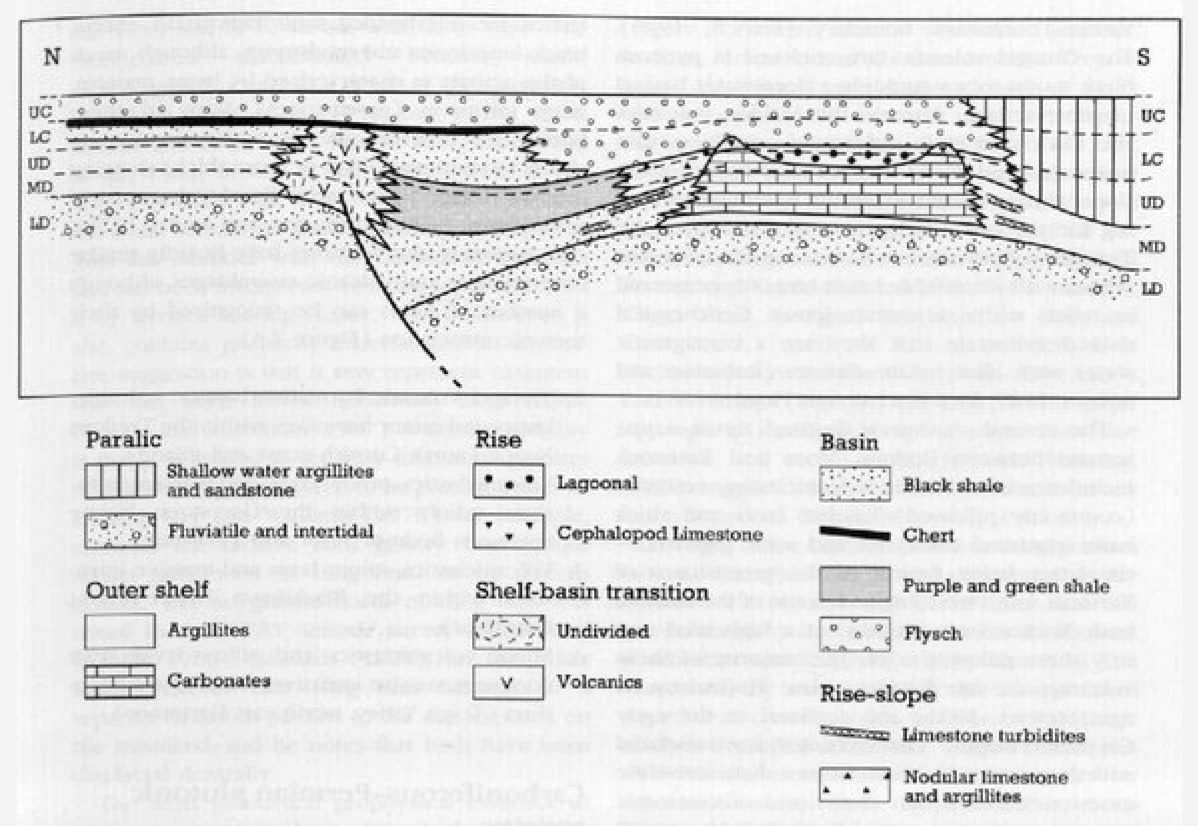

(Figure 2.7) Generalized facies relationships throughout the Devonian and Carboniferous of central south-west England (after Selwood and Thomas, 1986b). LD = Lower Devonian; MD = Middle Devonian; UD = Upper Devonian; LC = Lower Carboniferous; UC = Upper Carboniferous.

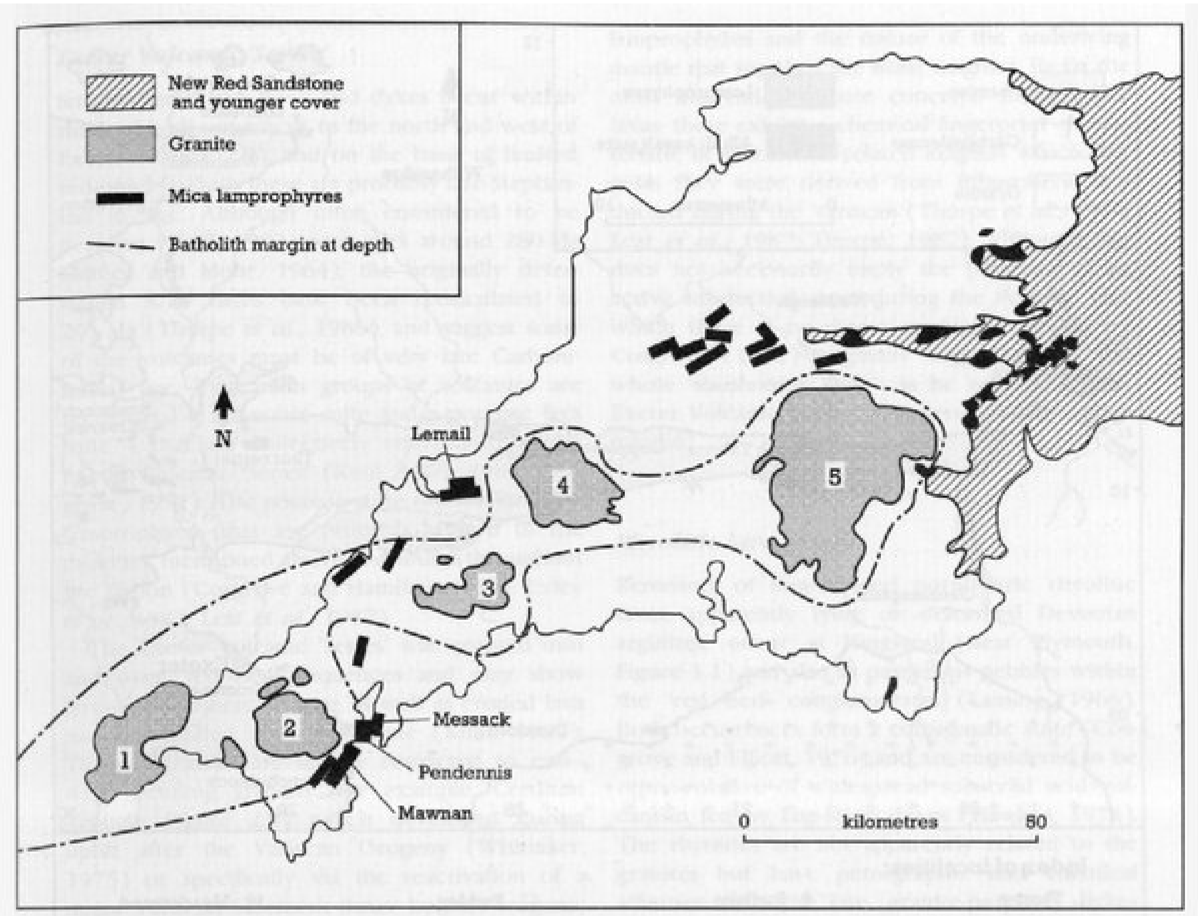

(Figure 2.8) Geological outline map of south-west England, showing the distribution of mica lamprophyres relative to the exposed Cornubian granite batholith (grey) and its geophysically determined margin (after Leat et al., 1987). The Exeter Volcanic 'Series' is shown within the New Red Sandstone outcrop and younger Mesozoic rocks (diagonal ruling). 1 =

Land's End Granite; 2 = Carnmenellis Granite; 3 = St Austell Granite; 4 = Bodmin Moor Granite; 5 = Dartmoor Granite.

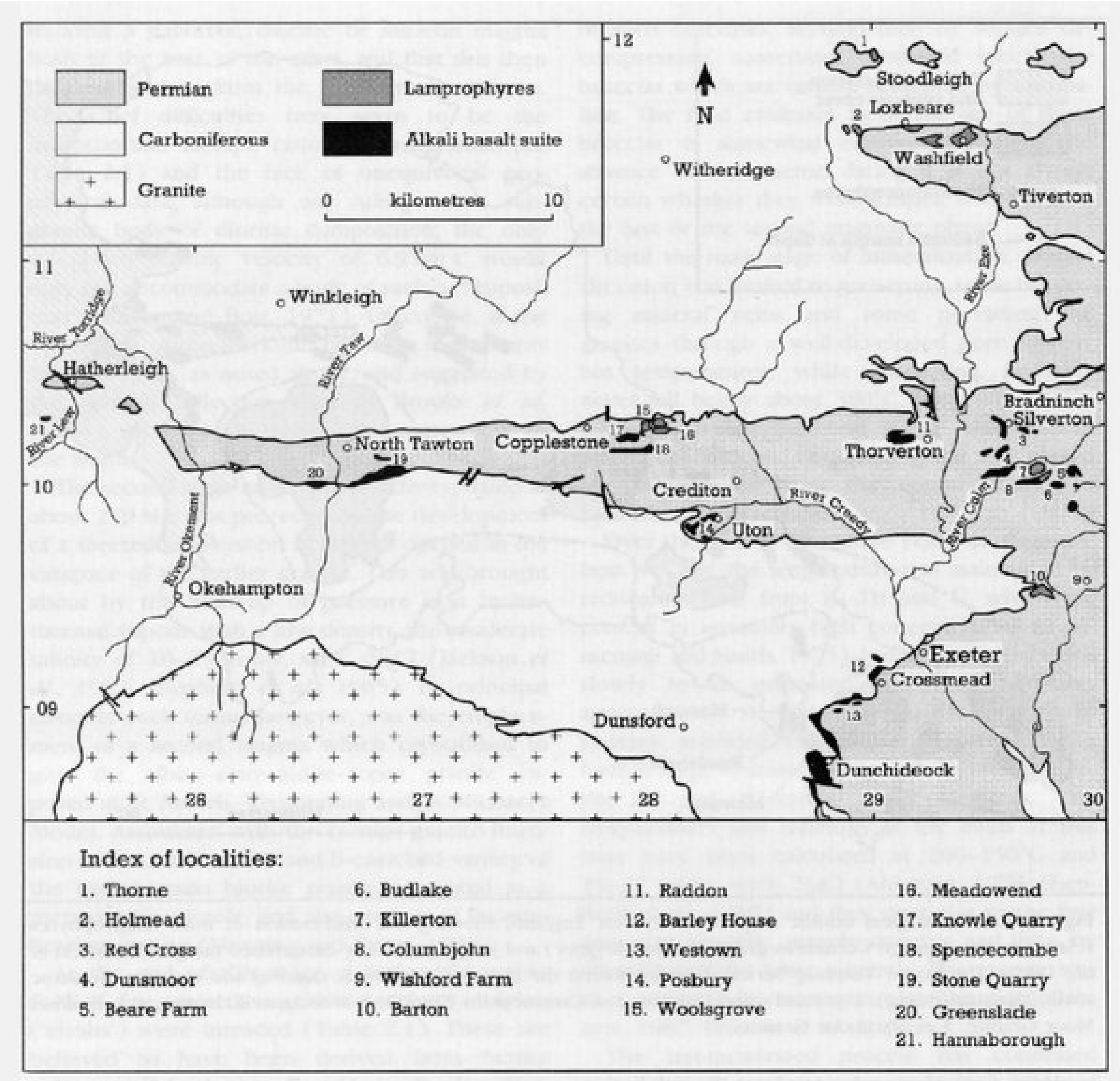

(Figure 2.9) Distribution of the two main magmatic groups within the Exeter Volcanic 'Series', mid-Devon (after Edmonds et al., 1969).

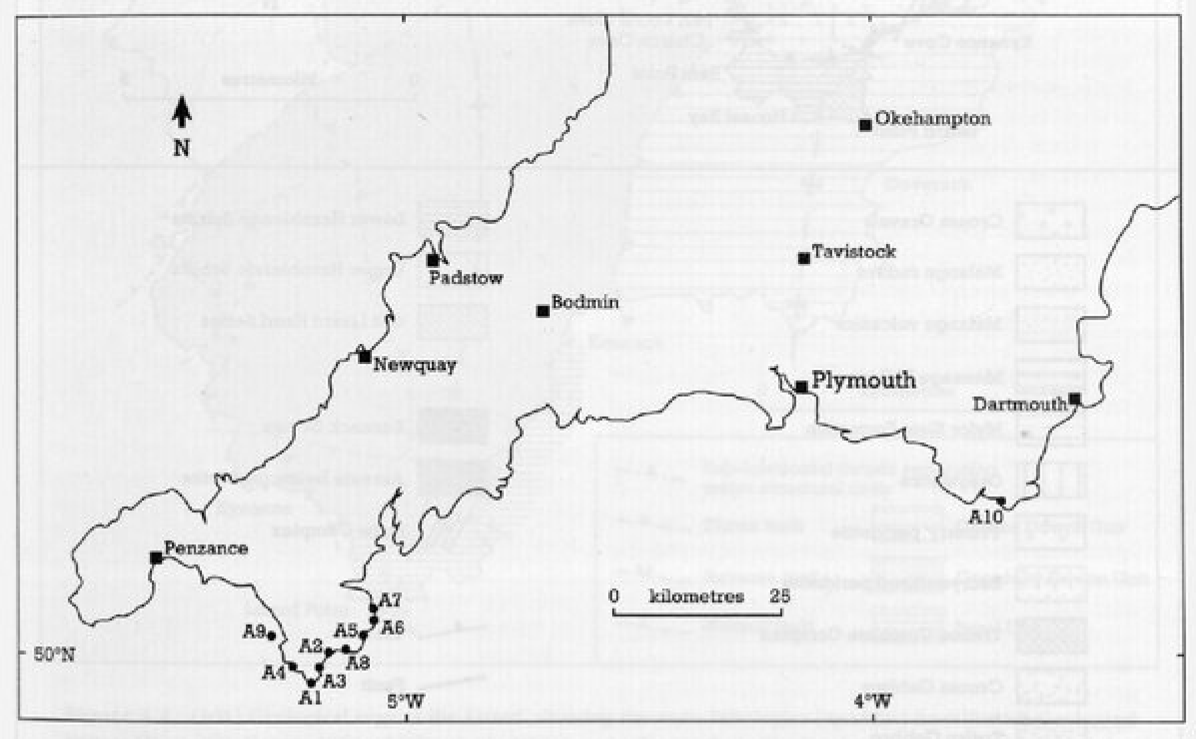

(Figure 3.1) Outline map of south-west England, showing the location of Group A sites.

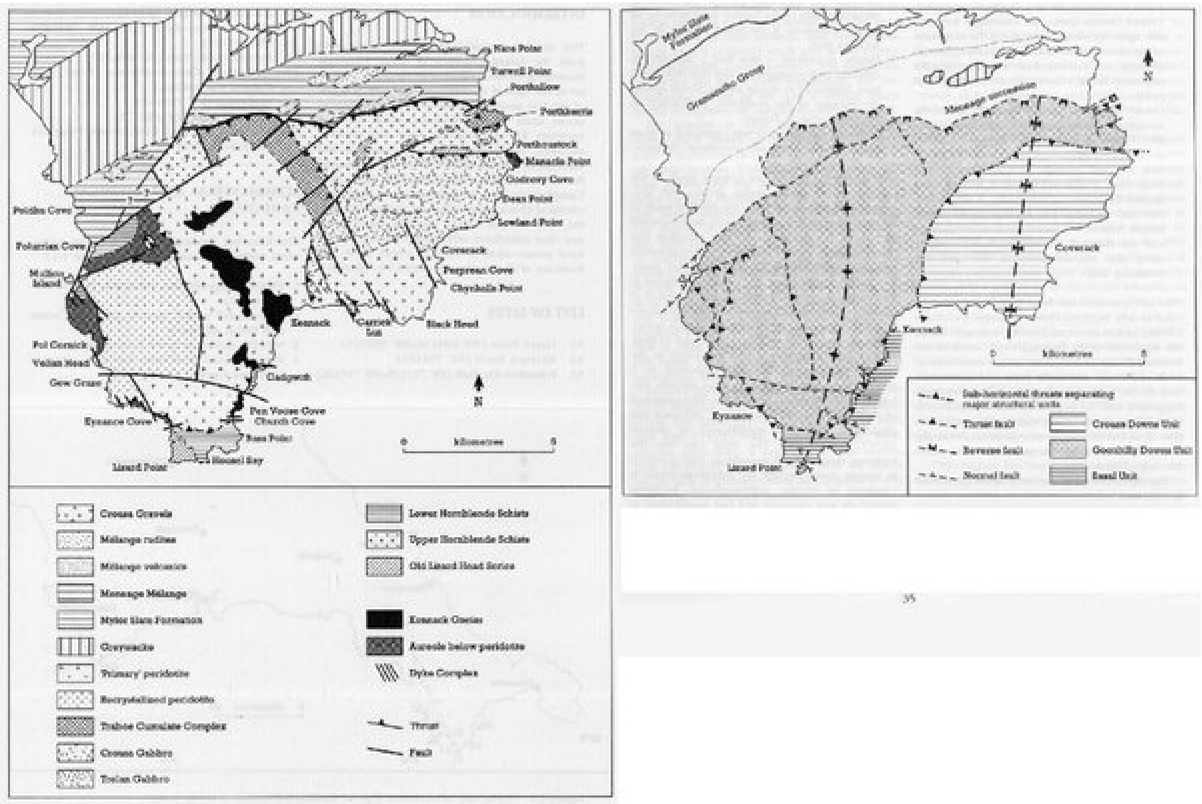

(Figure 3.2) (left) Geological map of the Lizard, showing the main lithologies (modified from British Geological Survey Sheet 359; Green, 1964a; Leake et al., 1990); and (above) their division into three tectonic units (after Bromley, 1979).

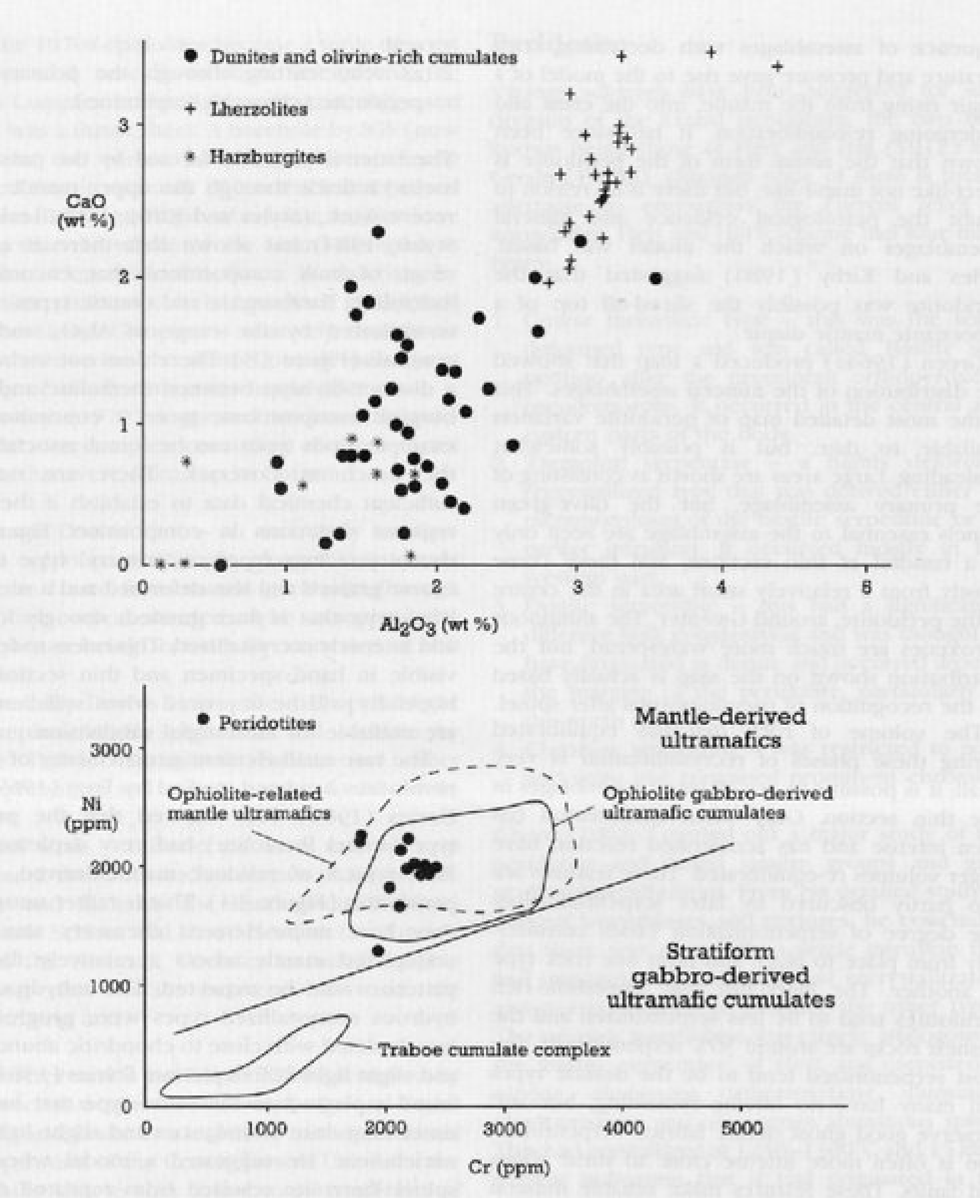

(Figure 3.3) Distribution of Al_2O_4—CaO and Ni—Cr in Lizard peridotites, dunites and ultramafic cumulates (data from Parker, 1970; Kirby, 1979a; Leake and Styles, 1984) relative to typical ophiolite- and stratiform-related ultramafics (data from Rivalenti et al. (1981) and the literature).

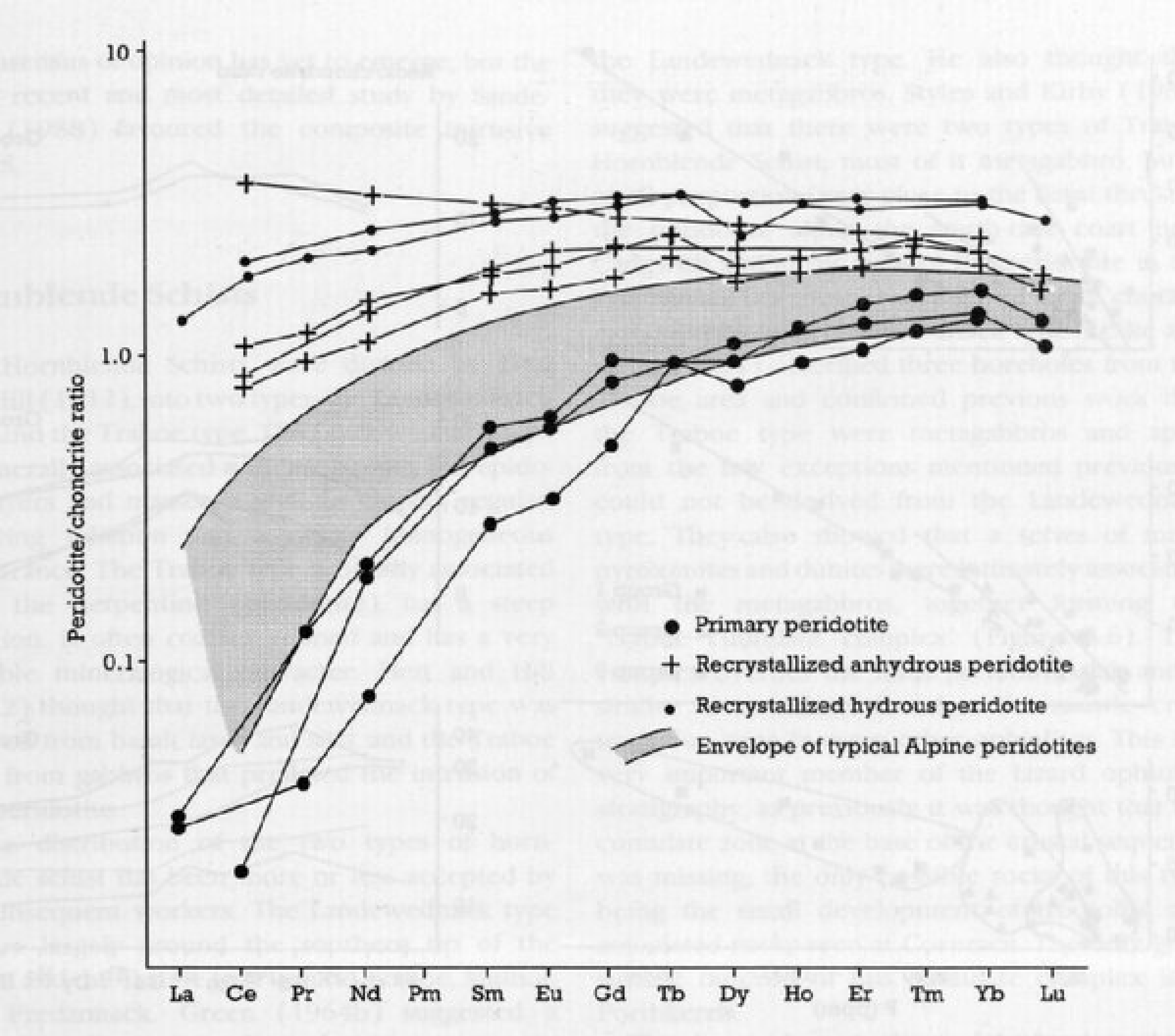

(Figure 3.4) Chondrite-normalized REE data for the different assemblages of the Lizard peridotite (from Frey, 1969; Davies, 1984) and typical Alpine peridotites (data from Frey, 1984).

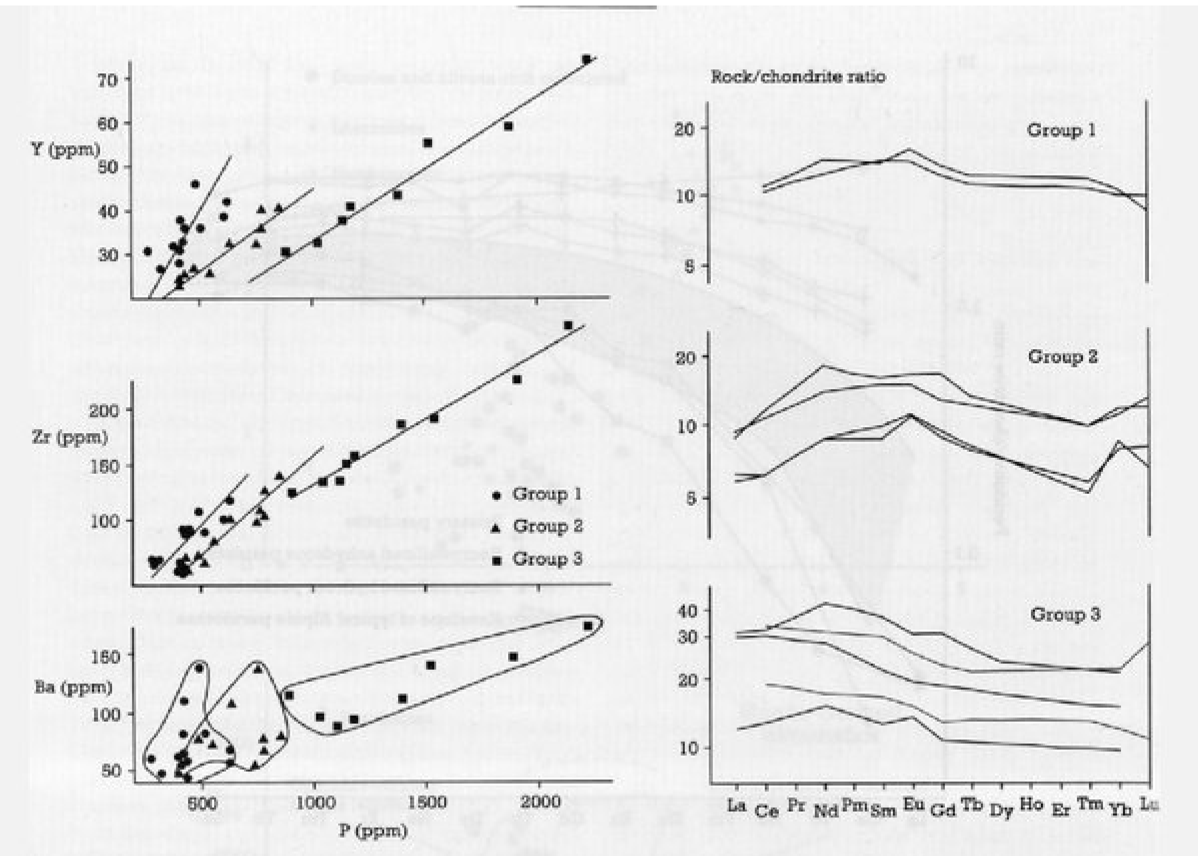

(Figure 3.5) Incompatible-element and normalized REE patterns for the Lizard basaltic dykes, showing the distinctions between the three chemical groups (data from Davies, 1984; Kirby, 1984).

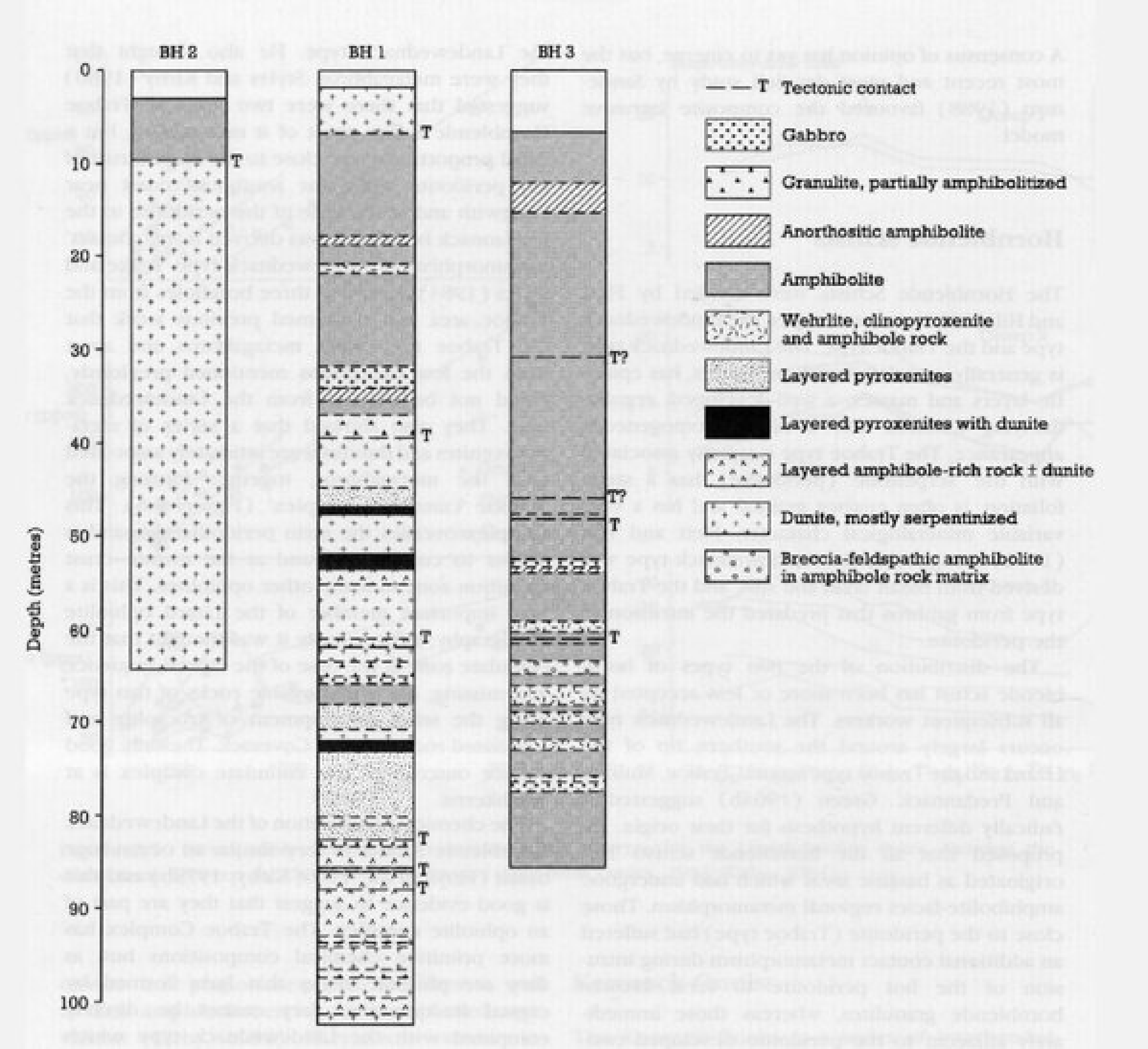

(Figure 3.6) Lithological borehole logs for the Traboe ultramafic—mafic cumulate complex at Traboe, Lizard area (data from Leake and Styles, 1984).

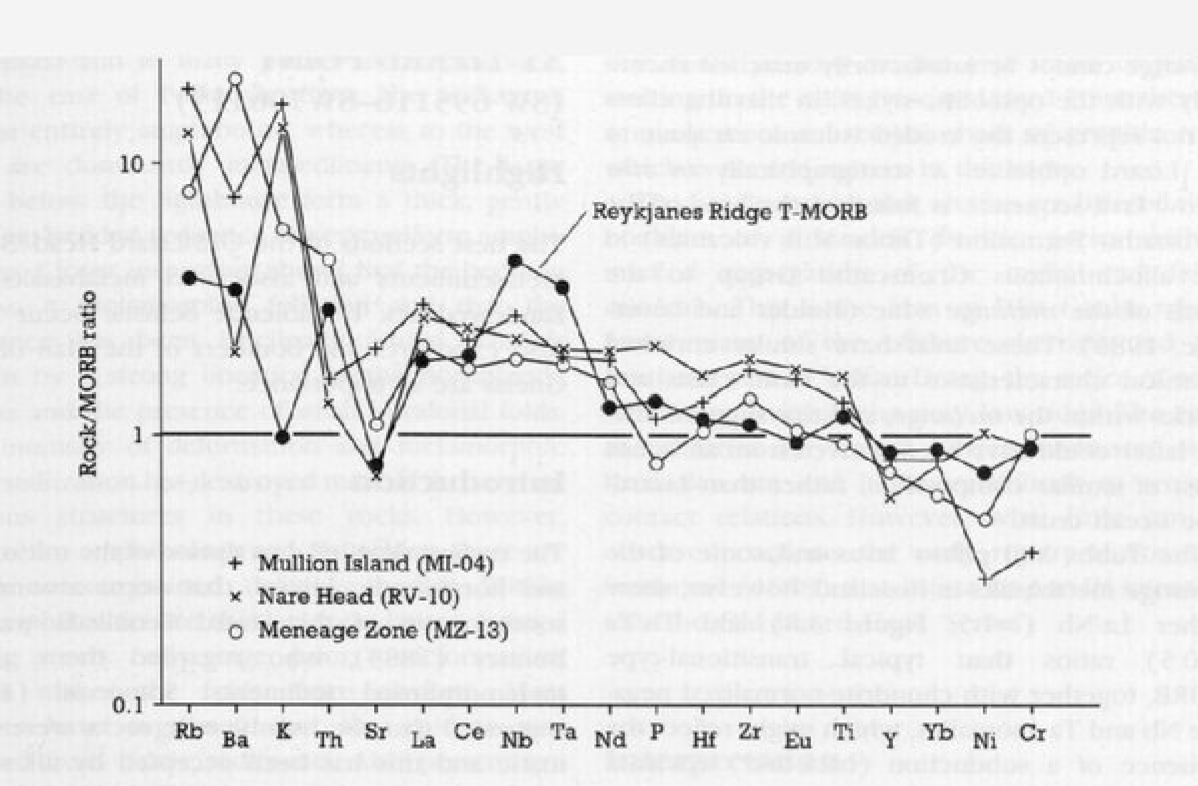

(Figure 3.7) MORB-normalized multi-element patterns for selected mélange metabasalts compared with an example of transitional-type MORB from the Reykjanes Ridge.

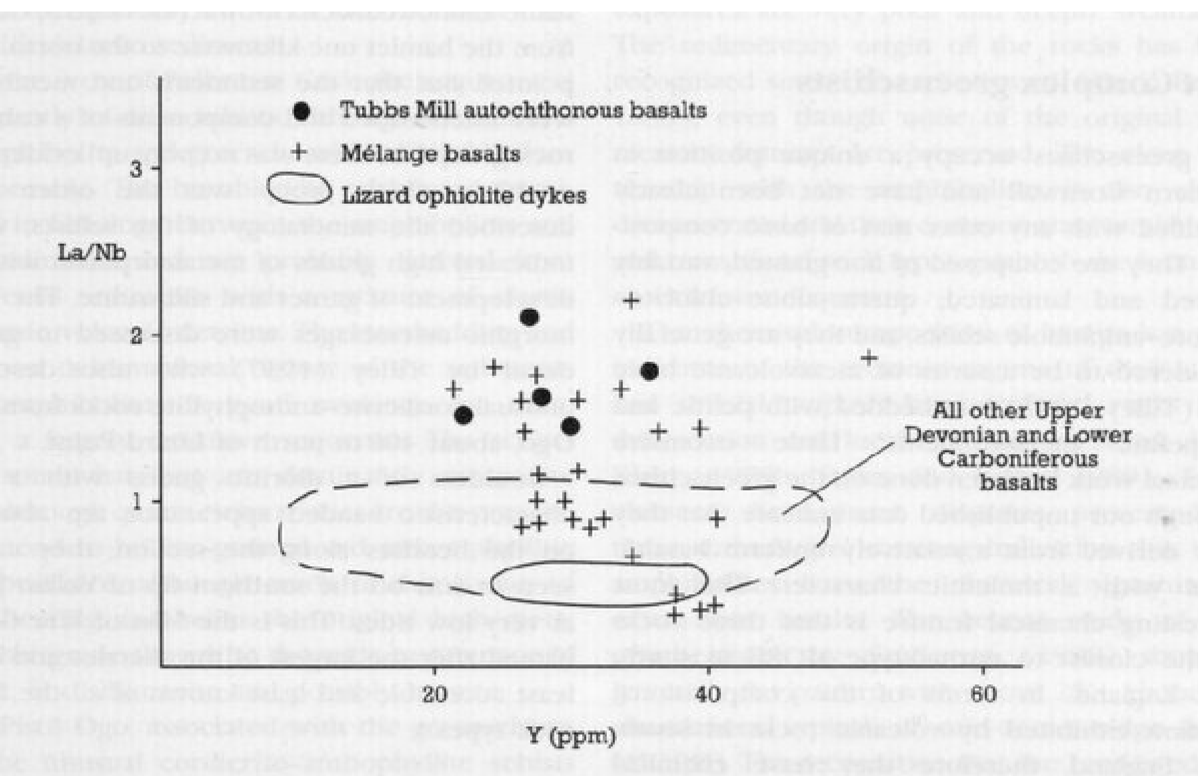

(Figure 3.8) Diagram showing the variation in the La/Nb ratio for the Tubbs Mill pillow lavas and some of the mélange metabasaltic clasts relative to the Lizard dykes and Upper Devonian—Lower Carboniferous basic volcanics from south-west England.

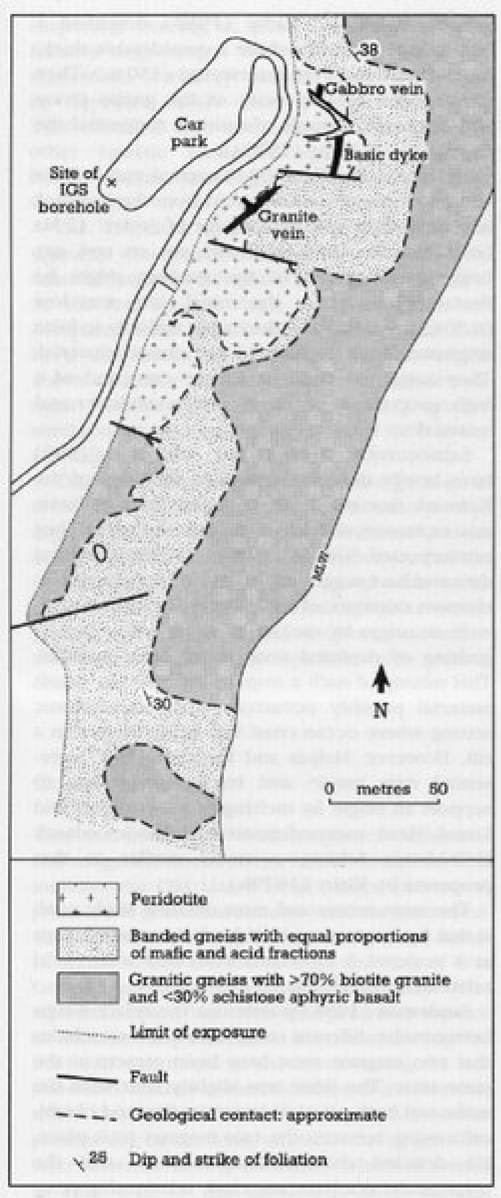

(Figure 3.9) Geological sketch map of the Kennack Sands site (A2).

(Figure 3.10) Banded gneiss, Kennack Sands. (Photo: M.T. Styles.)

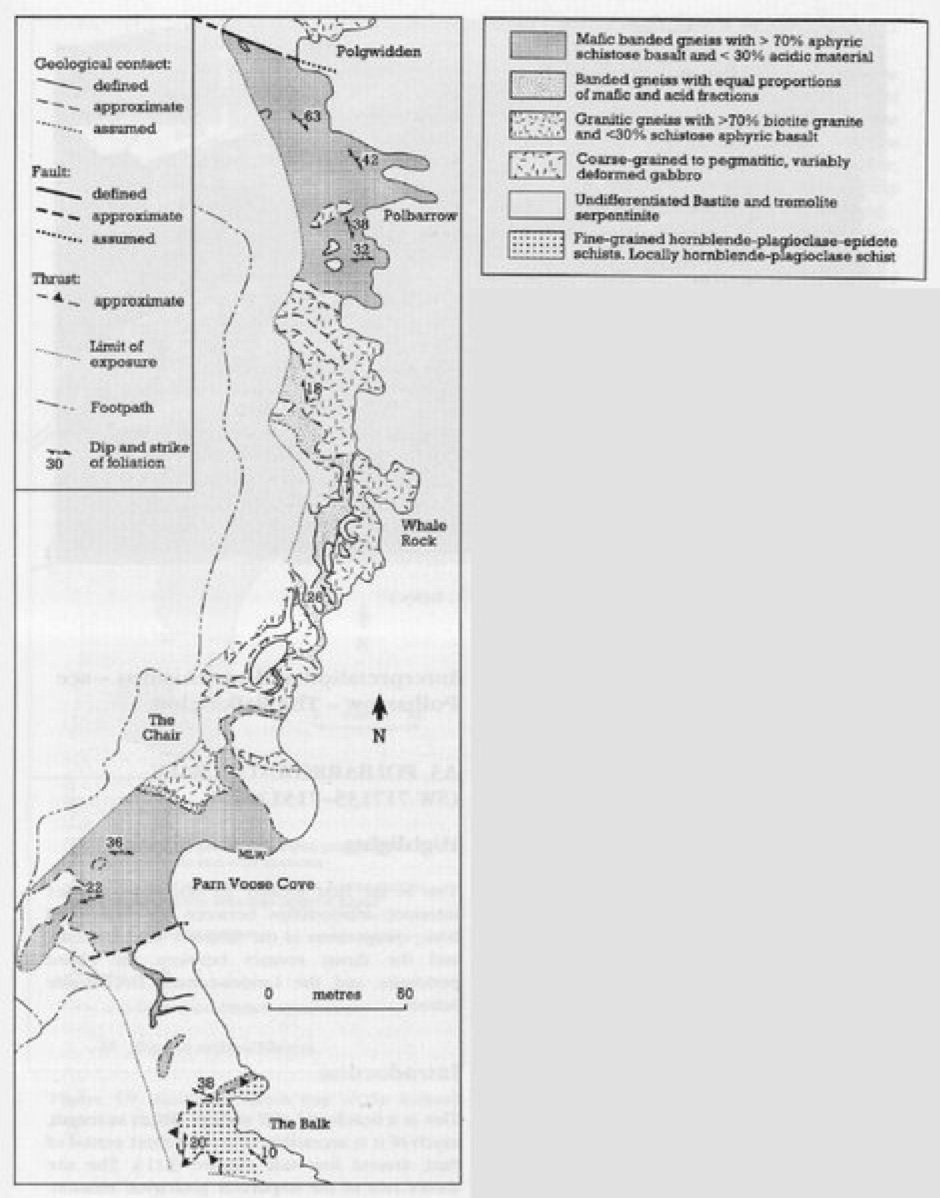

(Figure 3.11) Geological sketch map of the Polbarrow—The Balk site (A3) (after Sandeman, 1988).

(Figure 3.12) Acid-veined gabbro at Parn Voose. (Photo: M.T. Styles.)

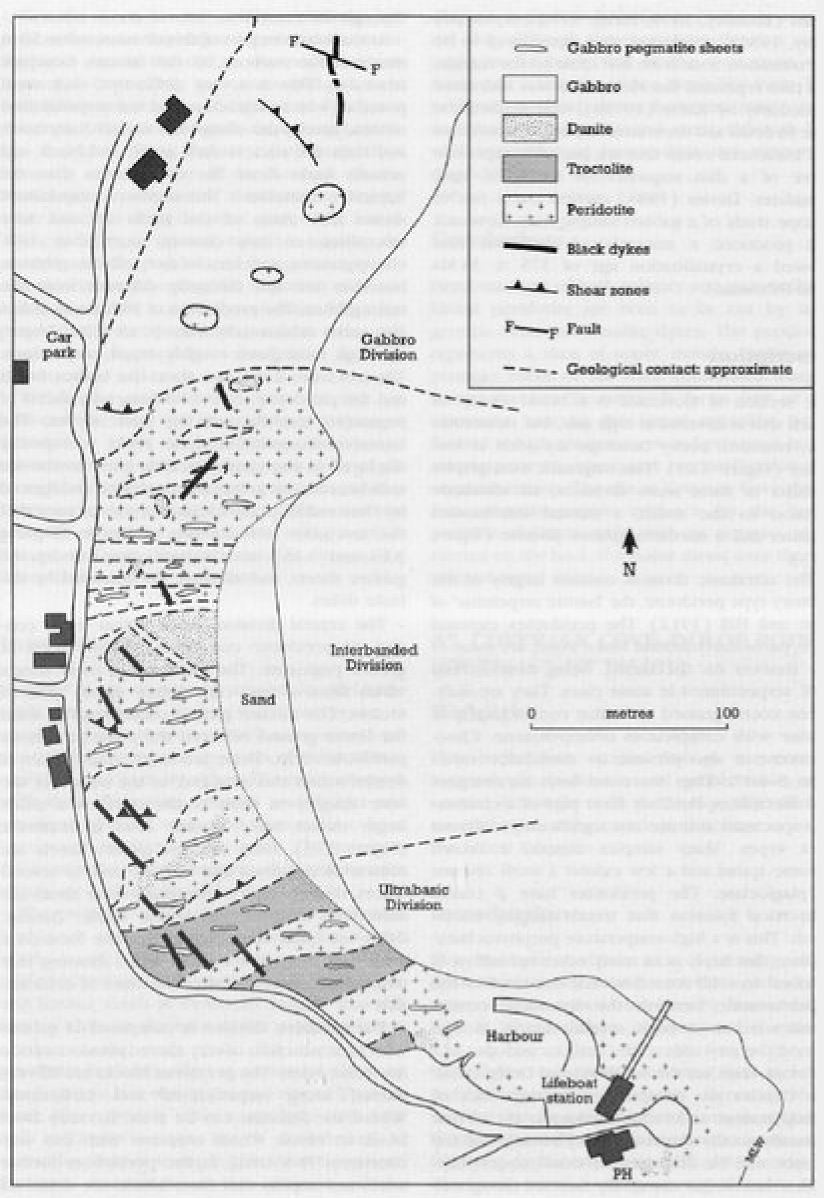

(Figure 3.13) Geological sketch map of the Coverack site (A5).

(Figure 3.14) Xenoliths of peridotite enclosed within troctolite, Coverack Beach. (Photo: M.T. Styles.)

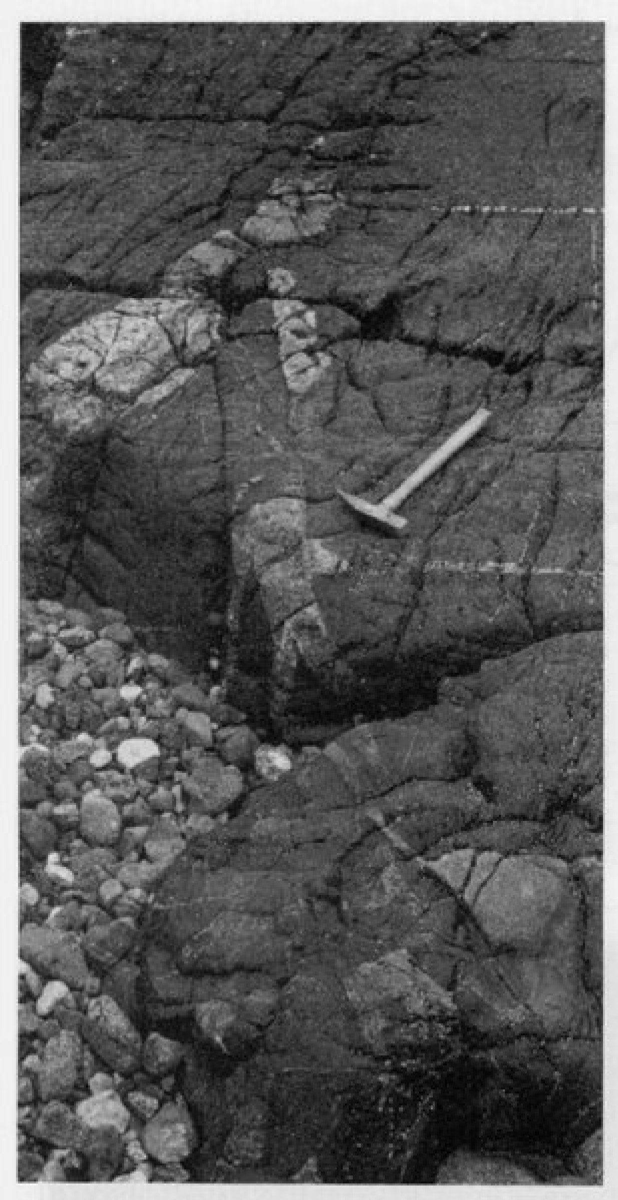

(Figure 3.15) Troctolite veining peridotite, Coverack. (Photo: M.T. Styles.)

(Figure 3.16) Sheeted, basic dykes at Porthoustock Point. The dykes locally form about 80% of the outcrop with only thin gabbroic screens separating them. (Photo: M.T. Styles.)

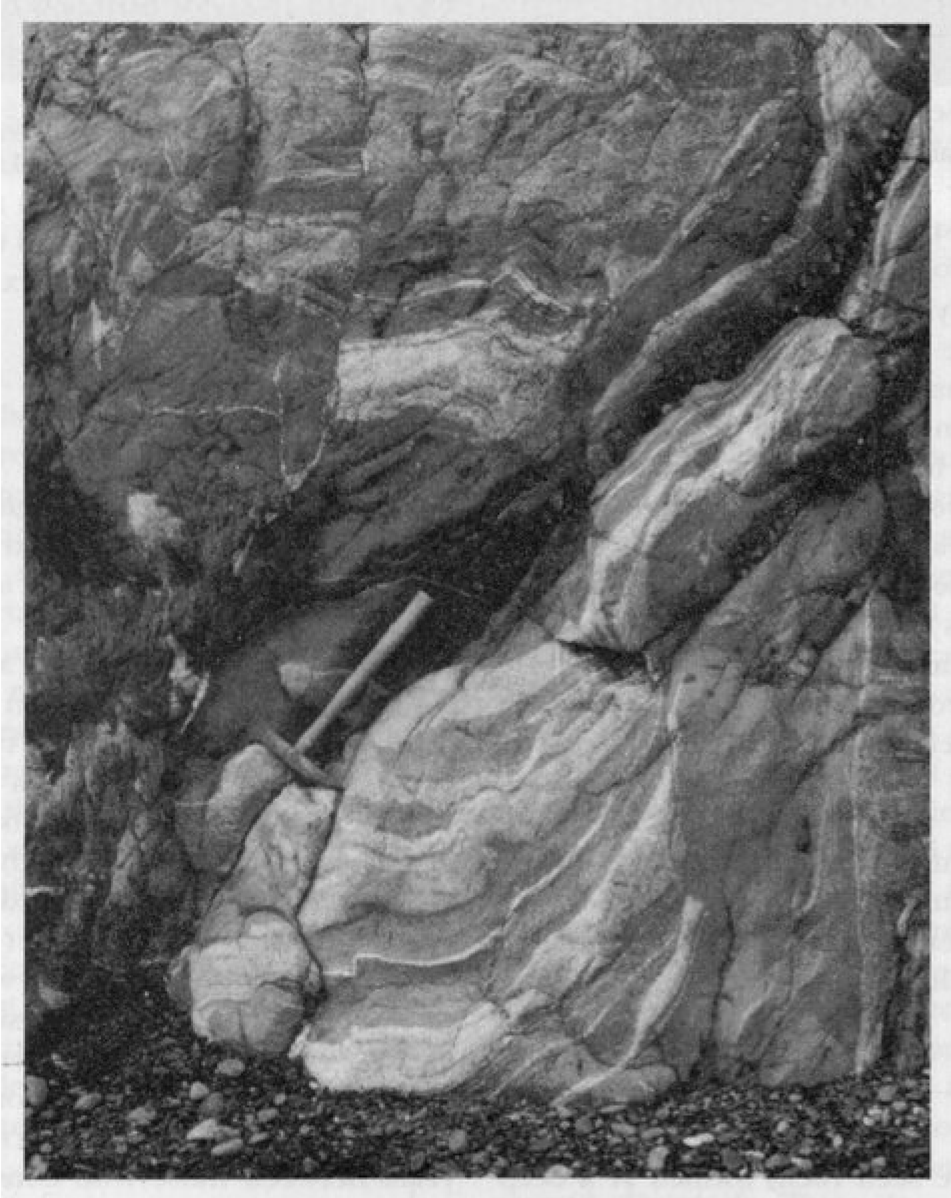

(Figure 3.17) Interlayered basic and ultrabasic cumulate rocks, Traboe-type schists, Porthkerris. (Photo: M.T. Styles.)

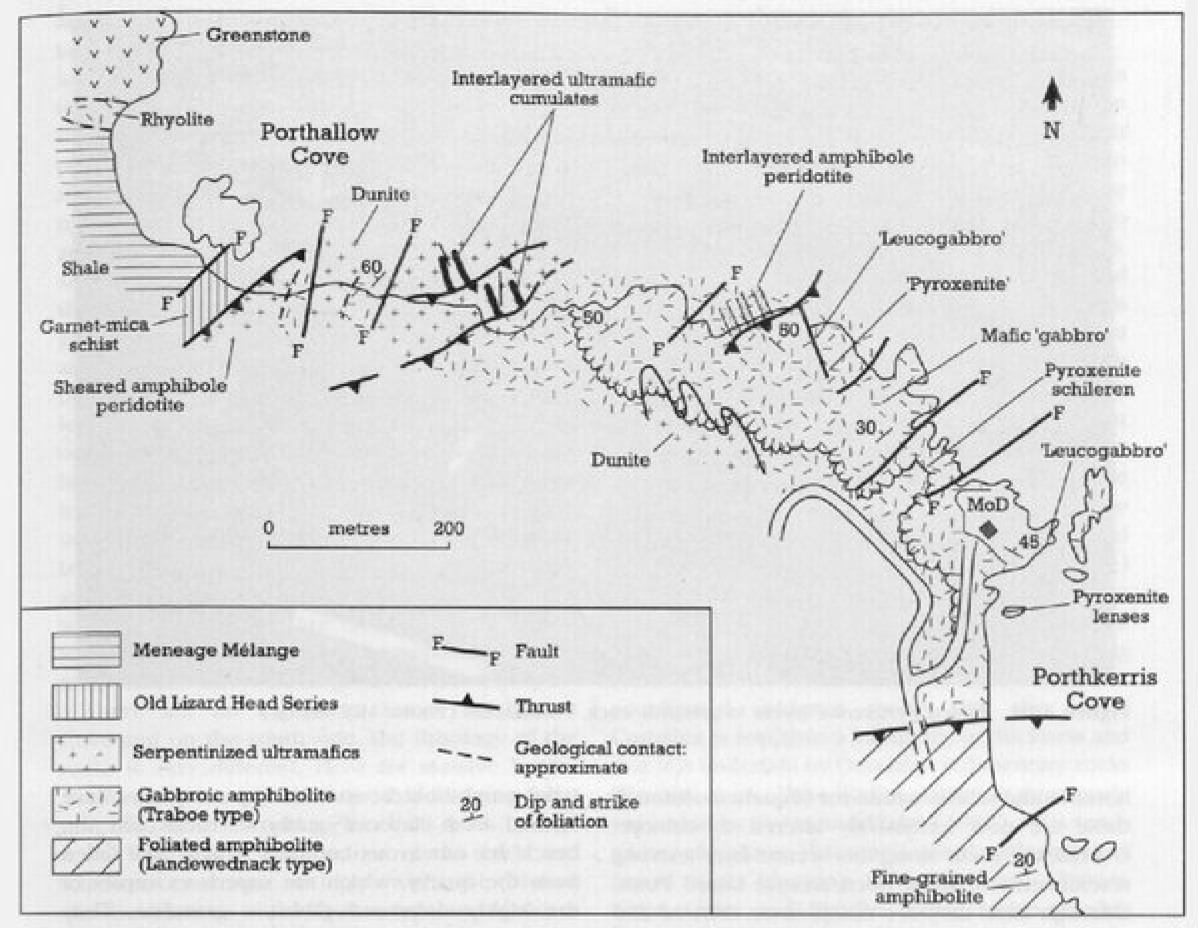

(Figure 3.18) Geological sketch map of the Porthallow Cove—Porthkerris Cove site ( )

(Figure 3.19) Folded pyroxenite layers in gabbroic rock, Porthkerris. (Photo: M.T. Styles.)

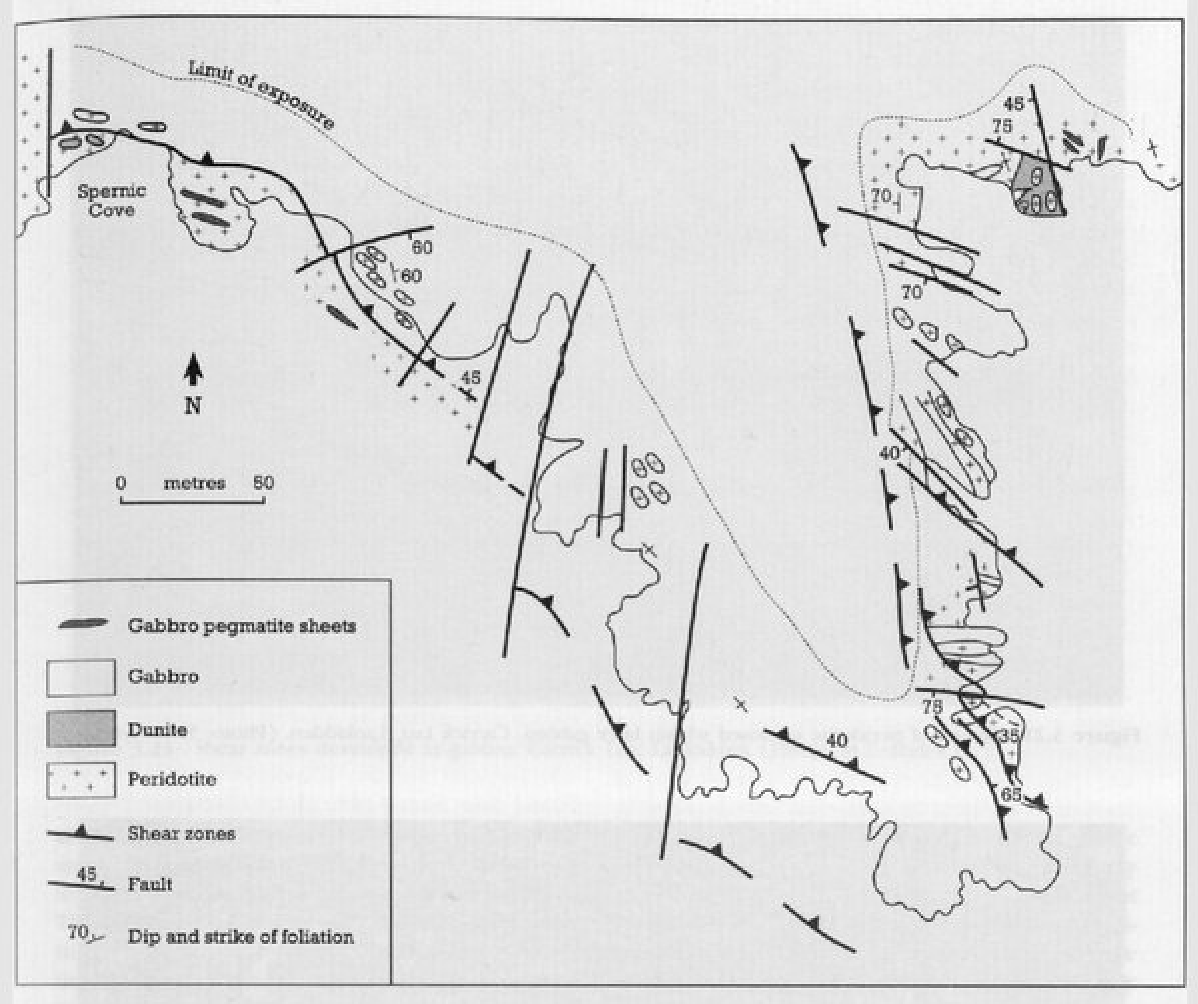

(Figure 3.20) Geological sketch map of the Lankidden site (A8) showing distribution of outcrops between landward exposures and low-water reefs.

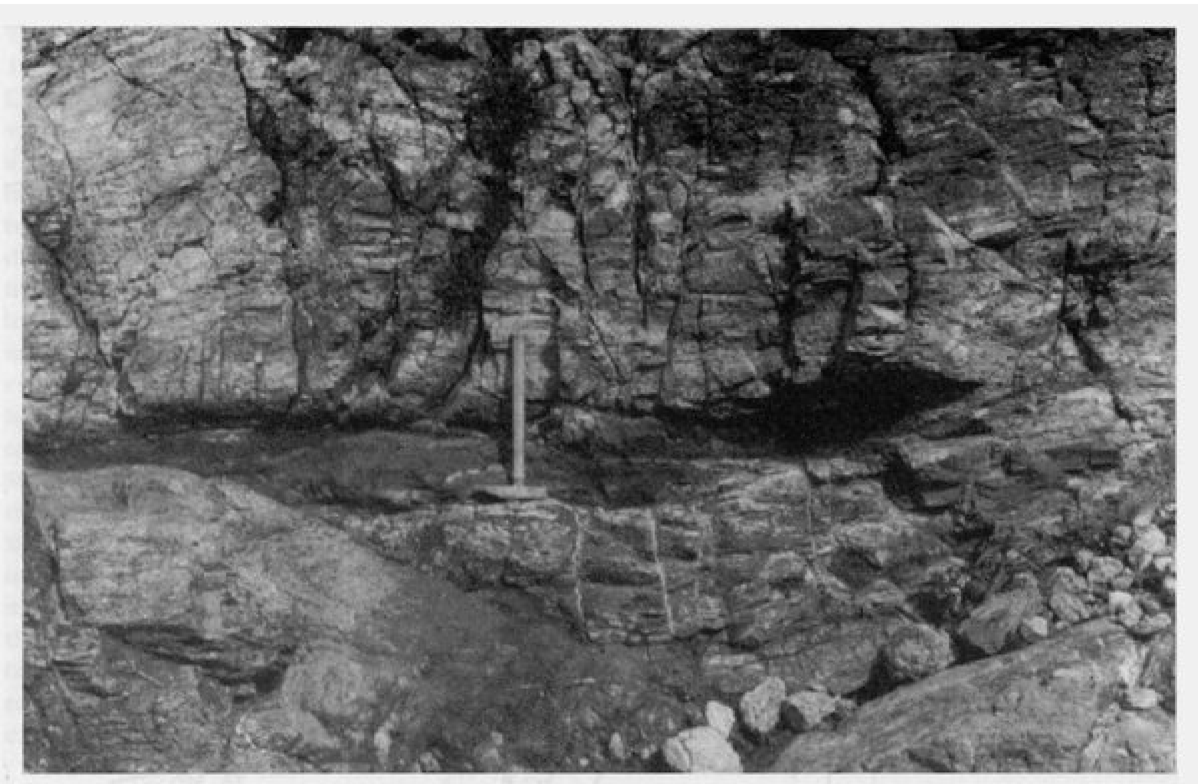

(Figure 3.21) Lenses of peridotite enclosed within later gabbro, Carrick Luz, Lankidden. (Photo: M.T. Styles.)

(Figure 3.22) Flaser gabbro, Carrick Luz, Lankidden. (Photo: M.T. Styles.)

(Figure 3.23) Shear zones developed in gabbro, Carrick Luz, Lankidden. (Photo: M.T. Styles.)

(Figure 3.24) A spectacular development of pillow lavas, of Frasnian age, on Mullion Island. (Photo: P.A. Floyd.)

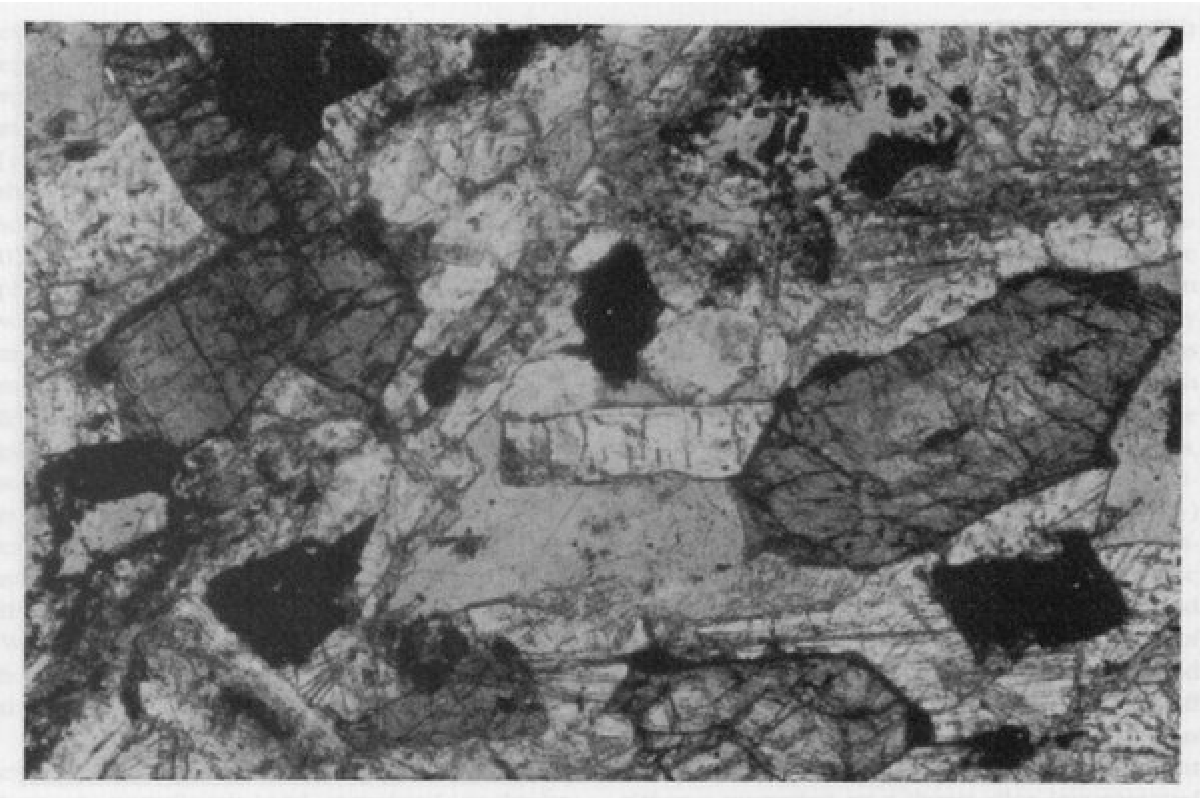

(Figure 3.25) Photomicrograph of pillow lava from Mullion Island. Primary plagioclase, zoned clinopyroxene and ilmenite are set in a secondary pumpellyite-facies mineral matrix. (Photo: P.A. Floyd.)

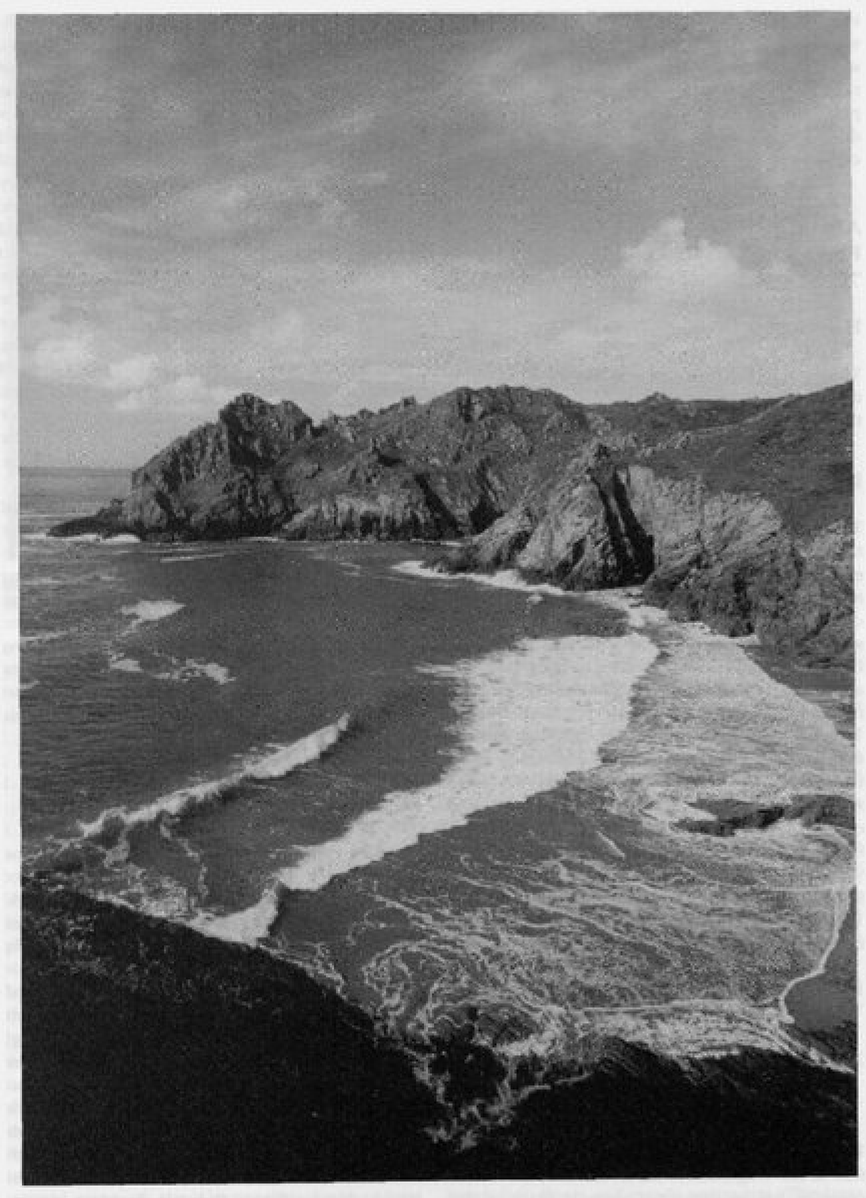

(Figure 3.26) The rocky cliffs of Elender Cove expose metavolcanic greenschists of the Start Complex. Elender Cove, near Prawle Point, Devon. (Photo: David Noton Photography.)

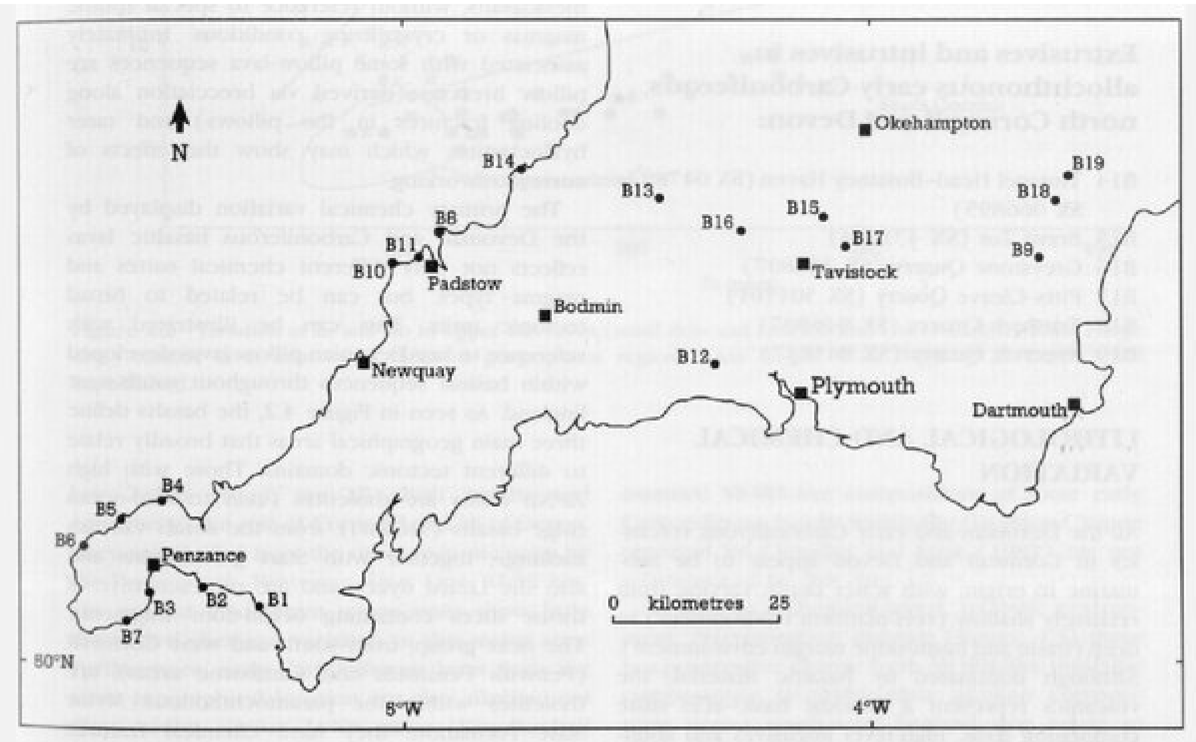

(Figure 4.1) Outline map of south-west England showing the location of Group B sites.

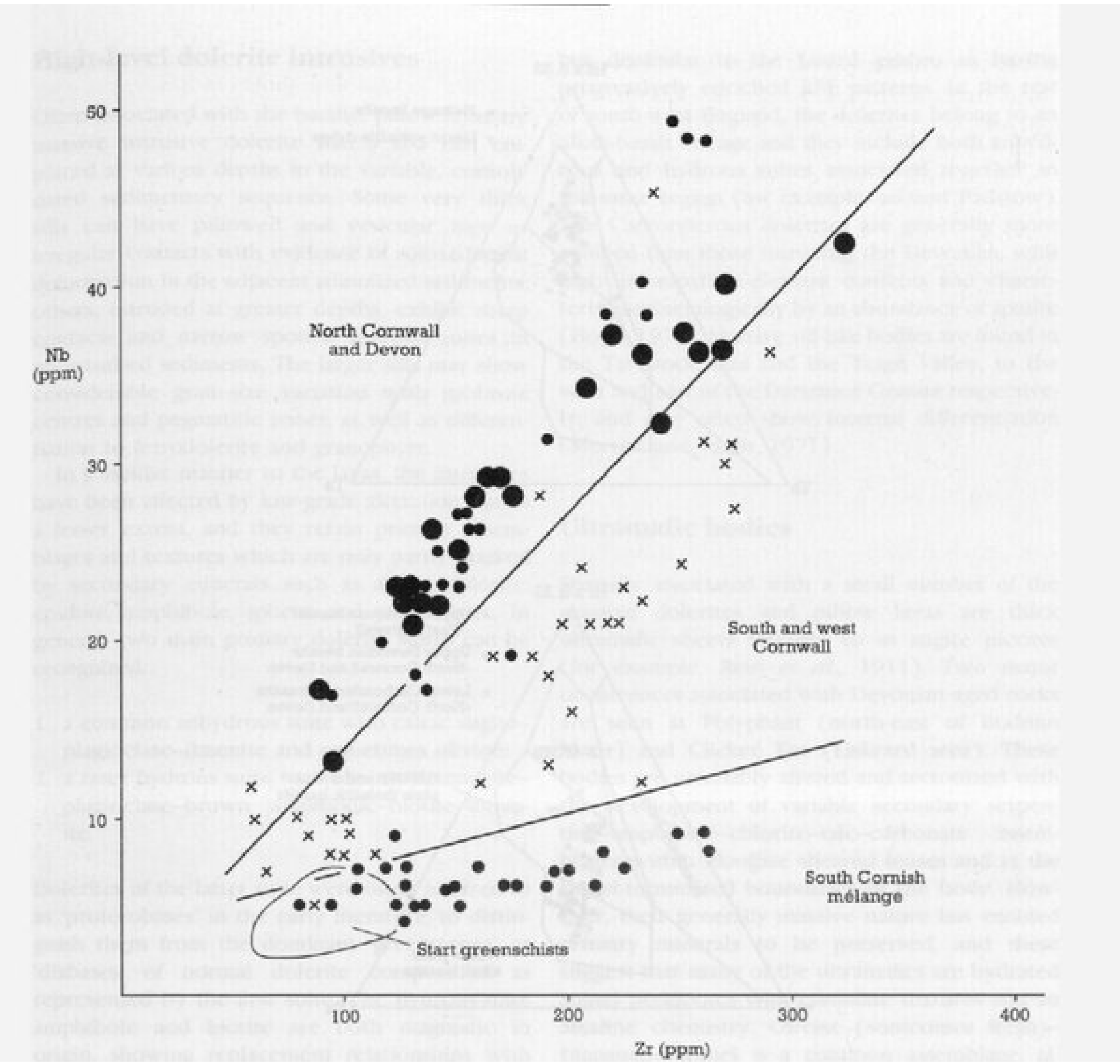

(Figure 4.2) Variation of Zr and Nb in Upper Devonian (small dots and crosses) and Lower Carboniferous (large dots) basaltic lavas relative to different geographical regions. Data largely from Floyd et al. (1983) and unpublished.

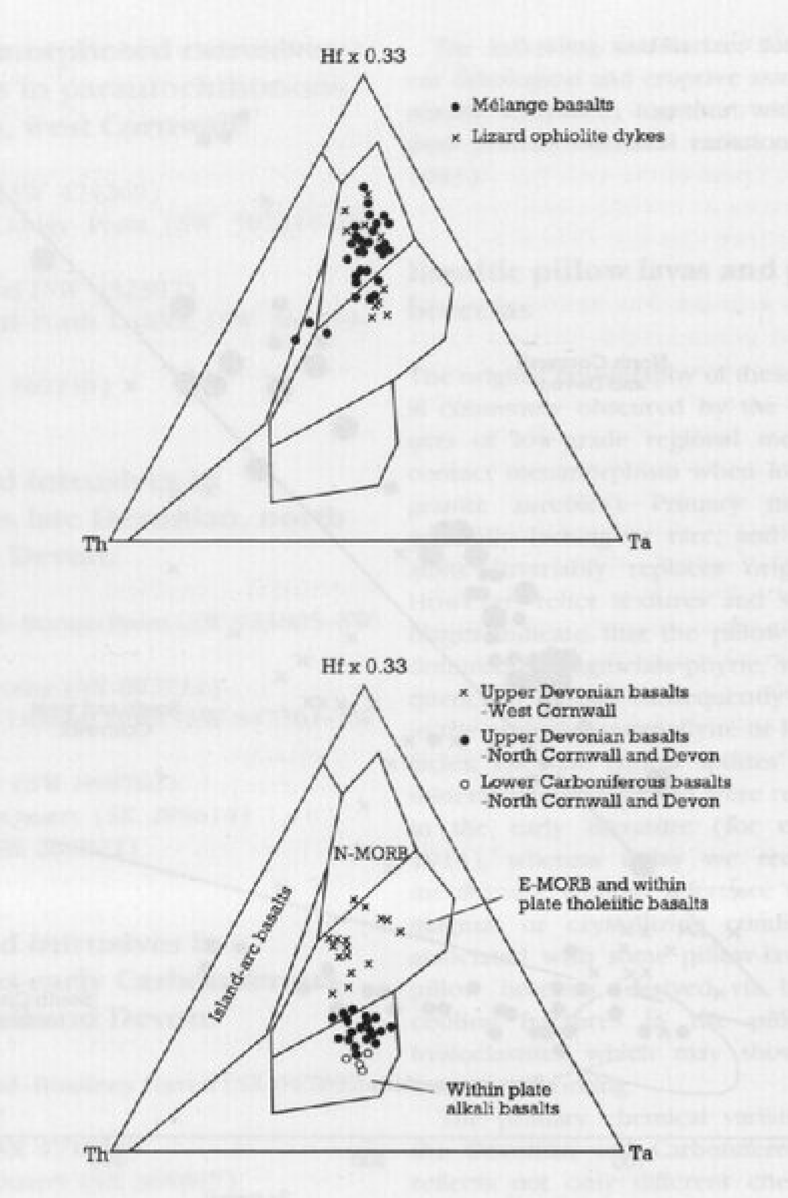

(Figure 4.3) Th—Hf—Ta variation in Devonian and Carboniferous basaltic rocks from different tectonic units and regions in south-west England. Tectonic discrimination fields from Wood (1980).

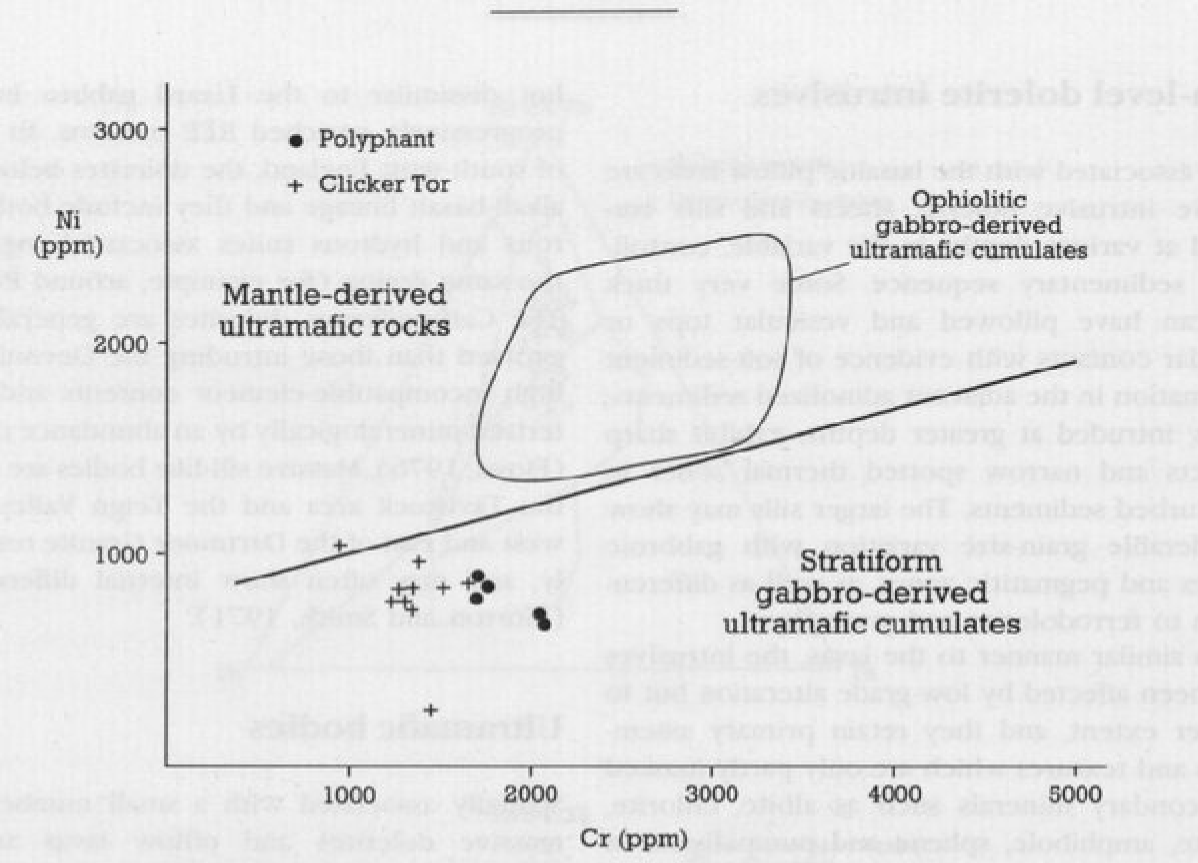

(Figure 4.4) Distribution of Ni and Cr in Variscan ultramafic bodies associated with dolerites and pillow lavas relative to ophiolitic and stratiform cumulates (boundaries from Figure 3.3).

(Figure 4.5) Apparently discordant relationship between a basic intrusive body (on the right) and adjacent foliated sediments of Lower Devonian age (on the left). Porthleven, Cornwall. (Photo: P.A. Floyd.)

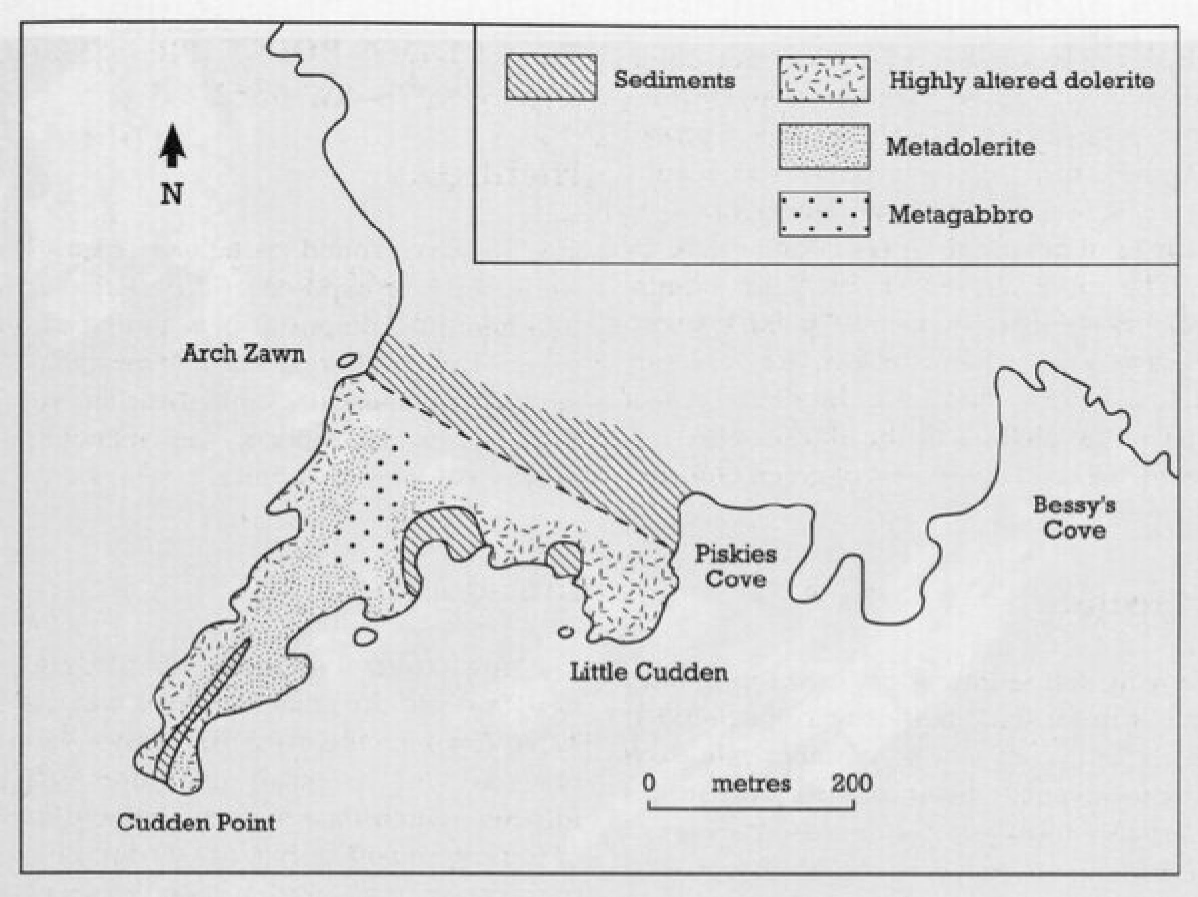

(Figure 4.6) Simplified map of the Cudden Point greenstone body.

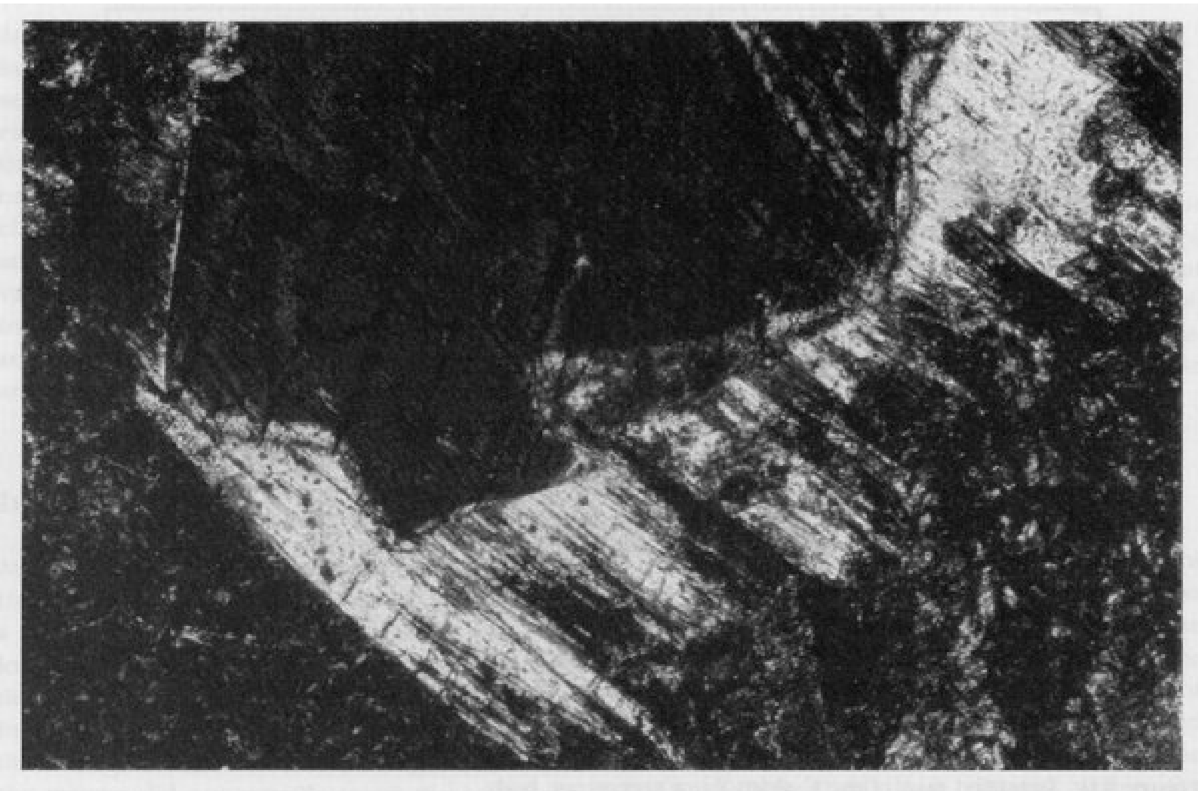

(Figure 4.7) Photomicrograph of the coarser facies of the Cudden Point greenstone showing primary augite partly replaced by a fringe of actinolite (cross polars). (Photo: P.A. Floyd.)

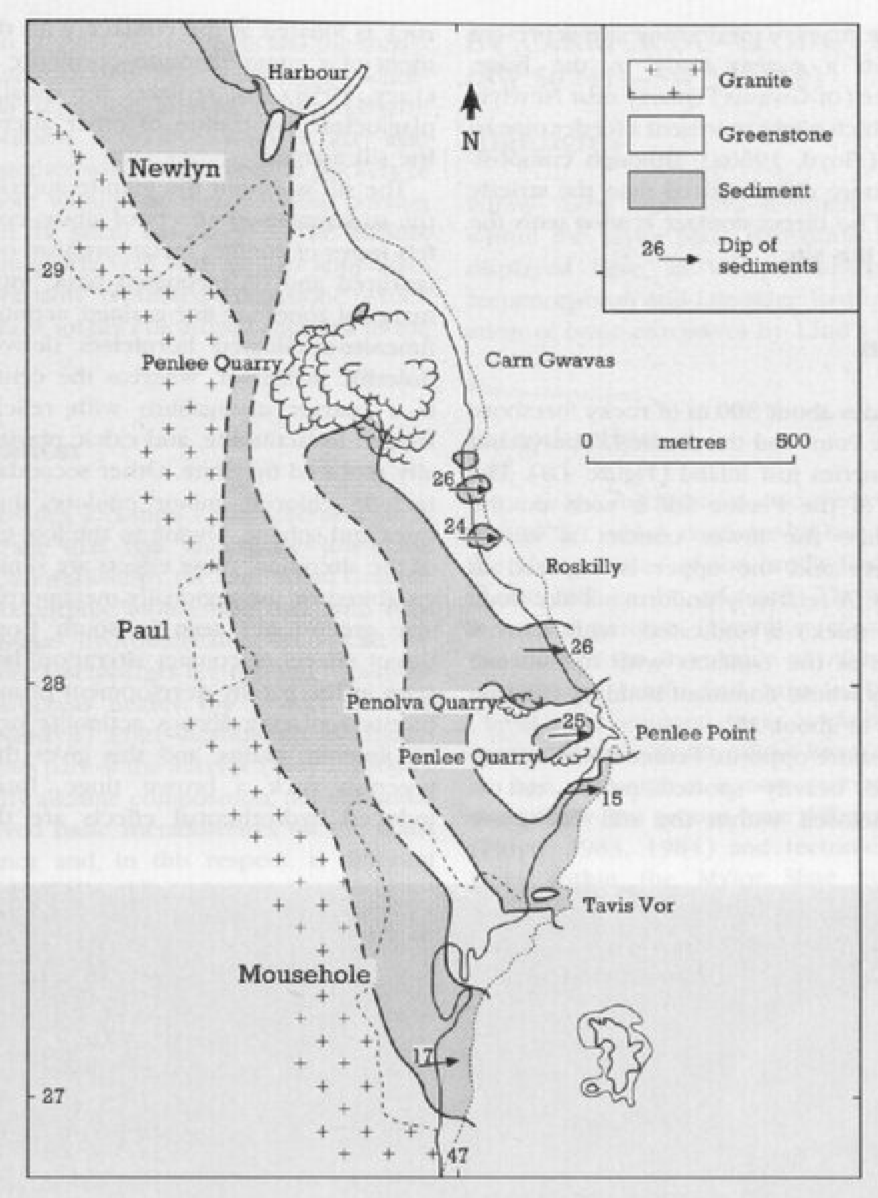

(Figure 4.8) Geological map of the Mousehole—Newlyn section of the Land's End Granite aureole, showing the distribution of the dolerite sills around Penlee Point (after Floyd, 1966a).

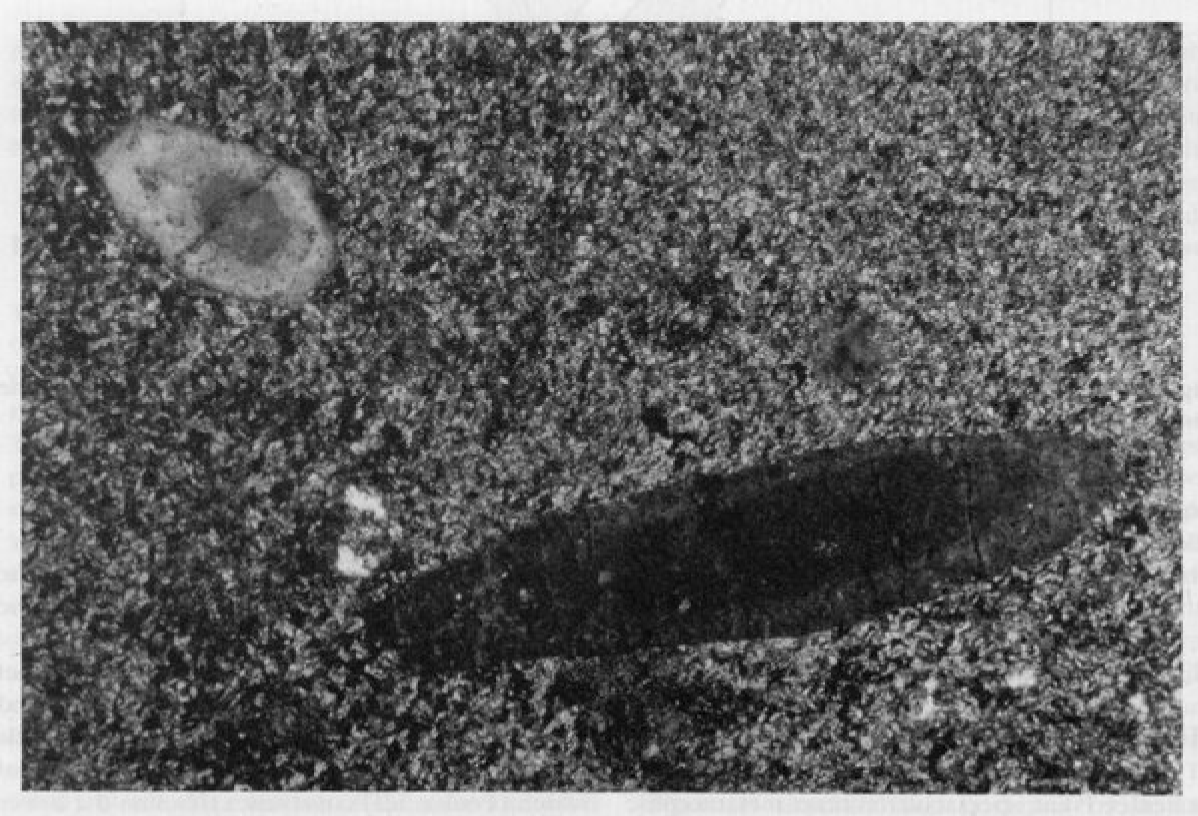

(Figure 4.9) Photomicrograph showing late zoned tourmaline replacing chloritic matrix of contact metamorphosed Penlee dolerite (cross polars). (Photo: P.A. Floyd.)

(Figure 4.10) View of the pillow-lava sequence at Clodgy Point, Penwith, Cornwall. (Photo: P.A. Floyd.)

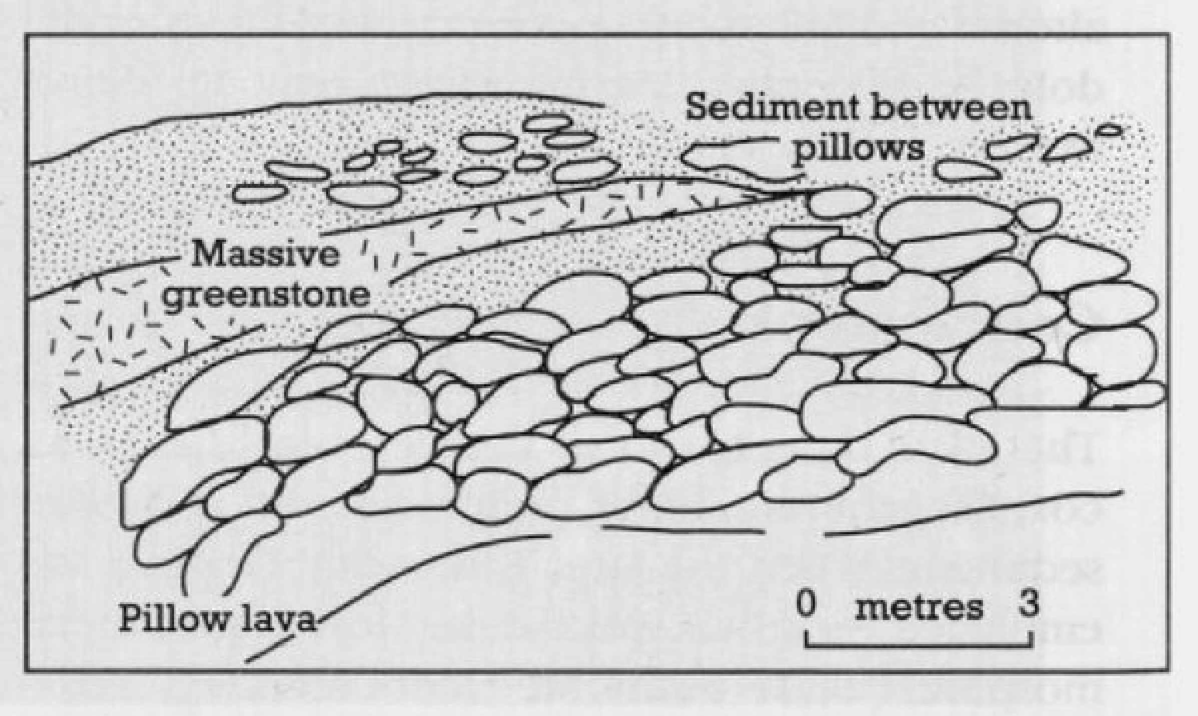

(Figure 4.11) Relationship between Upper Devonian pillow lavas and interlayered pelitic sediment, Clodgy Point, Penwith Peninsula.

(Figure 4.12) Polygonal cooling cracks on pillow-lava sequence at Clodgy Point, Penwith, Cornwall. (Photo: P.A. Floyd.)

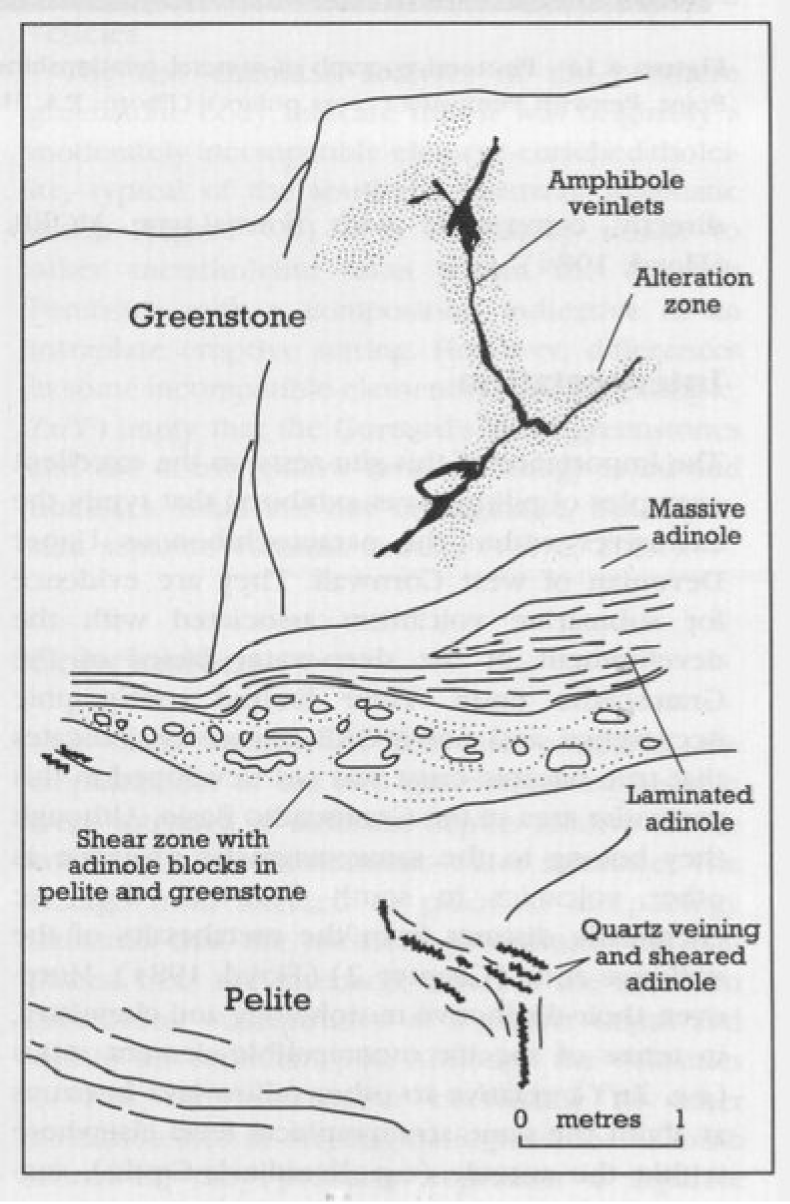

(Figure 4.13) Sketch of the tectonized contact between adinolized sediments and greenstone, Clodgy Point, Penwith Peninsula.

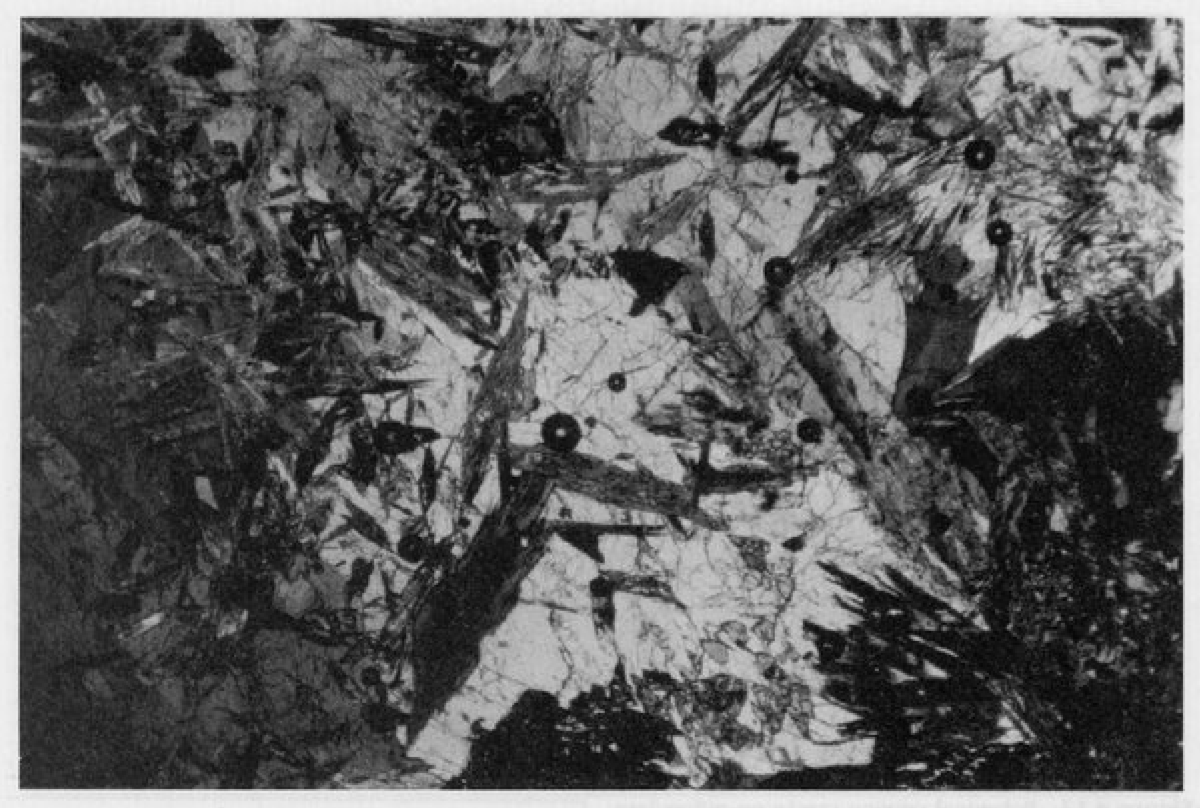

(Figure 4.14) Photomicrograph of mineral relationships in late amphibole-rich hydrothermal veins, near Clodgy Point, Penwith Peninsula (cross polars). (Photo: P.A. Floyd.)

(Figure 4.15) The two greenstone masses of Gurnard's Head. The intervening hollow is underlain by metasediments. Gurnard's Head, Cornwall. (Photo: P.A. Floyd.)

(Figure 4.16) Sheared and flattened L. per Devonian pillow lavas associated with the massive greenstone body at Gurnard's Head, Cornwall. (Photo: P.A. Floyd.)

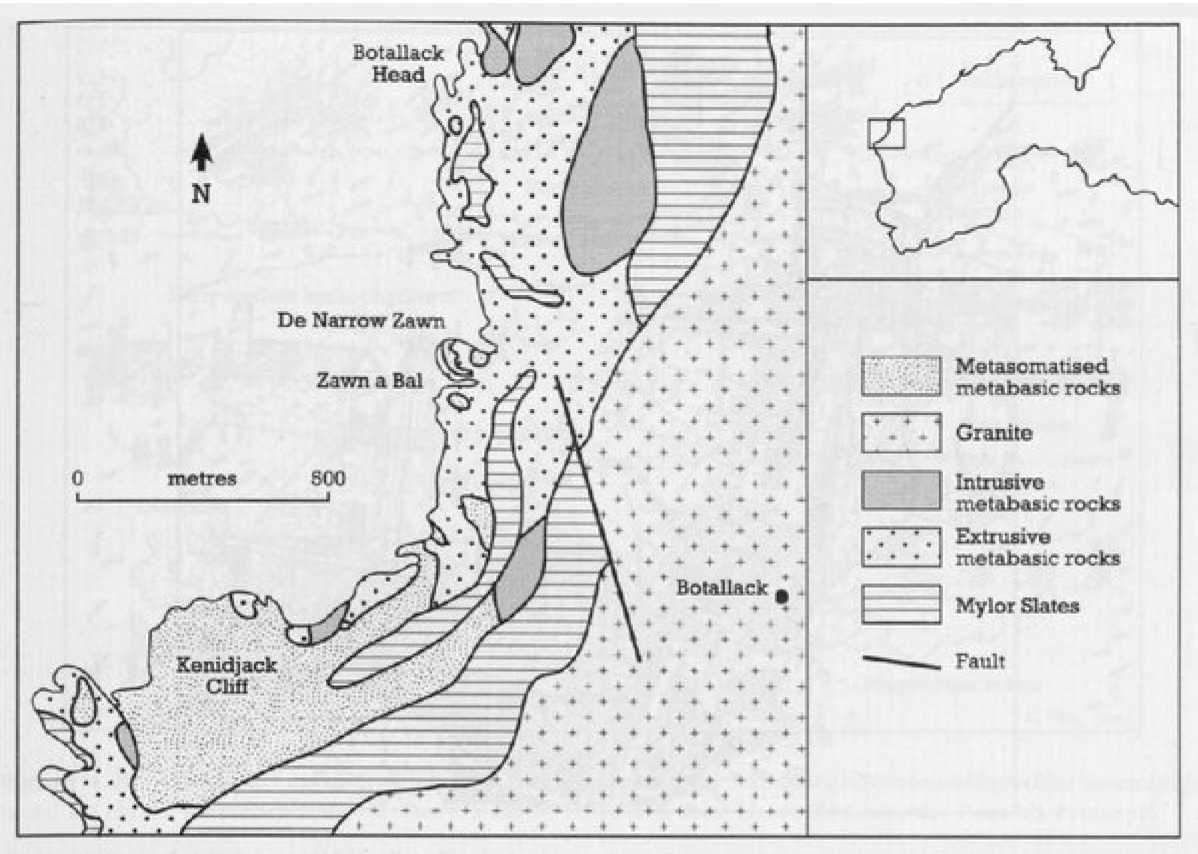

(Figure 4.17) Geological map of the Botallack—Cape Cornwall section of the Land's End aureole, Penwith Peninsula (after Goode and Merriman, 1987).

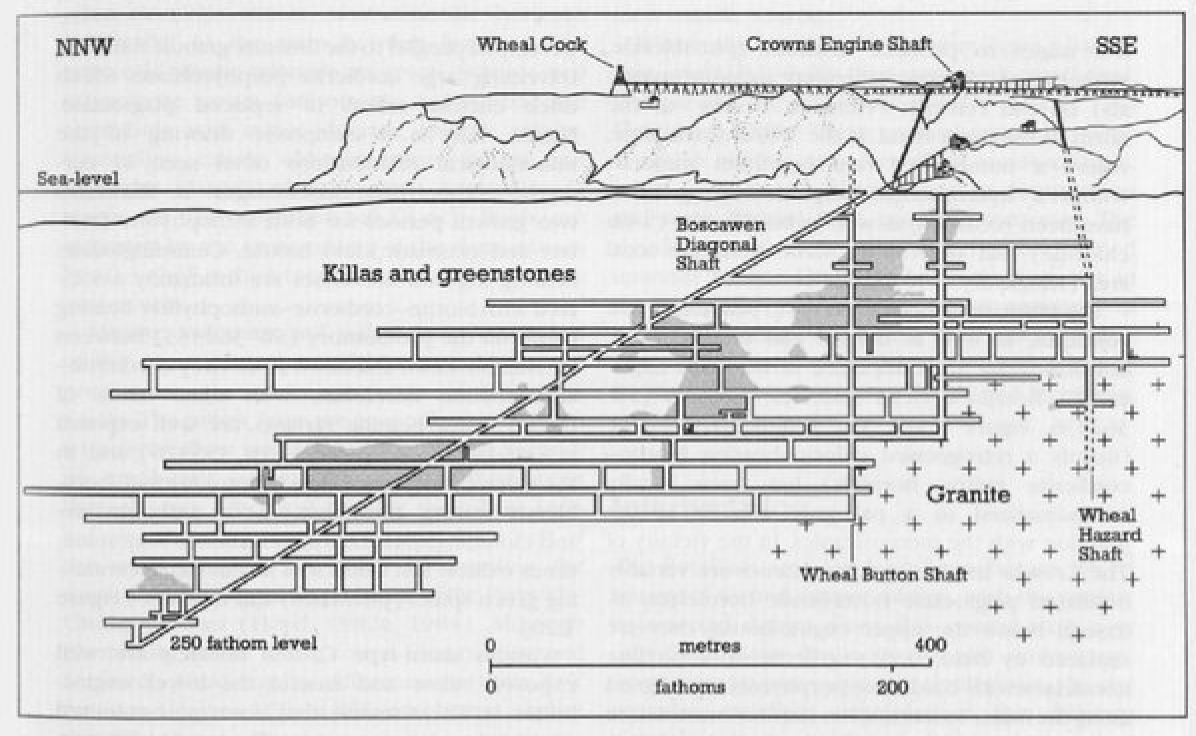

(Figure 4.18) Section through the Botallack Mine, showing the sub-sea-floor workings and famous diagonal shaft, near St Just, Penwith Peninsula (after Embrey and Symes, 1987).

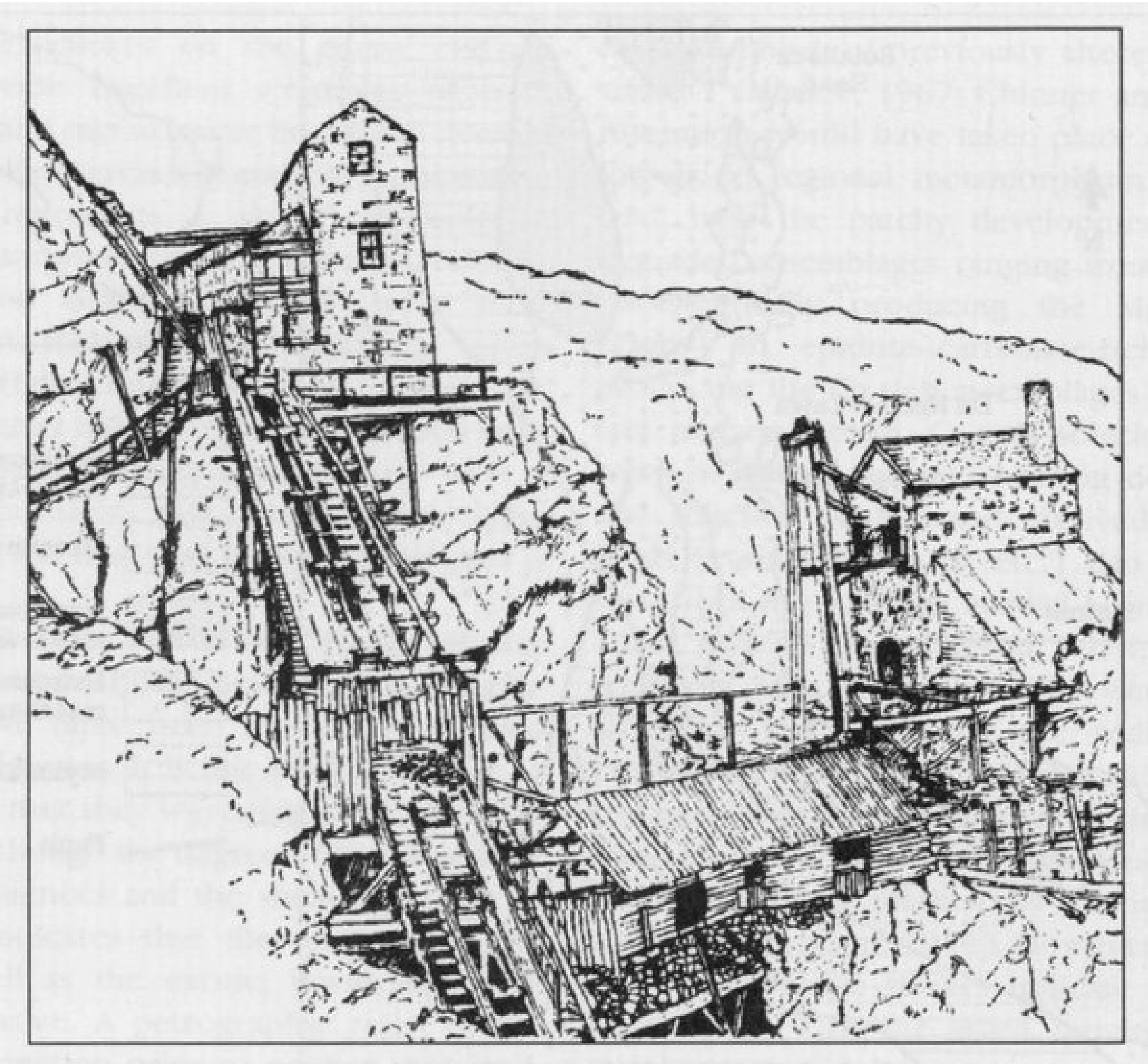

(Figure 4.19) Line drawing of the cliff-edge engine-houses of the Botallack Mine and the beginning of the diagonal shaft at The Crowns, near St Just, Penwith Peninsula (reproduced from Barton, 1965).

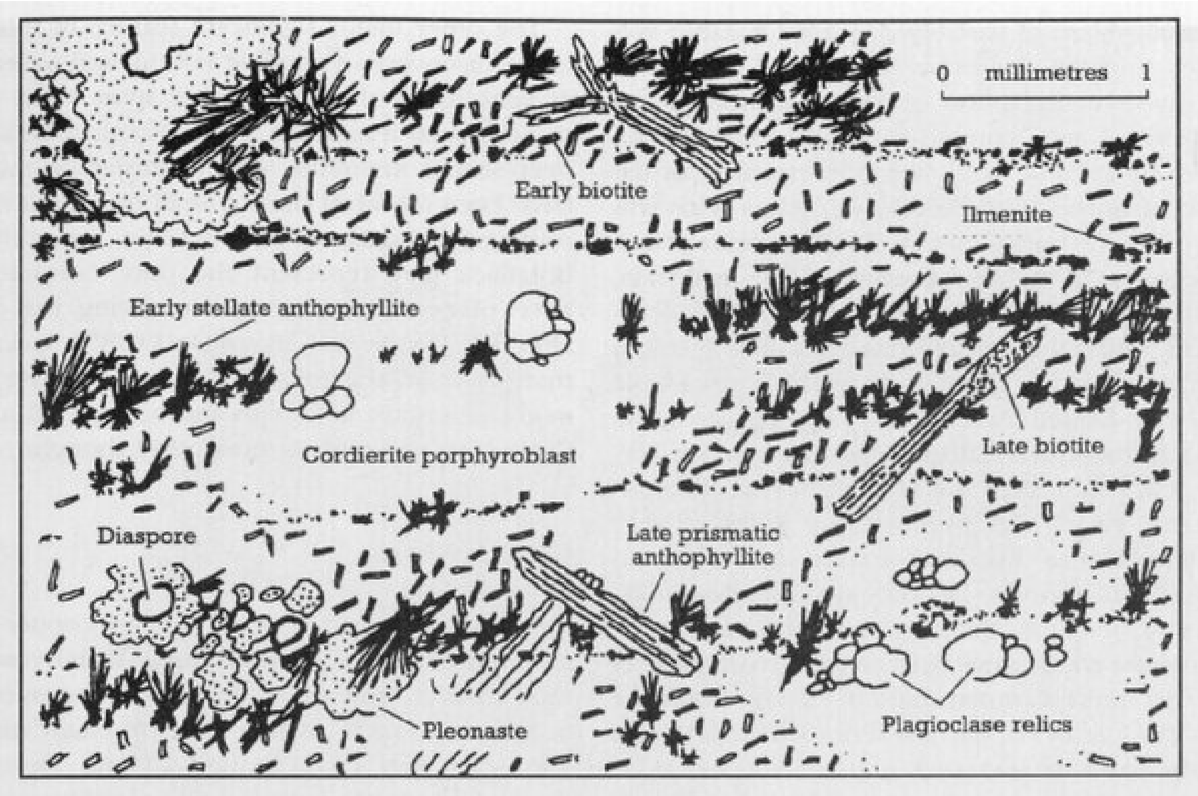

(Figure 4.20) Composite drawing of mineral relationships in the biotite—cordierite—anthophyllite assemblage, based on exotic hornfelses from the Zawn a Bal to Kenidjack area, Land's End aureole, Penwith Peninsula.

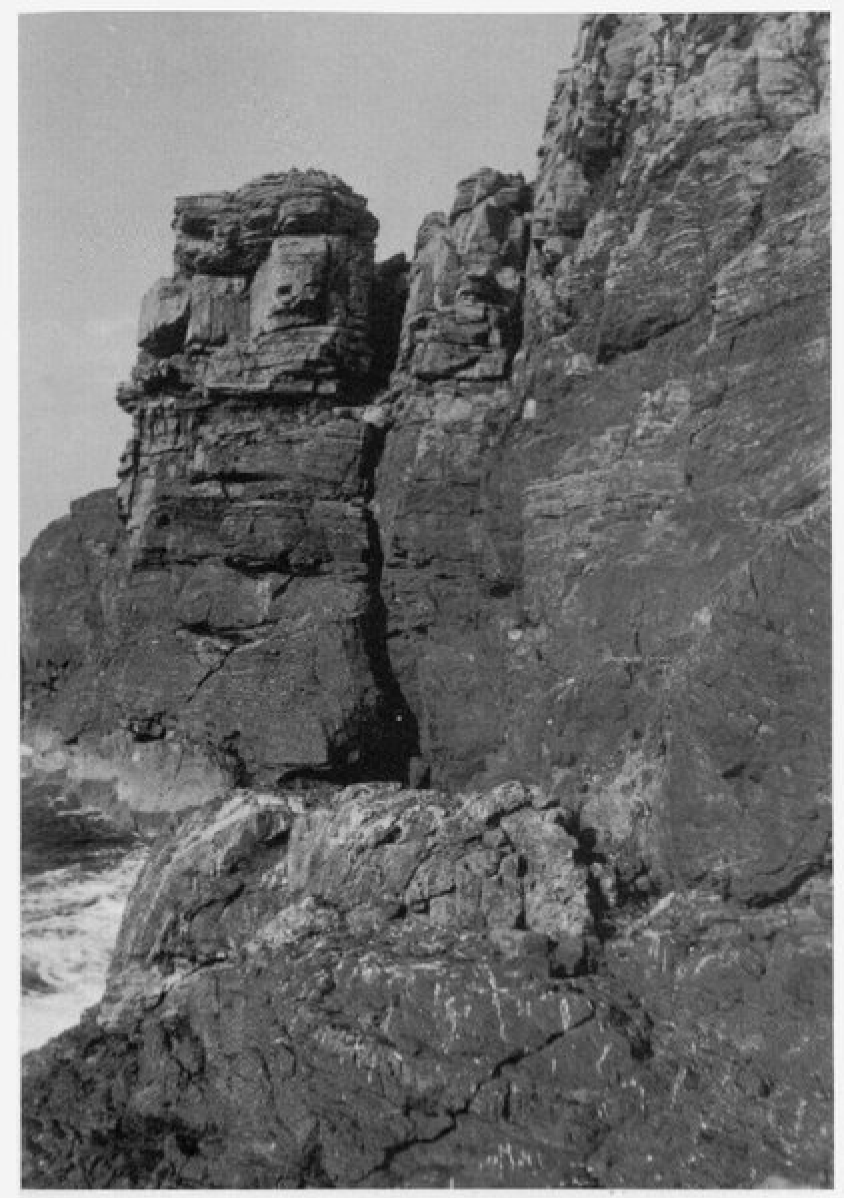

(Figure 4.21) Massive cliff section composed of various banded, amphibole-hearing, basic hornfelses of volcanic origin. In, the foreground is a small irregular raft of metasediment caught up during the emplacement of the basalts. Tater-du. Cornwall. (Photo: P.A. Floyd.)

(Figure 4.22) Typical, banded, basic hornfels of volcanic origin, composed of dark layers of hornblende and biotite, with light-coloured, segregation lenses of diopside. Tater-du, Cornwall. (Photo: P.A. Floyd.)

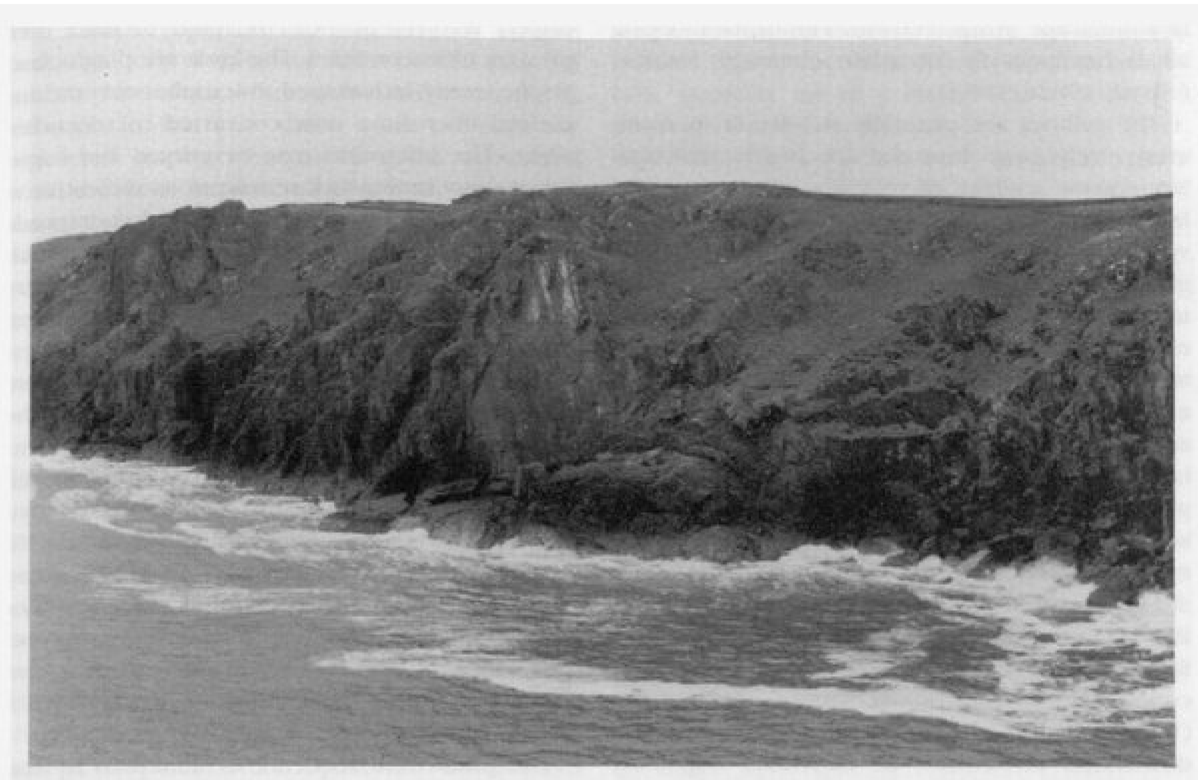

(Figure 4.23) View of Pentire Point cliffs showing Upper Devonian pillow-lava mounds. (Photo: P.A. Floyd.)

(Figure 4.24) Pillow-lava breccia formed by fragmentation on cooling soon after submarine extrusion. Pentire Point, Cornwall. (Photo: P.A. Floyd.)

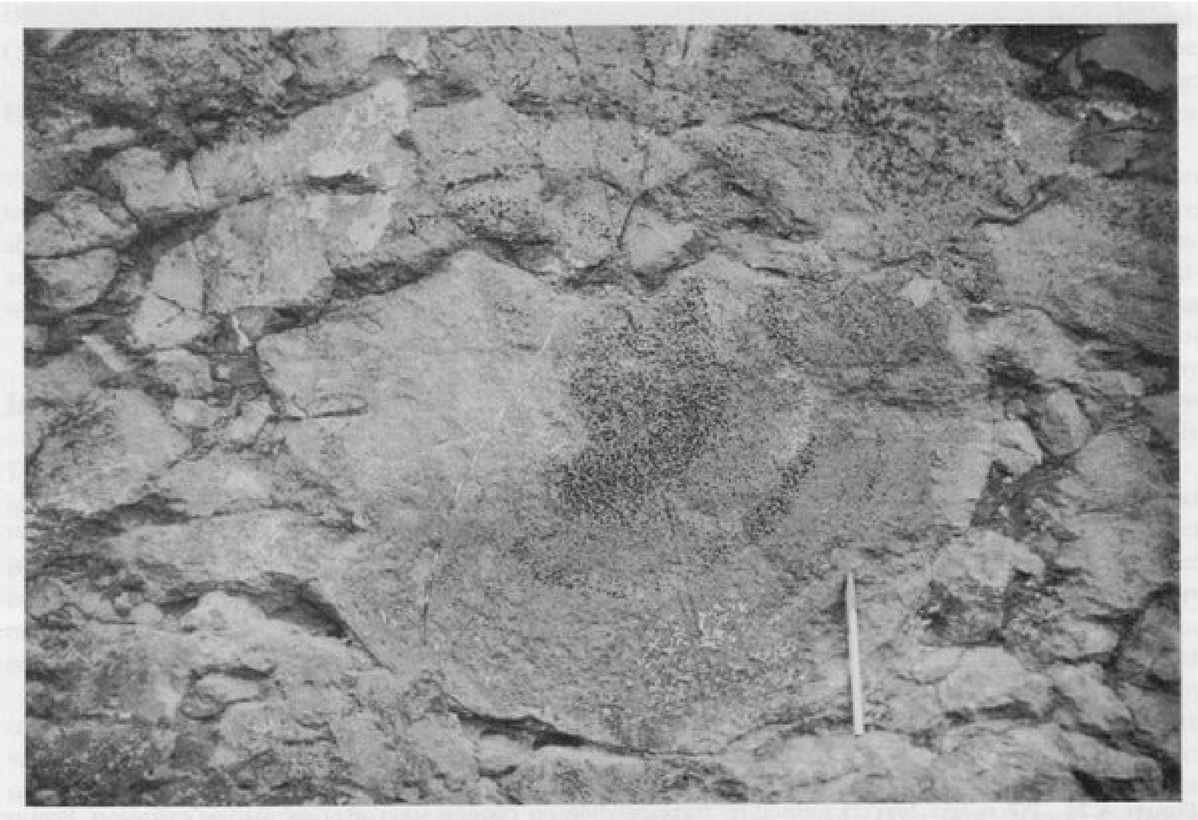

(Figure 4.25) In situ autobrecciation of a lava pillow. Pentire Point, Cornwall. (Photo: P.A. Floyd.)

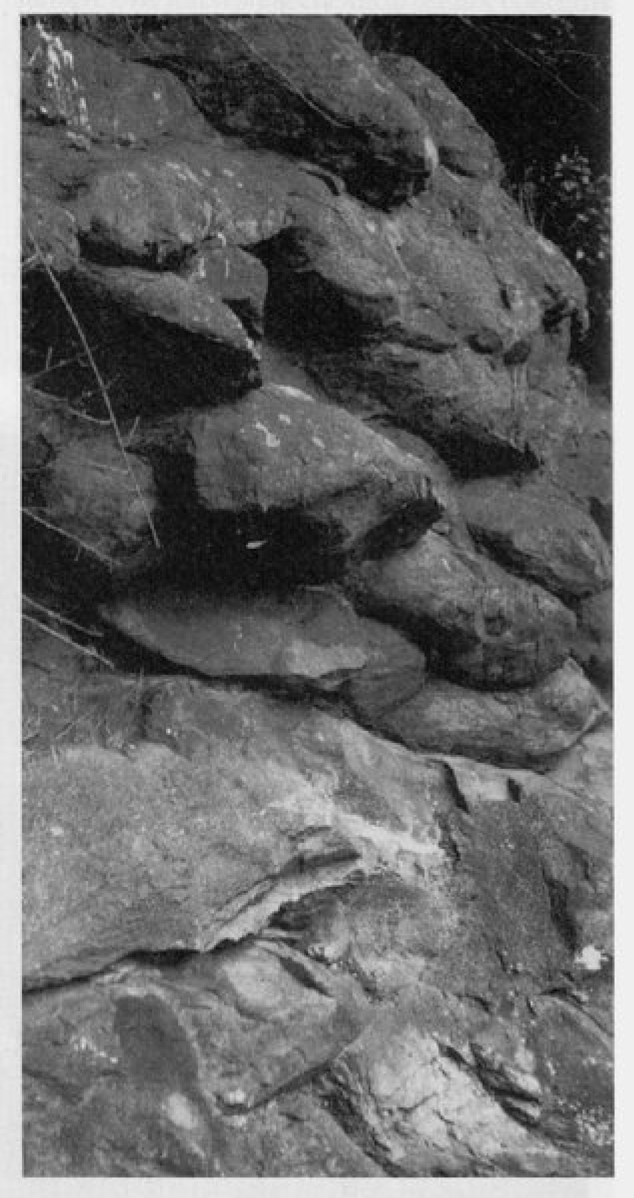

(Figure 4.26) Upper Devonian pillow lavas of alkali-basalt composition. Chipley Quarries, Devon. (Photo: PA. Floyd.)

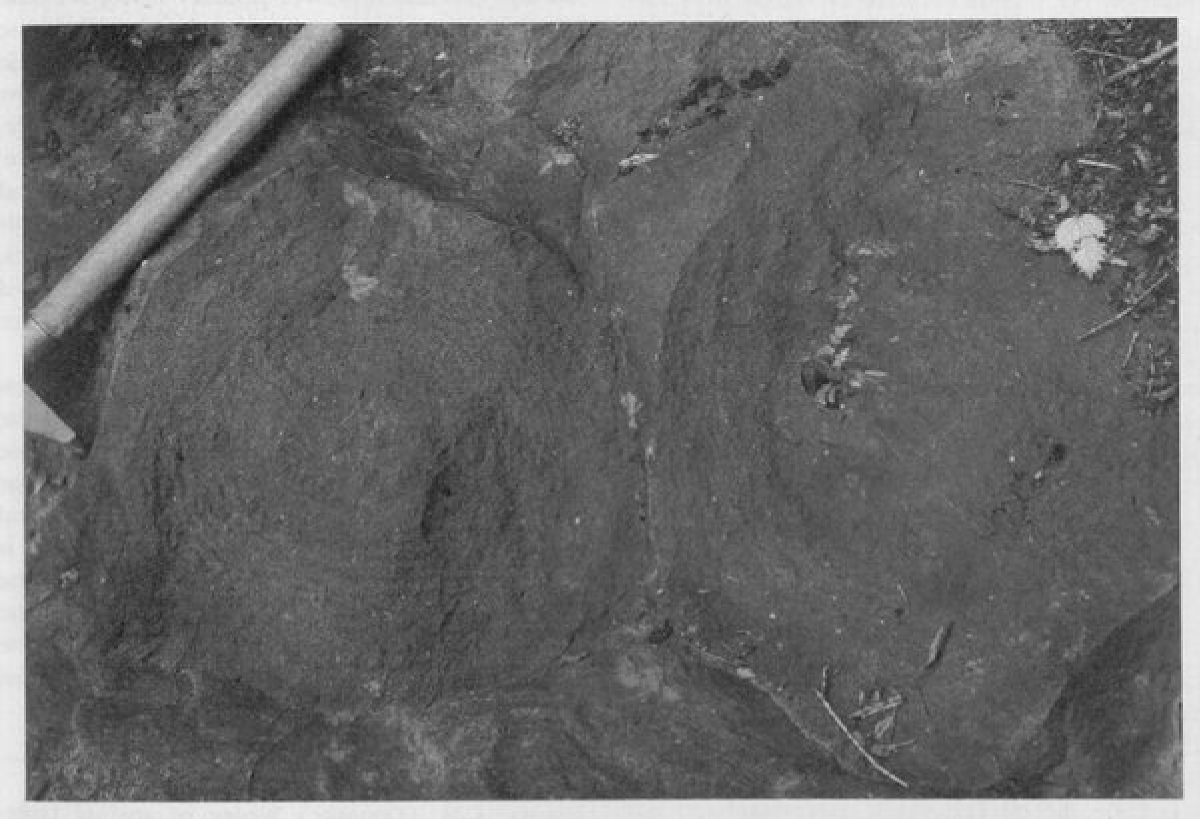

(Figure 4.27) Cross-section through two pillows showing the high degree of vesicularity and its concentric disposition. Chipley Quarries, Devon. (Photo: P.A. Floyd.)

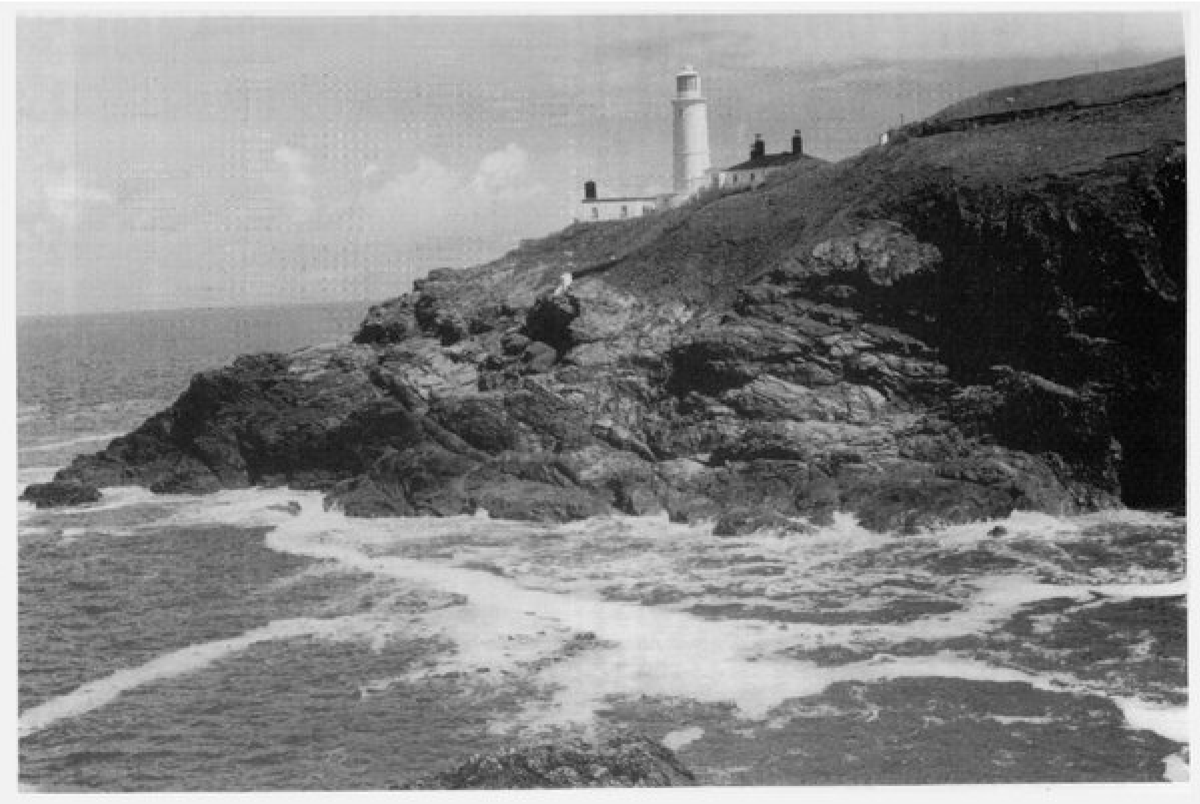

(Figure 4.28) (Opposite) Wedge of argillite (pale-coloured cliffs) resting on dark intrusive dolerite near sea-level. Trevose Head, Cornwall. (Photo: P.A. Floyd.)

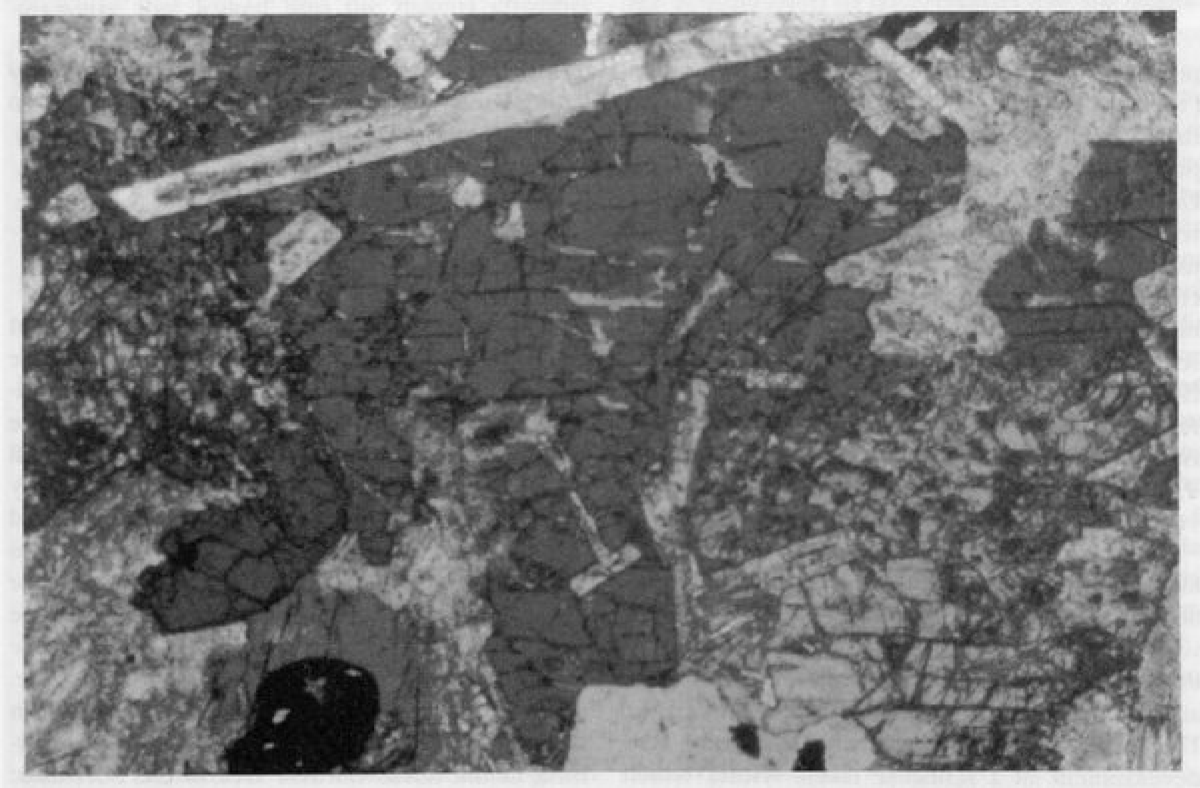

(Figure 4.29) Photomicrograph of a hydrous dolerite showing large irregular crystal of dark, primary, kaersutitic amphibole replacing colourless clinopyroxene (bottom right); long needle-like apatite crystal traverses the amphibole unaltered (top). Trevone Bay, Cornwall. (Photo: P.A. Floyd.)

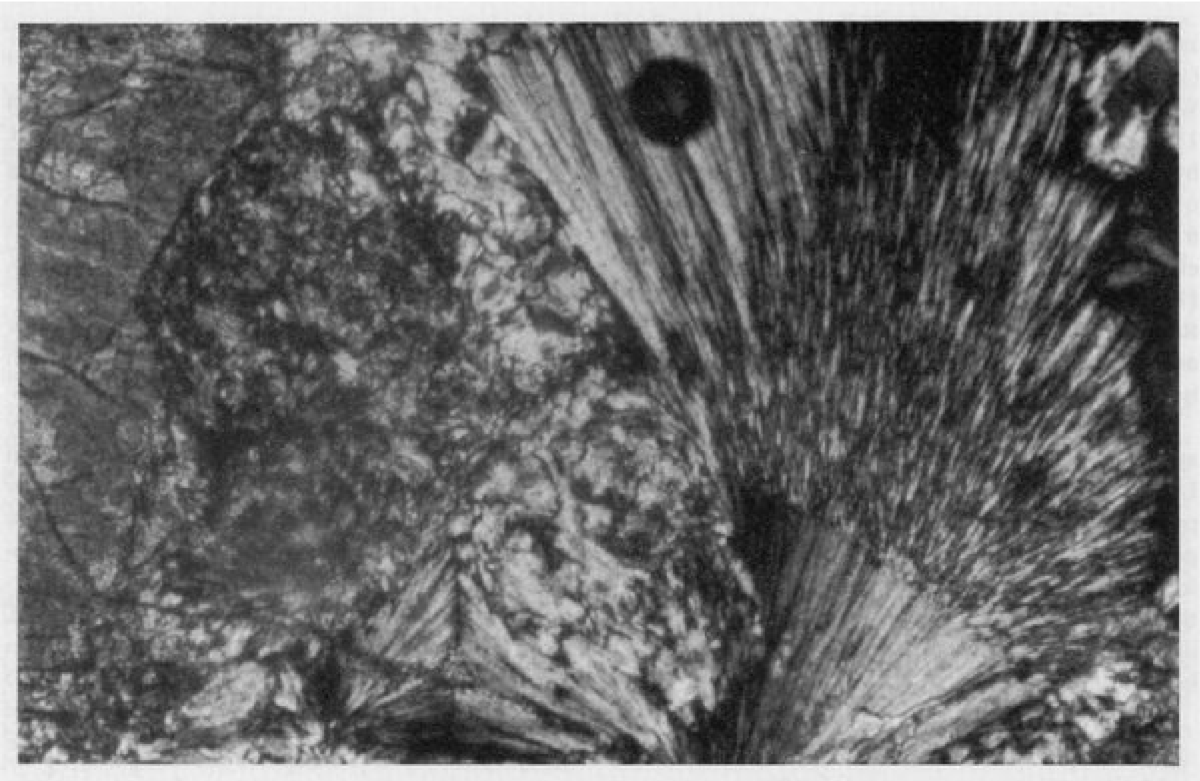

(Figure 4.30) Photomicrograph of a hydrous dolerite showing the fan-like growth of secondary Al-rich pumpellyite that replaced the original plagioclase. Trevone Bay, Cornwall. (Photo: P.A. Floyd.)

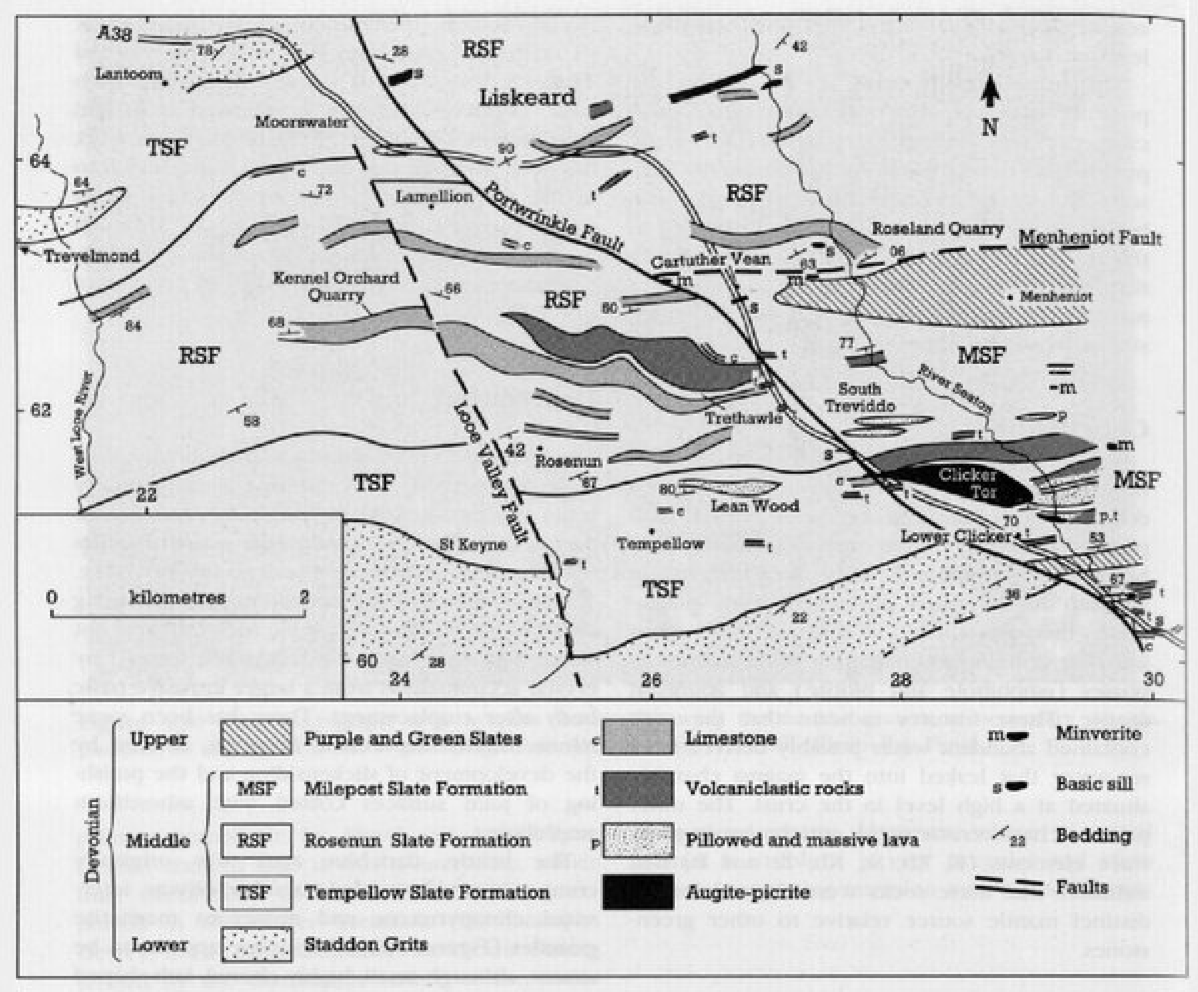

(Figure 4.31) Geological map of the area to the south of Liskeard showing the location of the Clicker Tor ultramafic body (after Burton and Tanner, 1986).

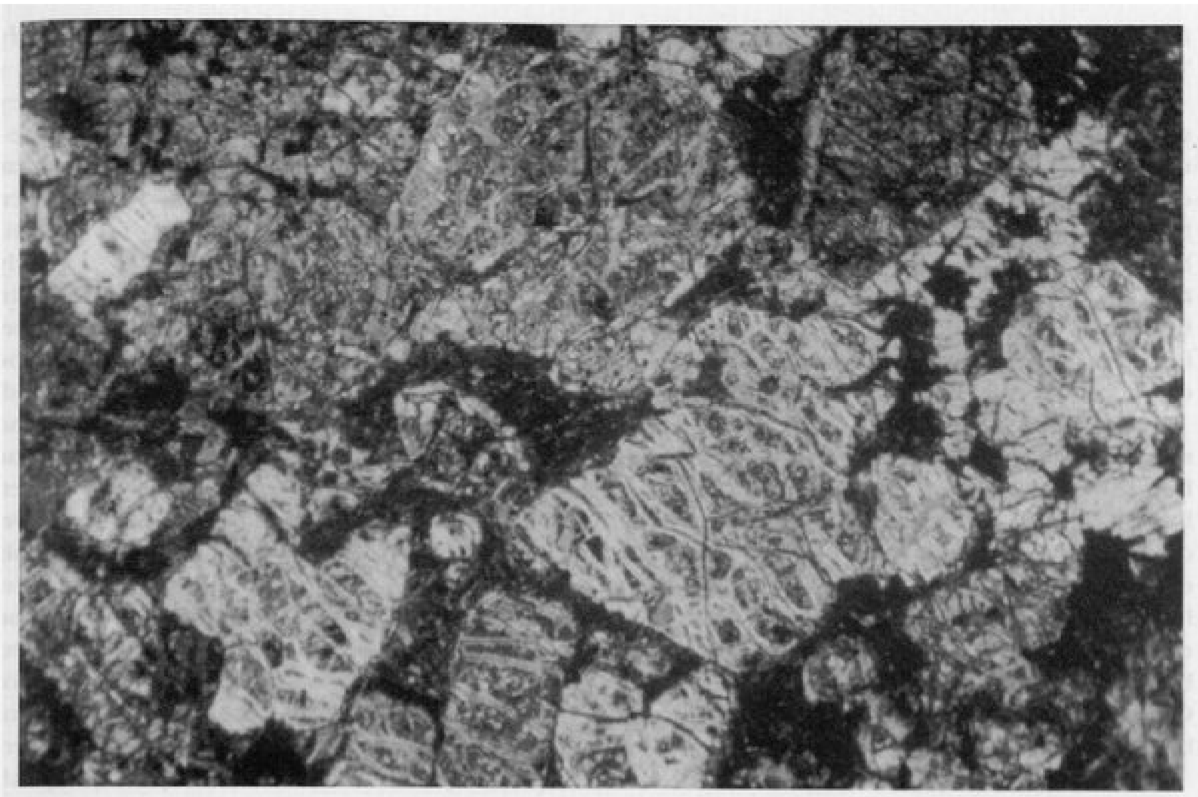

(Figure 4.32) Photomicrograph of partly altered olivine crystals (with veins) and intercumulus pyroxene in the ultramafic body at Clicker Tor, Cornwall. (Photo: P.A. Floyd.)

(Figure 4.33) Weathering of the Polyphant ultramafic body (hydrous picrite) showing a core boulder of serpentinite within a highly oxidized, degraded matrix. Polyphant, Cornwall. (Photo: P.A. Floyd.)

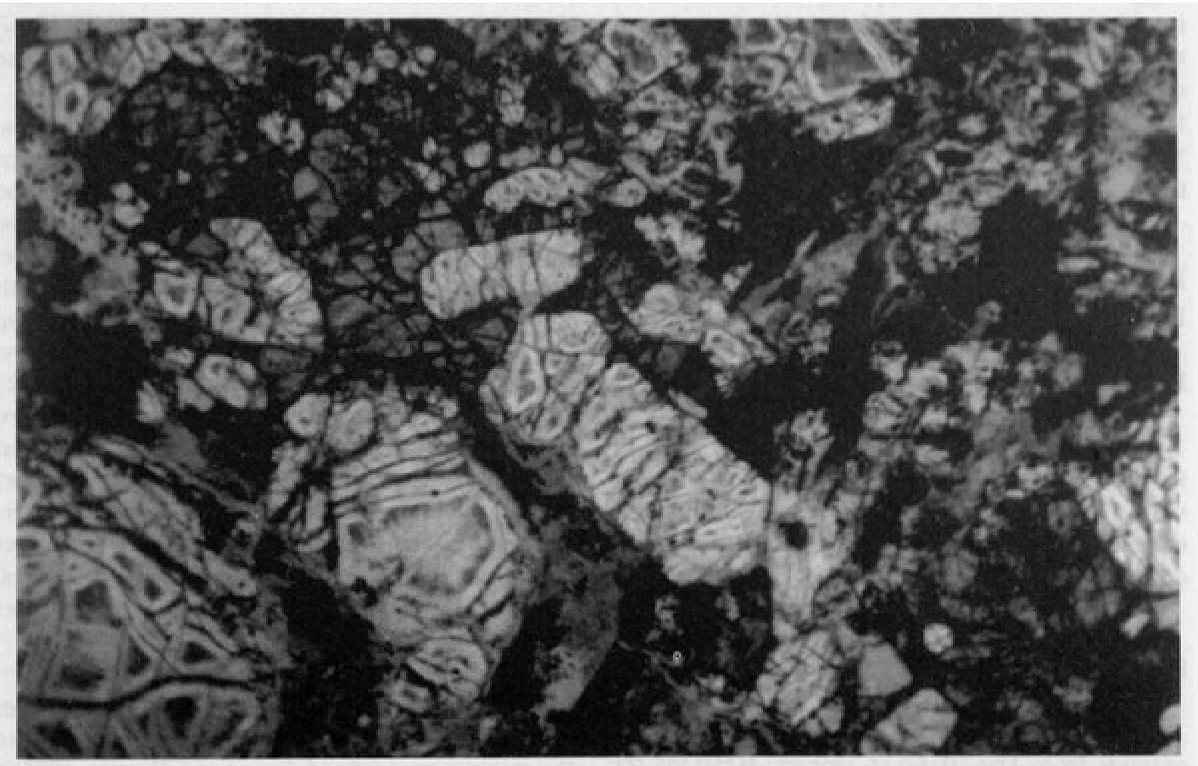

(Figure 4.34) Photomicrograph of the Polyphant hydrous picrite, showing serpentinized olivine crystals, pyroxene and dark kaersutitic amphibole (top left). Polyphant, Cornwall. (Photo: P.A. Floyd.)

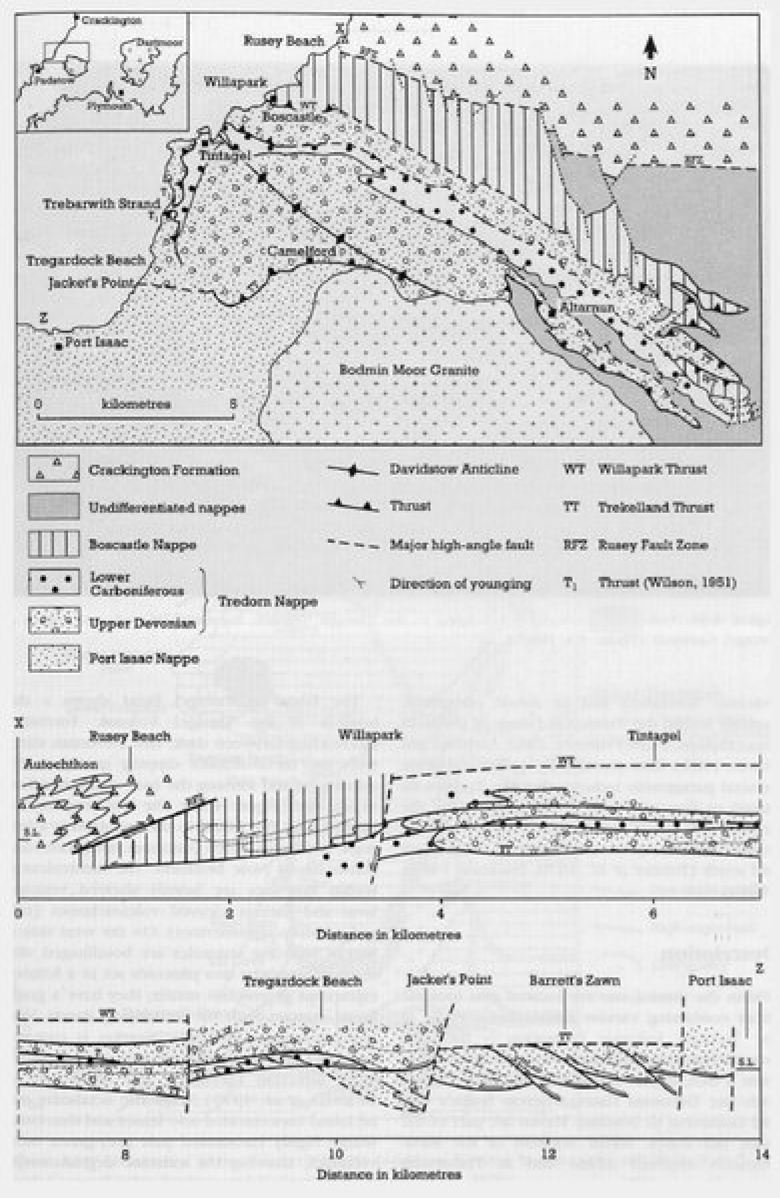

(Figure 4.35) (Opposite) Map and section of north Cornwall, showing the distribution and relationship of the major nappes (after Selwood and Thomas, 1986a). The Tintagel Volcanic Formation occurs in the Tredorn Nappe.

(Figure 4.36) Contorted greenschists belonging to the Tintagel Volcanic Formation at Gullastem, north of Tintagel, Cornwall. (Photo: P.A. Floyd.)

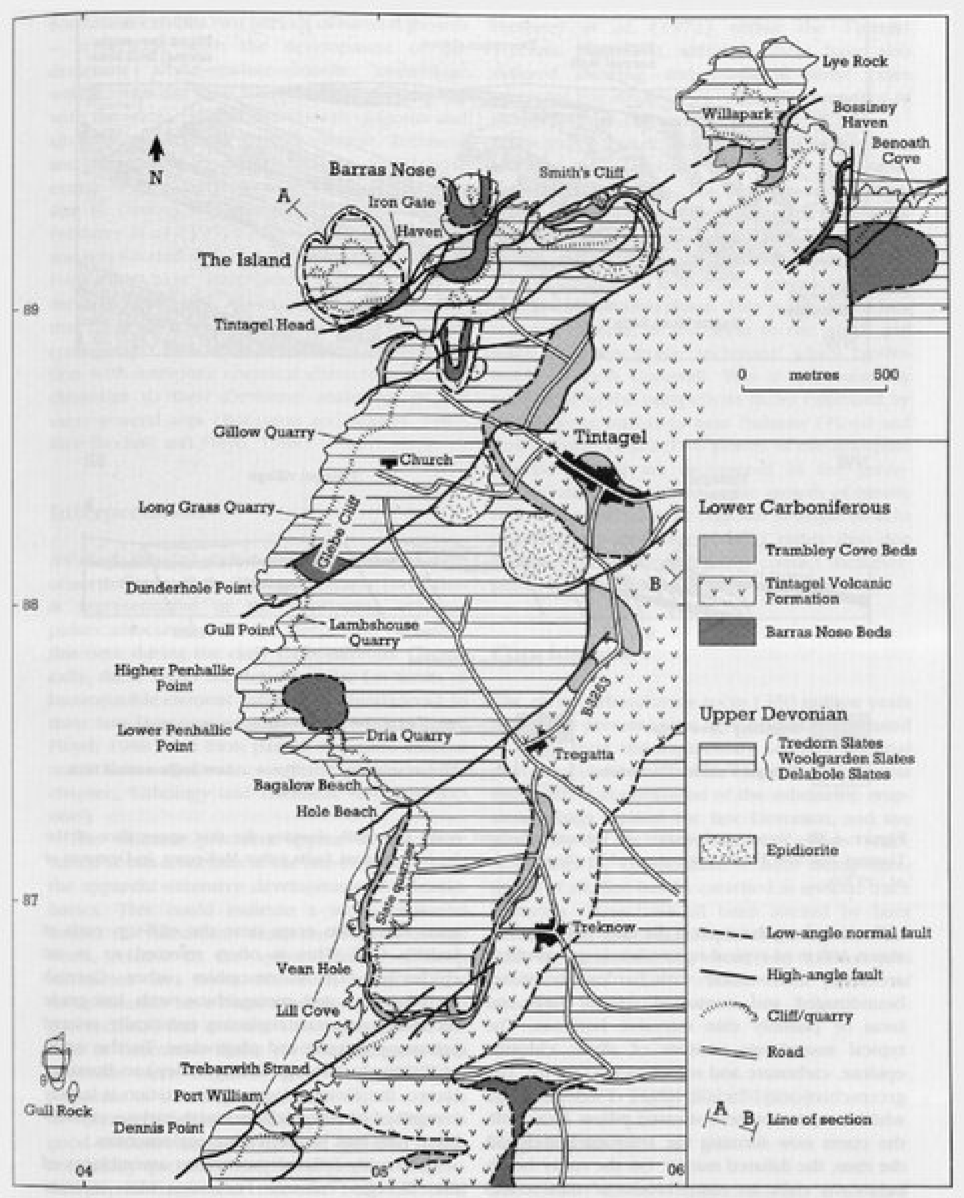

(Figure 4.37) Distribution of the Tintagel Volcanic Formation between Bossiney Bay and Trebarwith Strand, north Cornwall (after Freshney and McKeown, in Dearman et al., 1970).

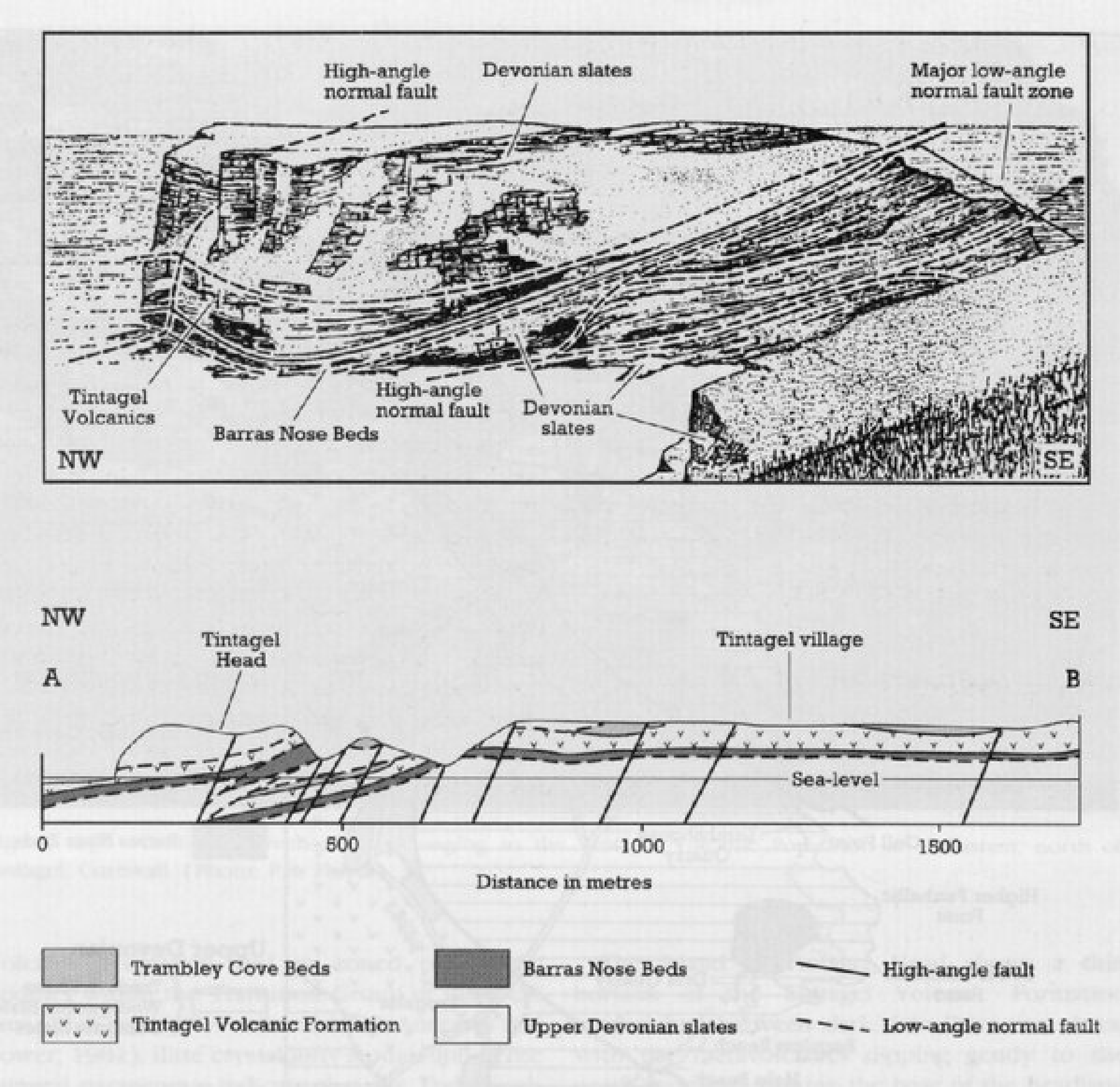

(Figure 4.38) Sketch and section of Tintagel headland, north Cornwall, showing the thin upper slice of the Tintagel Volcanic Formation truncated by thrusts and cut by later normal faults (after McKeown. in Dearman et al., 1970).

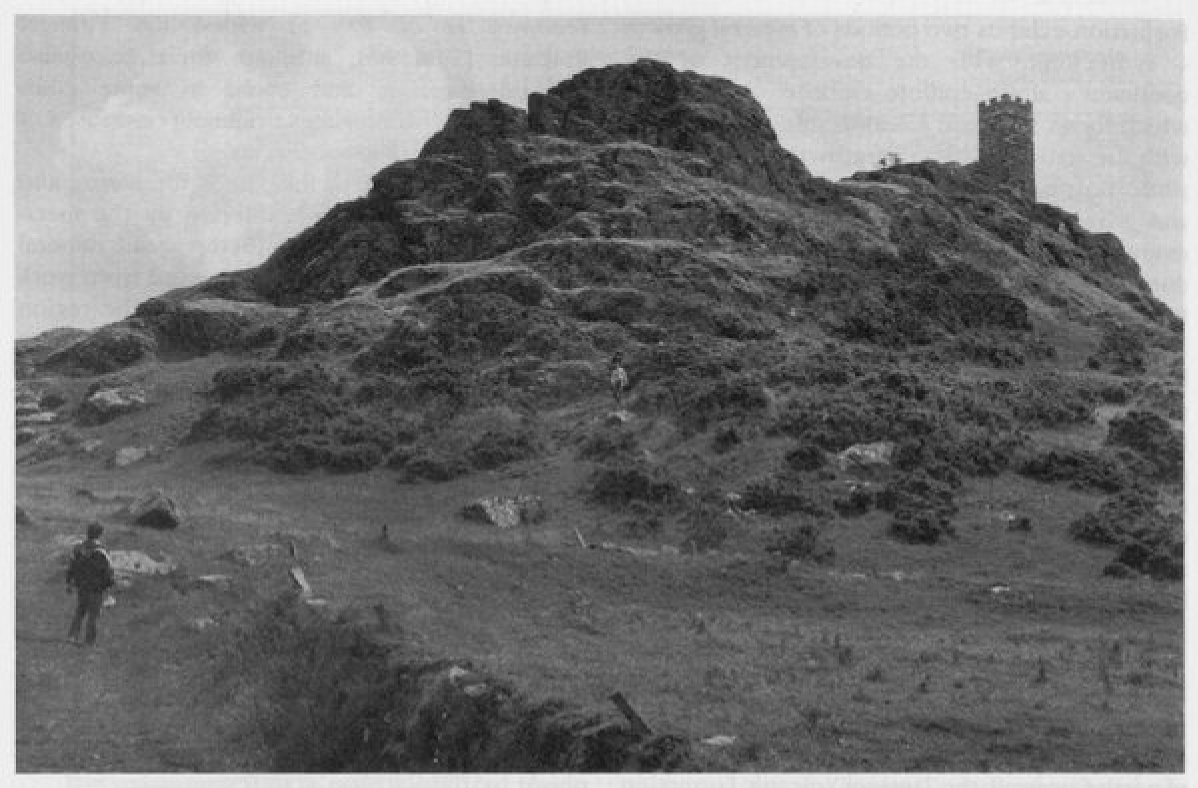

(Figure 4.39) The conical knoll of Brent Tor is composed of Lower Carboniferous basaltic pillow lavas and hyaloclastites which formed a near-emergent seamount with a reworked volcaniclastic apron. Brent Tor, Devon. (Photo: P.A. Floyd.)

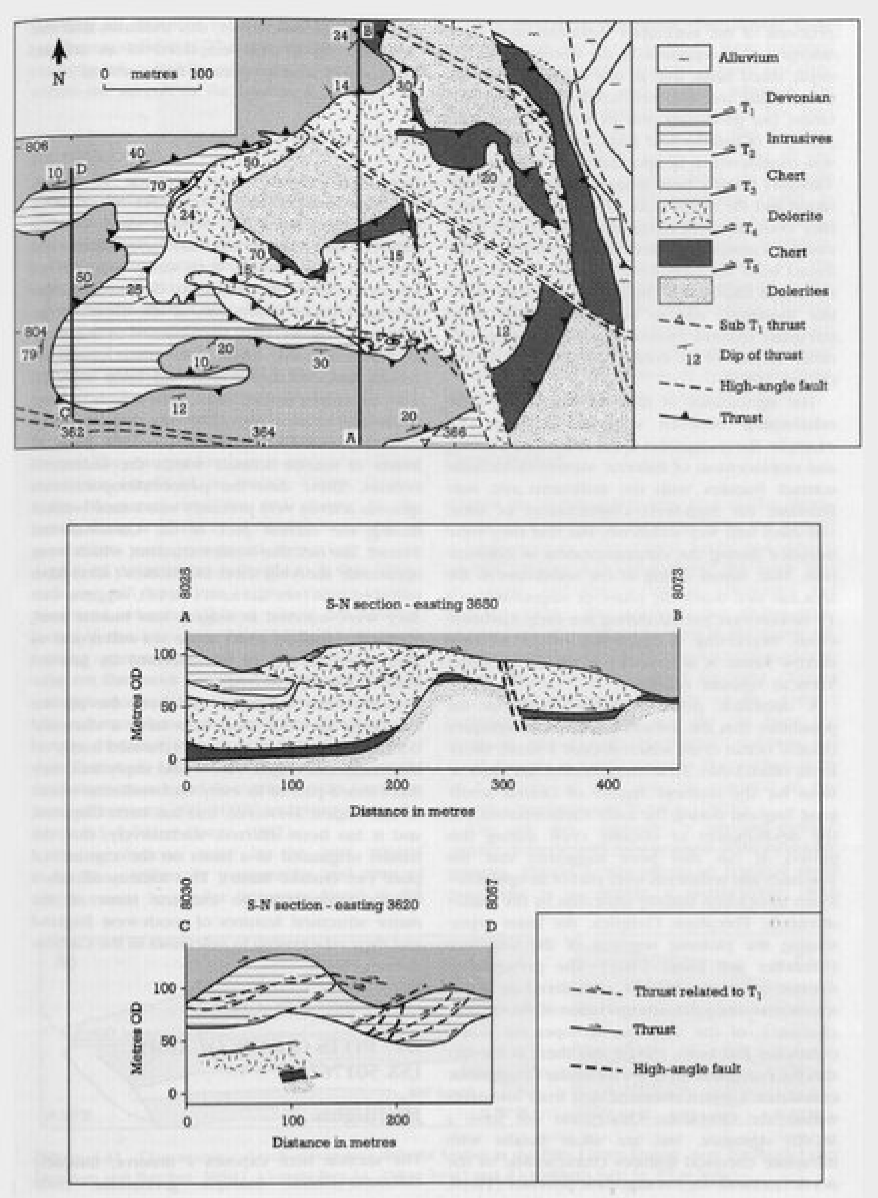

(Figure 4.40) Map and cross-sections of Greystone Quarry, showing the development of undulating thrust surfaces cutting dolerite and the transportation of Upper Devonian sediments over Lower Carboniferous volcanics by the major Greystone Thrust (after Turner, 1982).

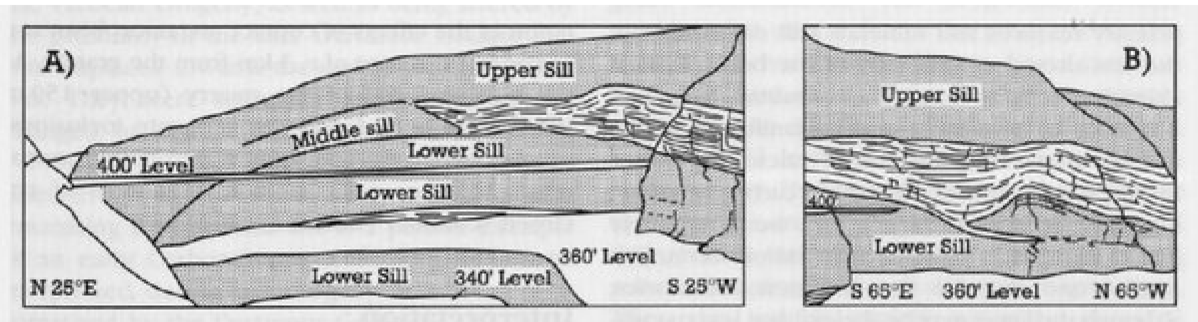

(Figure 4.41) Diagrammatic sketch of intrusive dolerite bodies in the Pitts Cleave Quarry, near Tavistock (after Dearman and Butcher, 1959). A) main face (c. 230 m long) and B) southern face (c. 85 m long).

(Figure 4.42) Well-developed columnar jointing in dolerite. Pius Cleave Quarry, Tavistock, Devon. (Photo: P.A. Floyd.)

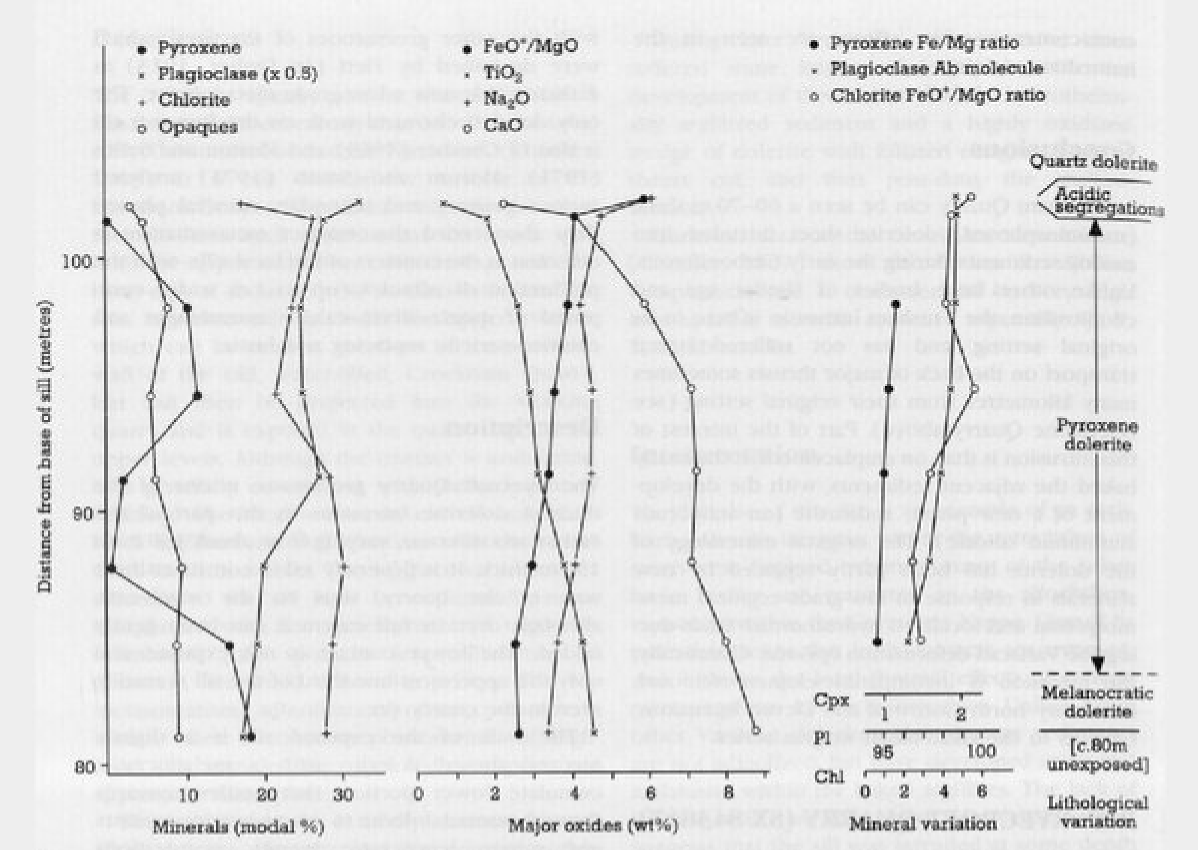

(Figure 4.43) Modal and chemical variation in thu• upper part of the Ryecroft dolerite sill, Teign Valley, east Devon (data from Morton and Smith, 1971).

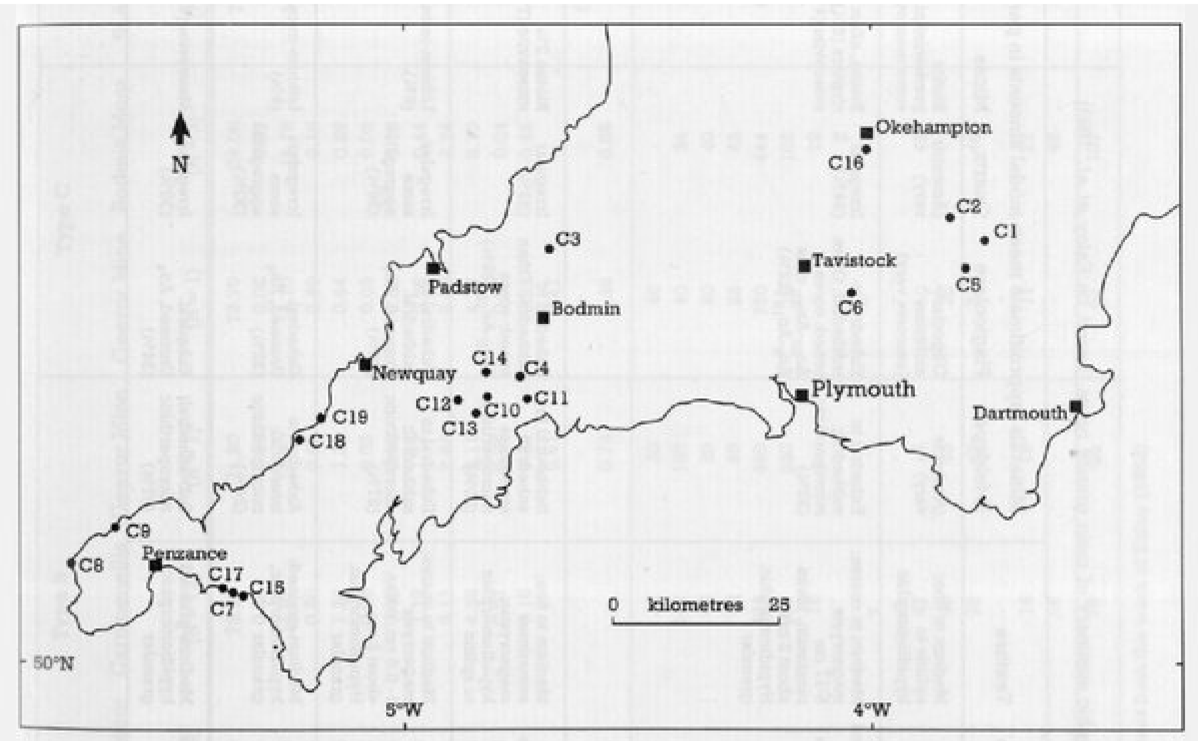

(Figure 5.1) Outline map of south-west England showing the location of Group C sites.

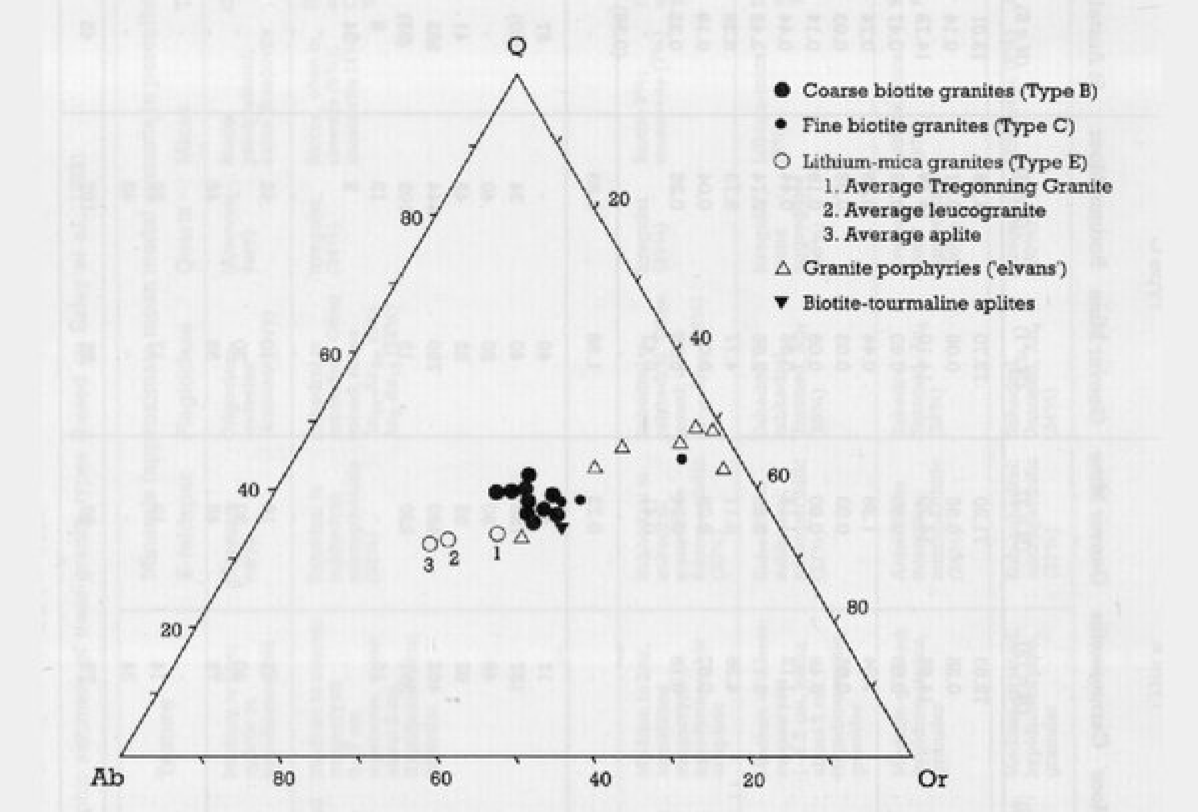

(Figure 5.2) Normative quartz-albite-orthoclase (Q-Ab-Or) diagram (after Exley and Stone, 1982, Figure 23.2).

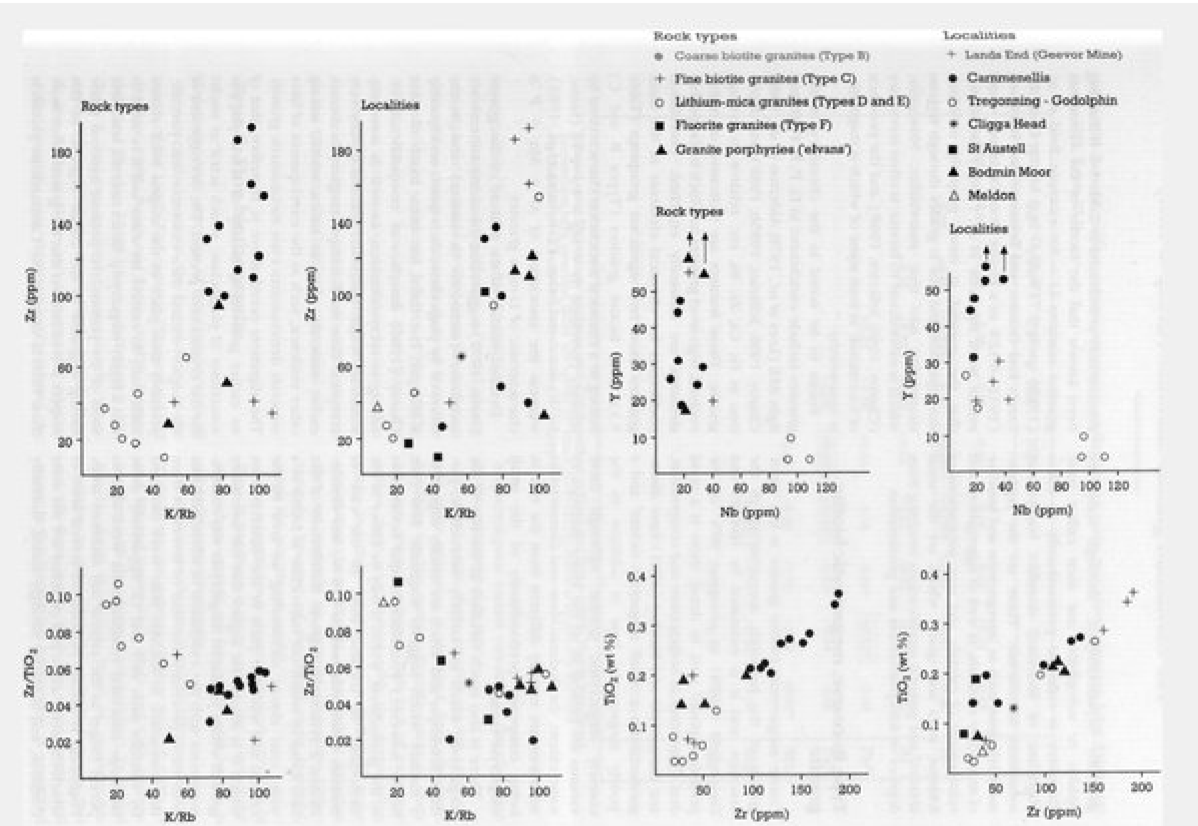

(Figure 5.3) Variation diagrams for Zr—K/Rb, Zr/TiO_2—K/Rb, Nb—Y and Zr—TiO_2 in south-west England granite types and different plutons (after Exley et al., 1983).

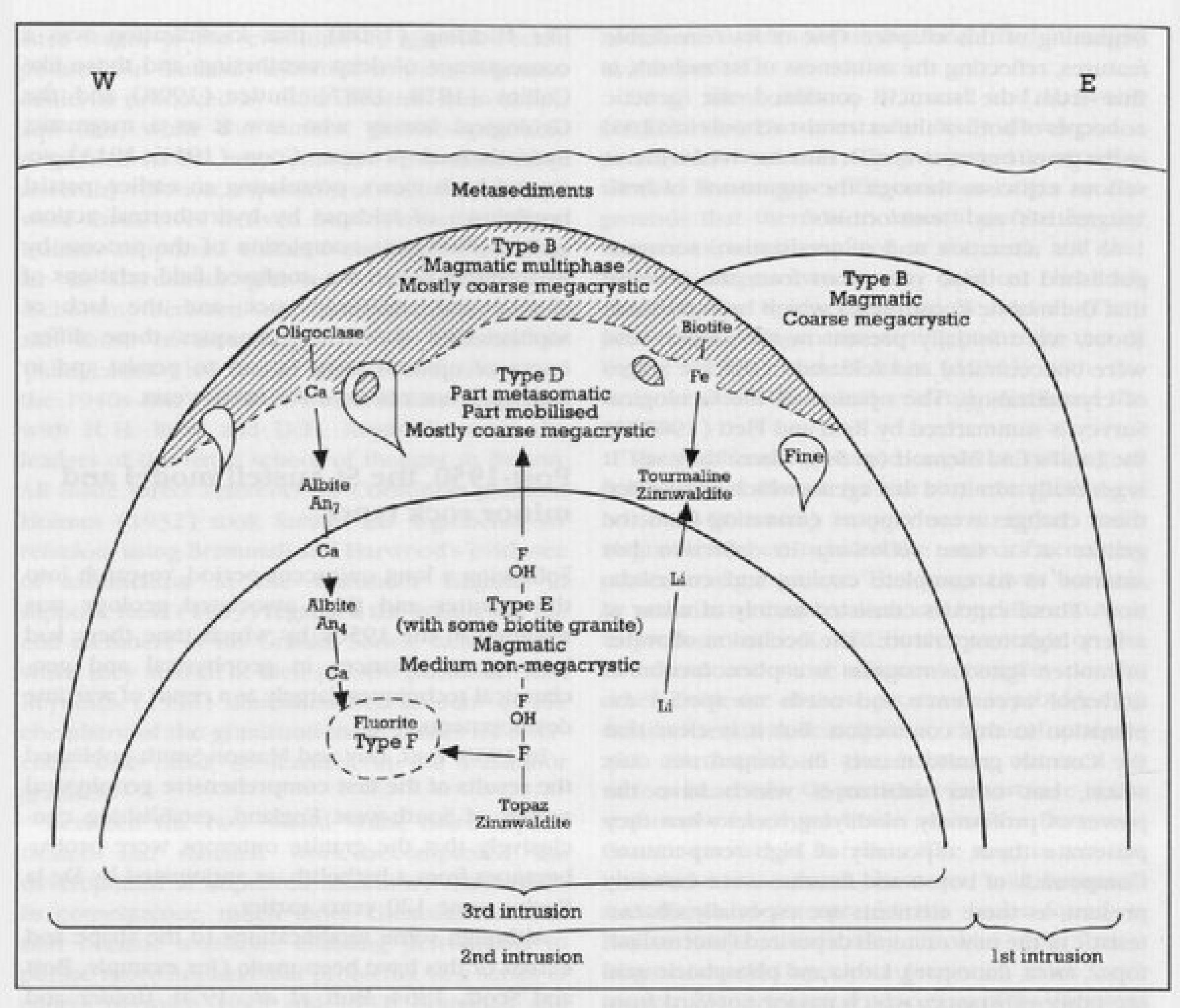

(Figure 5.4) The St Austell model. Diagram showing the first intrusion of Type-B granite (Table 5.1) cut by multiphase second intrusion of biotite granite, with metasomatic aureole of Type D caused by intrusion of Type E.

Type	Description	Texture	Minerals (approximate mean modal amounts in parentheses): K-feldspar	Plagioclase	Quartz	Micas	Tourmaline	Other	Other names in literature
A	Basic microgranite	Medium to fine; ophitic to hypidiomorphic	(Amounts vary)	Oligoclase-andesine (amounts vary)	(Amounts vary)	Biotite predominant; some muscovite	Often present	Hornblende, apatite, zircon, ore, garnet	Basic segregations (Reid et al., 1912); Basic inclusions (Brammall and Harwood, 1923, 1926)
B	Coarse-grained megacrystic biotite granite	Medium to coarse; megacrysts 5-17 cm maximum, mean about 2 cm. Hypidiomorphic, granular	Euhedral to subhedral; microperthitic (32%)	Euhedral to subhedral. Often zoned: cores An_{35}-An_{30}, rims An_{8}-An_{15} (22%)	Irregular (34%)	Biotite, often in clusters (6%); muscovite (4%)	Euhedral to anhedral. Often zoned. 'Primary' (1%)	Zircon, ore, apatite, andalusite, etc. (total, 1%)	Includes: Giant or tor granite (Brammall, 1926; Brammall and Harwood, 1923, 1932) = big-feldspar granite (Edmonds et al., 1968), coarse megacrystic granite (Hawkes and Dangerfield, 1978). Also blue or quarry granite (Brammall, 1926; Brammall and Harwood, 1923, 1932) = poorly megacrystic granite (Edmonds et al., 1968), coarse megacrystic granite (mesocrystic type) (Hawkes and Dangerfield, 1978), coarse megacrystic granite (small megacryst variant) (Dangerfield and Hawkes, 1981). Also medium-grained granite (Hawkes and Dangerfield, 1978), medium granites with few megacrysts and megacrysts very rare (Dangerfield and Hawkes, 1981). Biotite-muscovite granite (Richardson, 1923; Exley, 1959). Biotite granite, equigranular biotite granite, and globular quartz granite (Hill and Manning, 1987).
C	Fine-grained biotite granite	Medium to fine, sometimes megacrystic; hypidiomorphic to aplitic	Subhedral to anhedral; sometimes microperthitic (30%)	Euhedral to subhedral. Often zoned: cores An_{10}-An_{15} (26%)	Irregular (33%)	Biotite 3%; muscovite (7%)	Euhedral to anhedral. 'Primary' (1%)	Ore, andalusite, fluorite (total, <1%)	Fine granite, megacryst-rich and megacryst-poor types (Hawkes and Dangerfield, 1978; Dangerfield and Hawkes, 1981)
D	Megacrystic lithium-mica granite	Medium to coarse; megacrysts 1-8.5 cm, mean about 2 cm. Hypidiomorphic, granular	Euhedral to subhedral; microperthitic (27%)	Euhedral to subhedral. Unzoned, An_7 (26%)	Irregular; some aggregates (36%)	Lithium-mica (6%)	Euhedral to anhedral 'Primary' (4%)	Fluorite, ore, apatite, topaz (total, 0.5%)	Lithionite granite (Richardson, 1923). Early lithionite granite (Exley, 1959). Porphyritic lithionite granite (Exley and Stone, 1964). Megacrystic lithium-mica granite (Exley and Stone, 1982)
E	Equigranular lithium-mica granite	Medium-grained; hypidiomorphic, granular	Anhedral to interstitial; microperthitic (24%)	Euhedral. Unzoned, An_4 (32%)	Irregular; some aggregates (30%)	Lithium-mica (9%)	Euhedral to anhedral (1%)	Fluorite, apatite (total, 2%); topaz (3%)	Late lithionite granite (Exley, 1959). Non-porphyritic lithionite granite (Exley and Stone, 1964). Medium-grained, non-megacrystic lithium-mica granite (Hawkes and Dangerfield, 1978). Equigranular lithium-mica granite (Exley and Stone, 1982). Topaz granite (Hill and Manning, 1987)
F	Fluorite granite	Medium-grained; hypidiomorphic, granular	Sub-anhedral; microperthitic (27%)	Euhedral. Unzoned, An_4 (34%)	Irregular (30%)	Muscovite (6%)	Absent	Fluorite (2%), topaz (1%), apatite (<1%)	Gilbertite granite (Richardson, 1923)

(Table 5.1) Petrographic summary of main granite types (based on Exley et al., 1983)

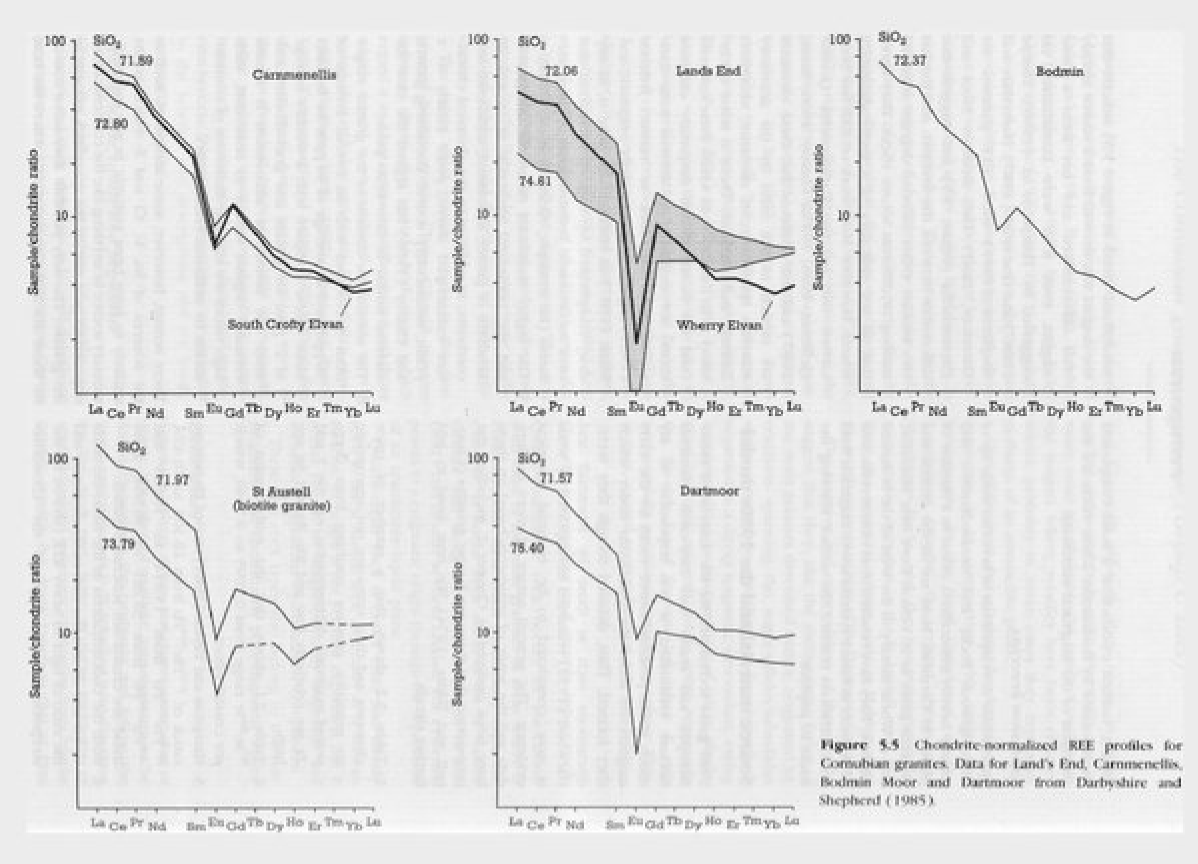

(Figure 5.5) Chondrite-normalized REE profiles for Corinthian granites. Data for Land's End, Carnmenellis, Bodmin Moor and Dartmoor from Darbyshire and Shepherd (1985).

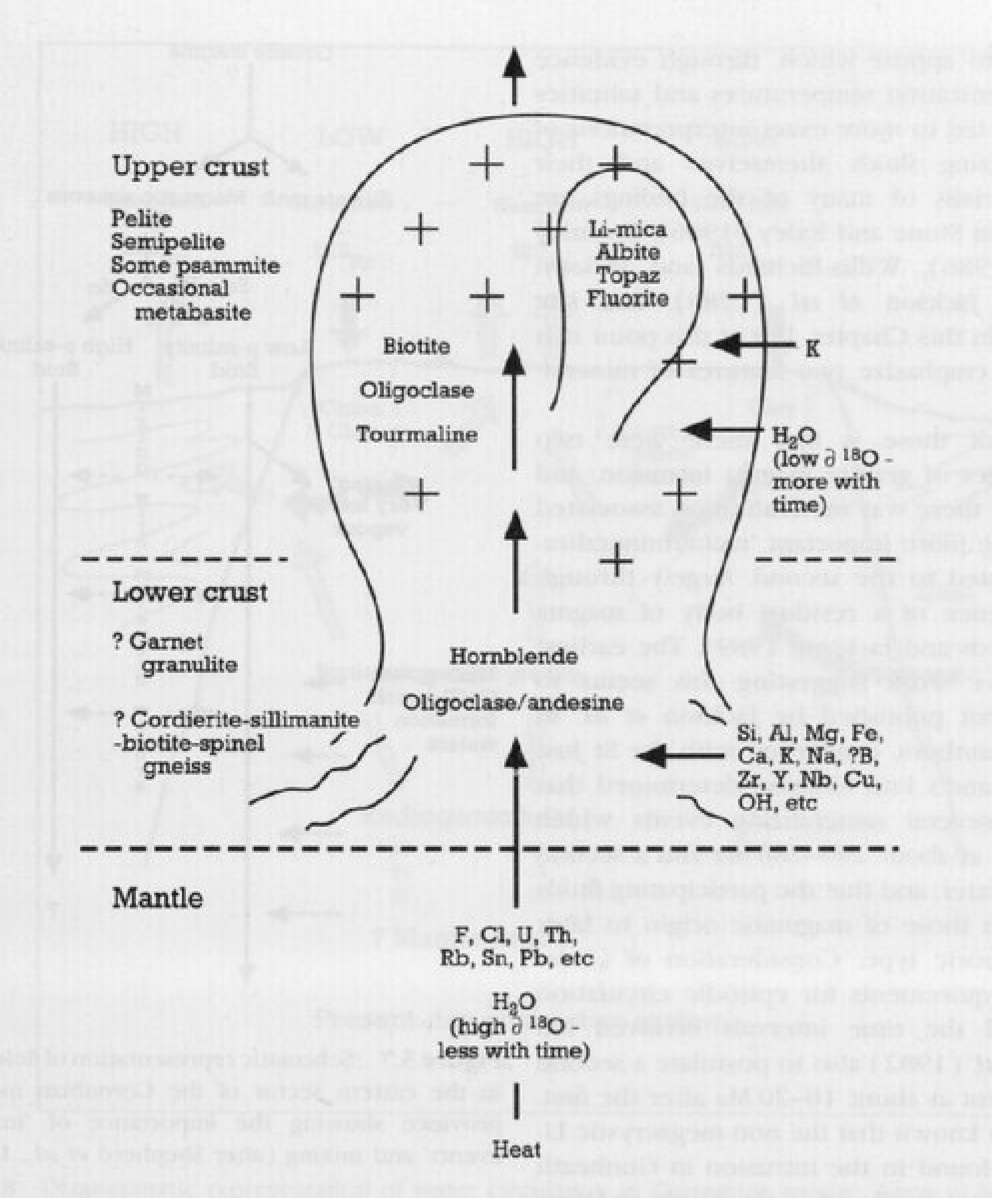

(Figure 5.6) The 1980s model. Granitic magma generated in the lower crust (but with mantle components) and evolving both by assimilating upper-crustal constituents and differentiating Li-mica granite magma. Magma becomes increasingly hydrated by drawing in increasing quantities of meteoric water during ascent.

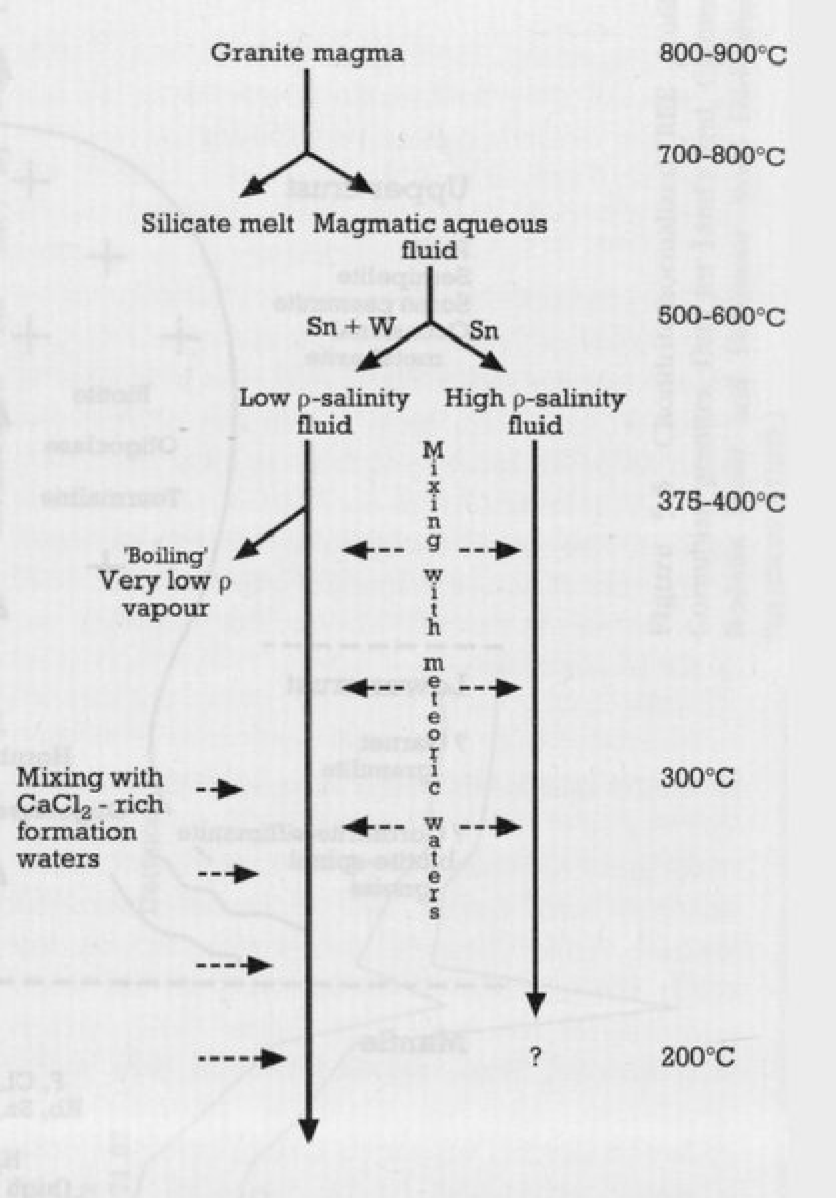

(Figure 5.7) Schematic representation of fluid evolution in the eastern sector of the Cornubian metallogenic province showing the importance of 'immiscibility events' and mixing (after Shepherd et al., 1985).

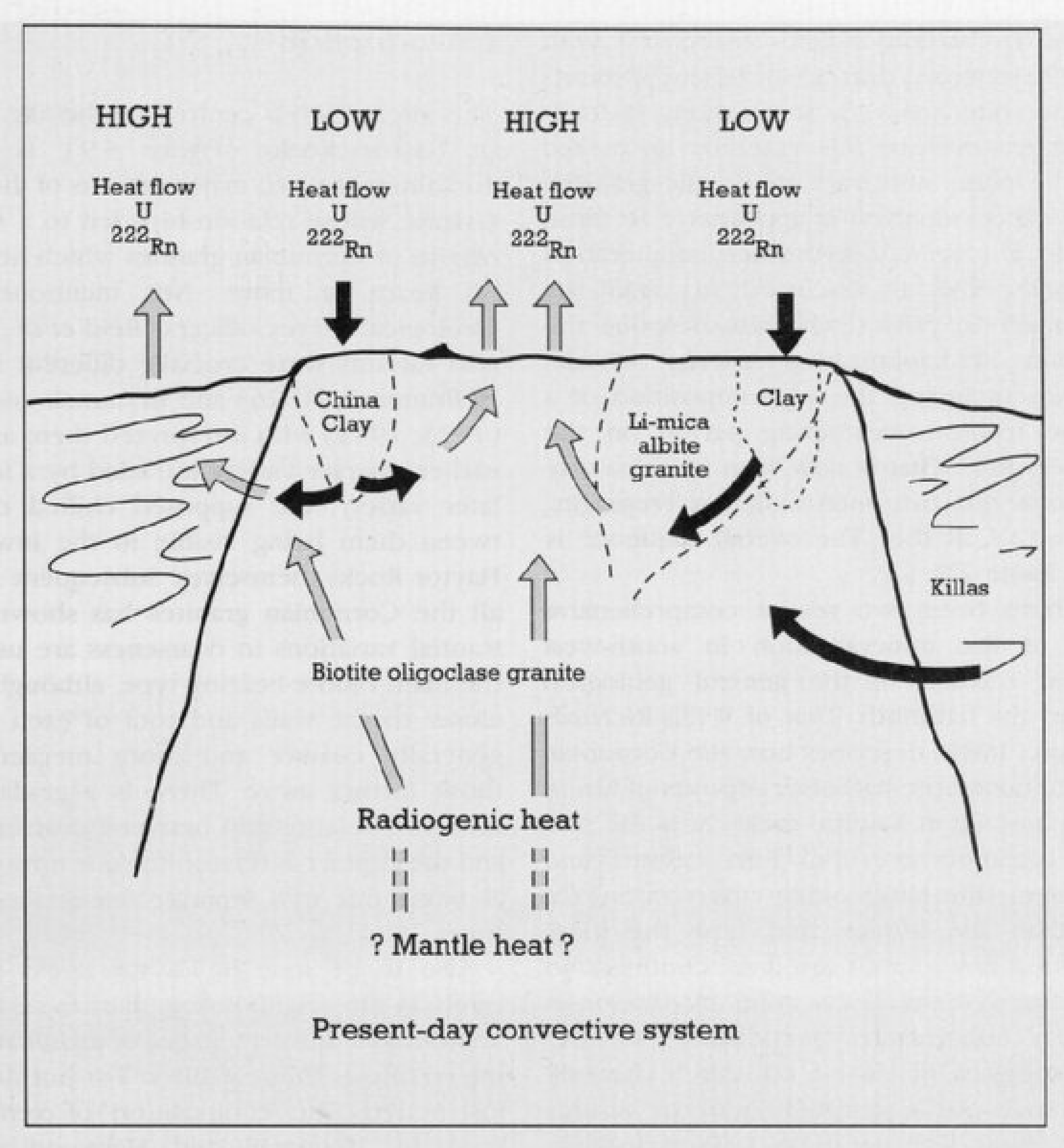

(Figure 5.8) Diagrammatic representation of water circulation in Cornubian granite. Areas of low heat flow, U and ^{222}Rn concentration are associated with china clay and indicate draw-down; areas of high heat flow, U and ^{222}R11 concentration indicate uprise (based on Durrance et al., 1982).

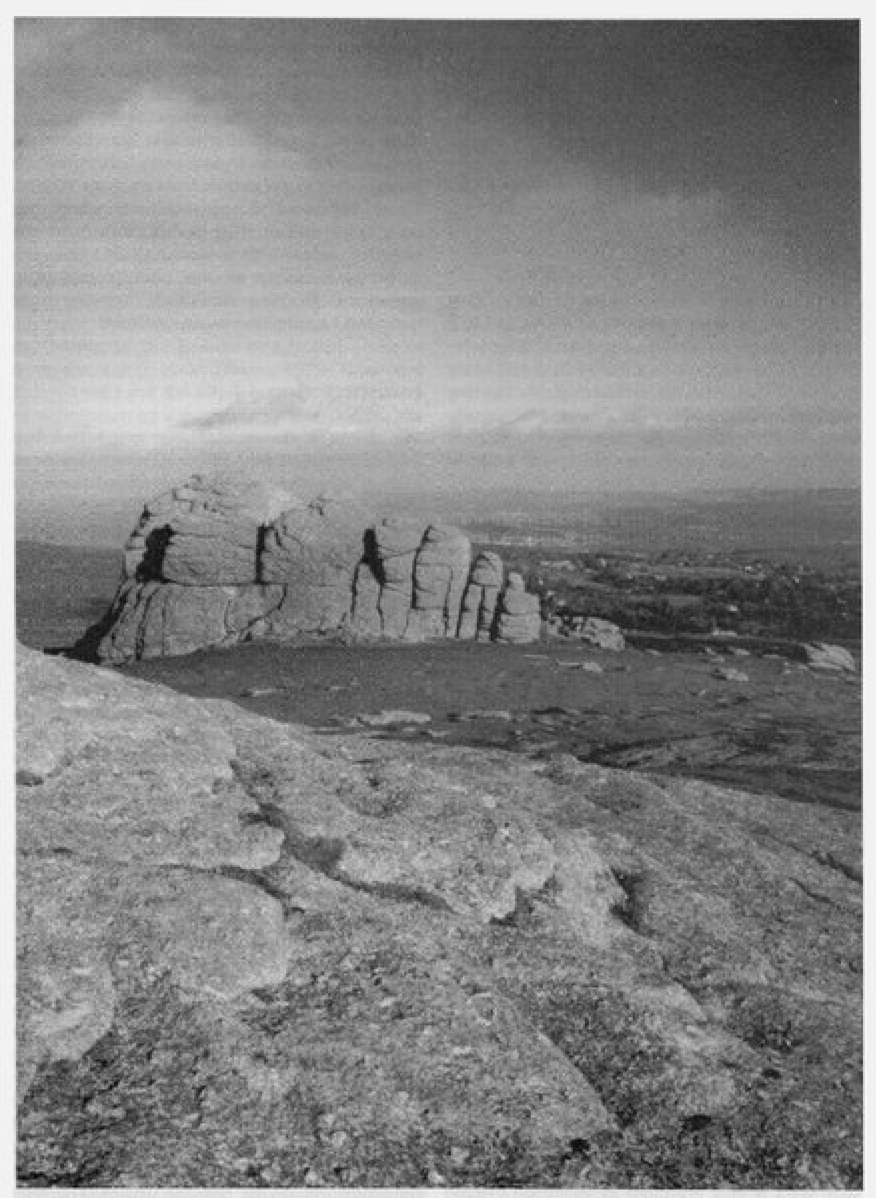

(Figure 5.9) Haytor Rocks, exposing the coarse megacrystic granite of Dartmoor. The megacrystic character of the granite is visible in the foreground exposure. (Photo: S. Campbell.)

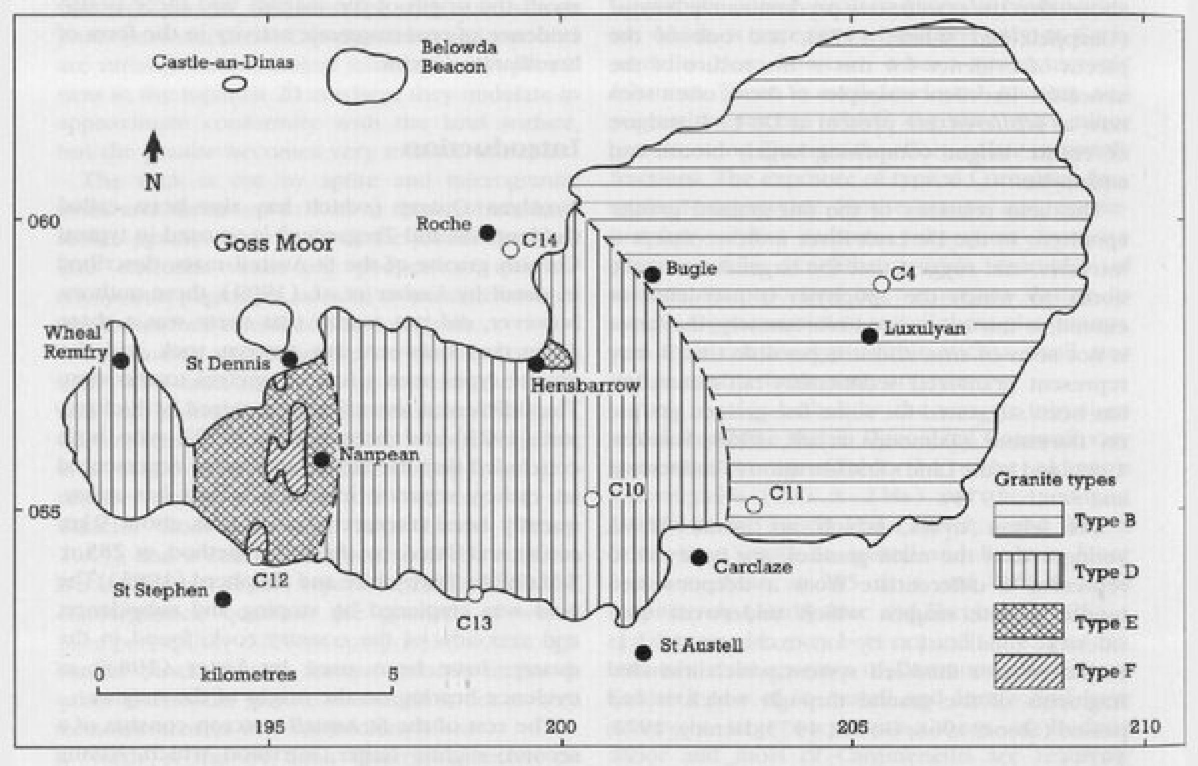

(Figure 5.10) Map of the St Austell Granite outcrop, showing the chief granite types, localities mentioned in the text (filled circles) and the following sites: C4 = Luxulyan Quarry; C10 = Wheal Martyn; C11 = Cam Grey Rock; C12 = Tregargus Quarries; C13 = St Mewan Beacon; and C14 = Roche Rock.

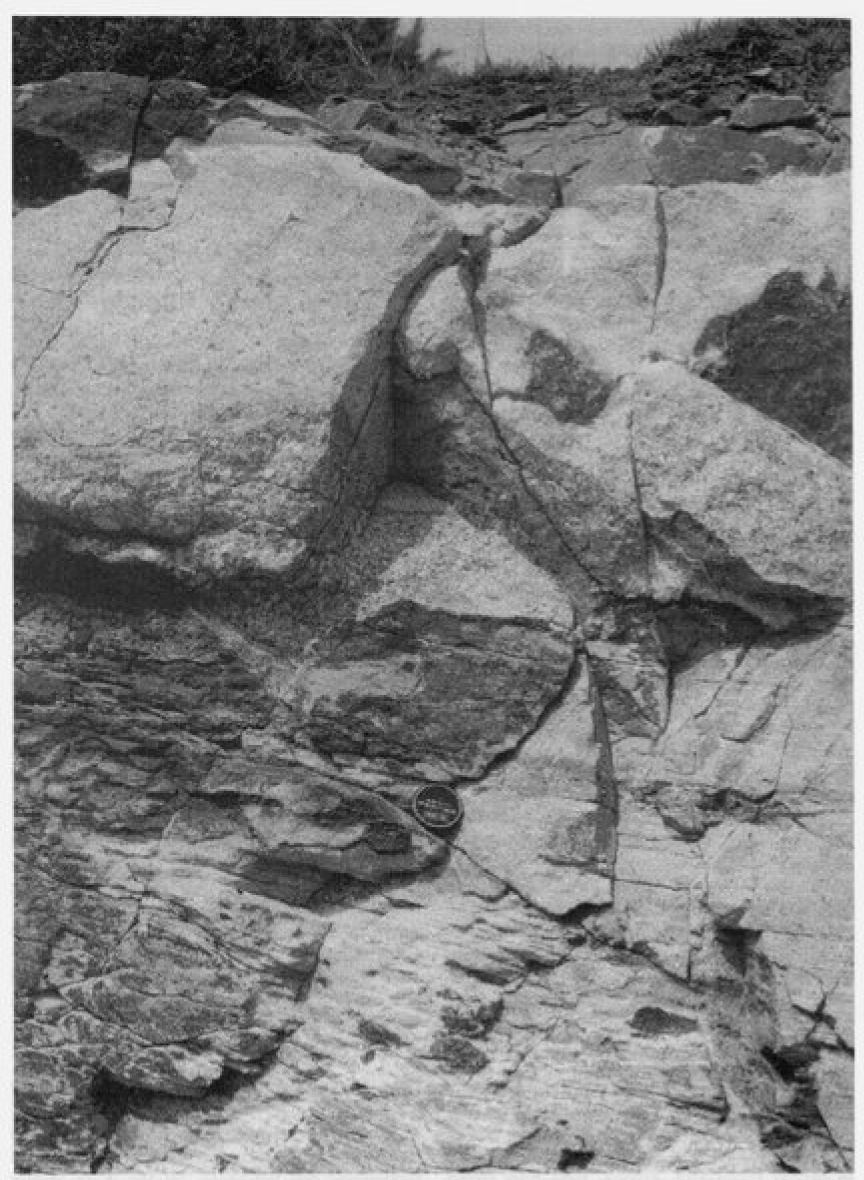

(Figure 5.11) Contact between Dartmoor Granite and Devonian slates, re-exposed after face cleaning by the Nature Conservancy Council in 1980. (Photo: Mj. Harley.)

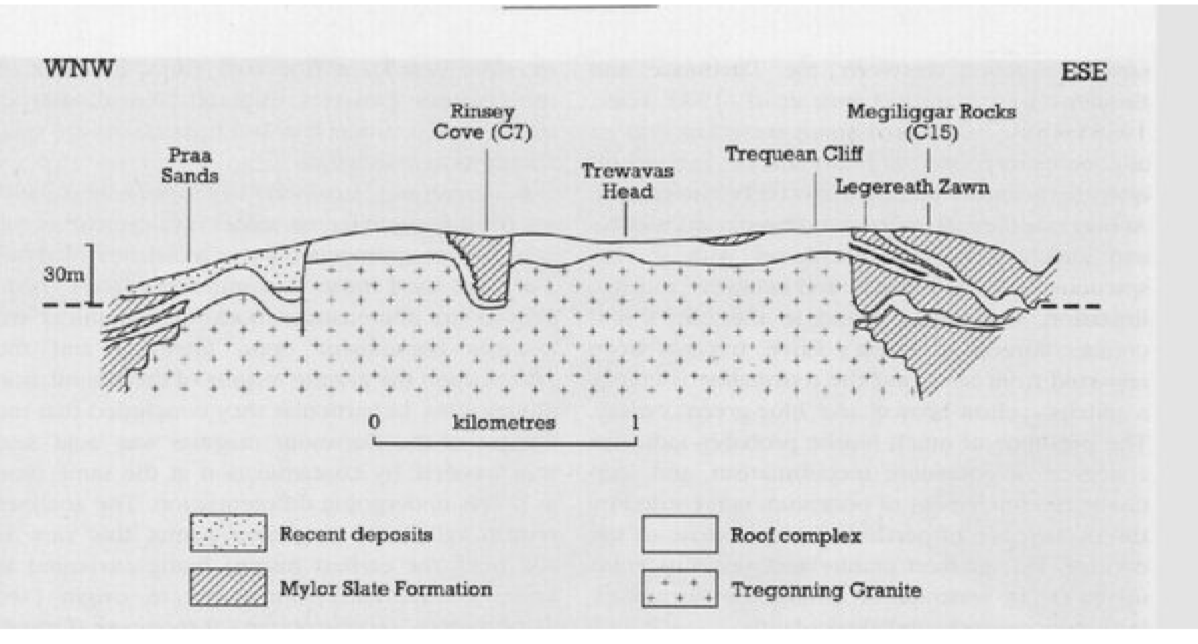

(Figure 5.12) Diagrammatic section across the Tregonning Granite, based on coastal exposures, showing the location of sites at Rinsey Cove (C7) and Megiliggar Rocks (C15) (after Exley and Stone, 1982, figure 21.2).

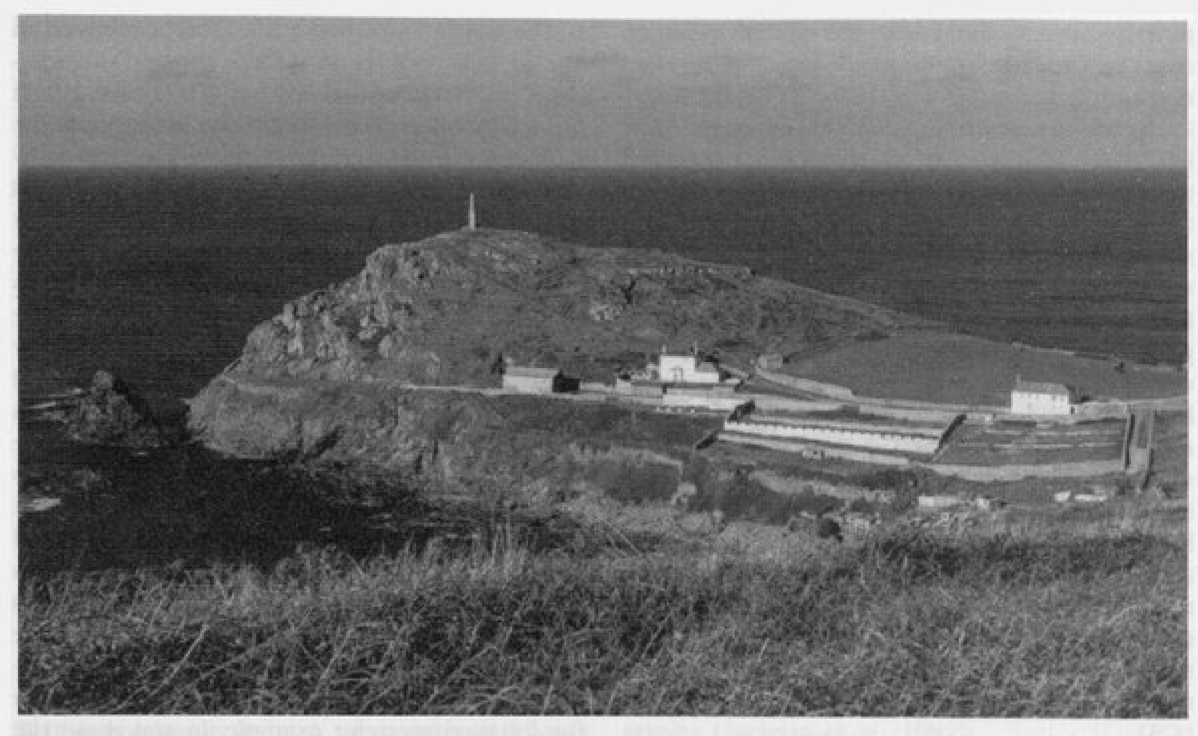

(Figure 5.13) The headland of Cape Cornwall which exposes contacts between Land's End Granite and adjacent metasediments. (Photo: S. Campbell.)

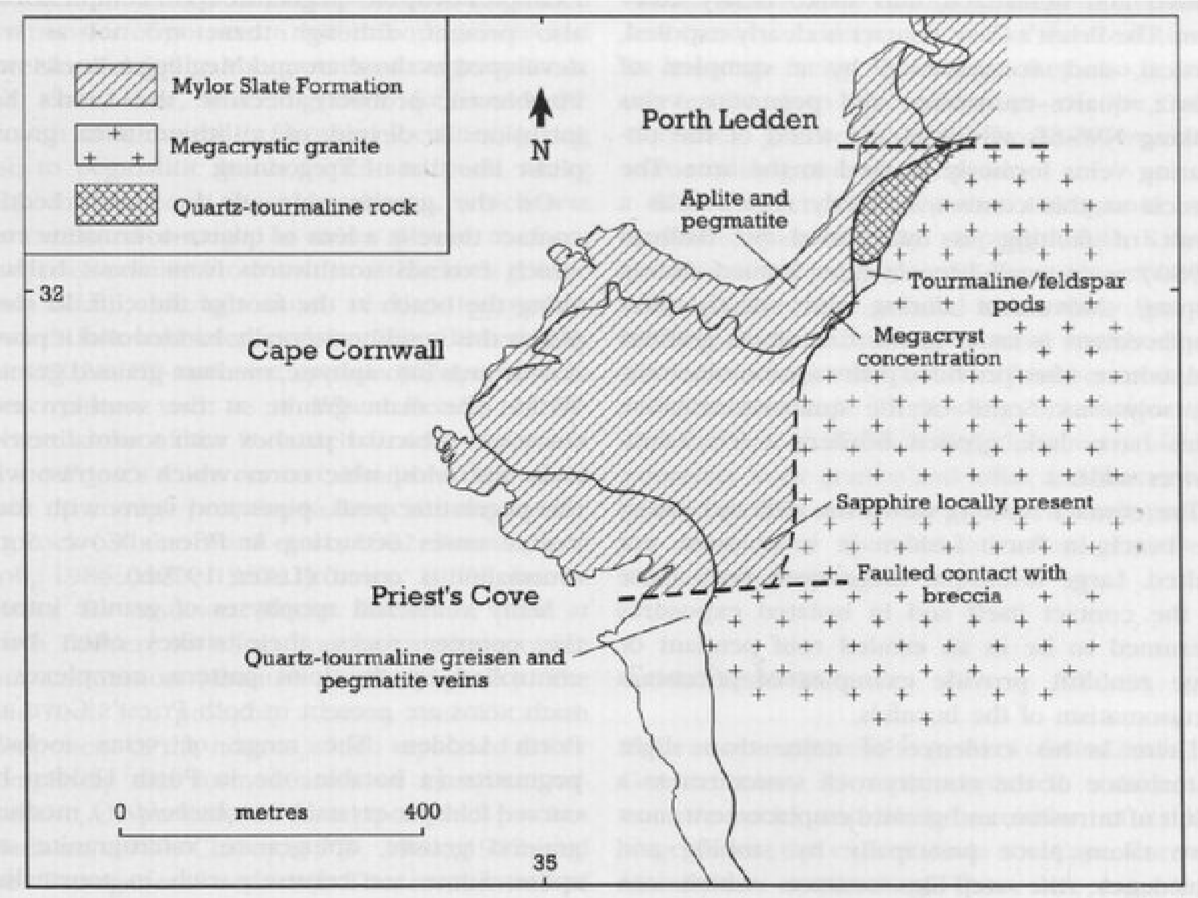

(Figure 5.14) Geological sketch map of the Cape Cornwall area (site (:8).

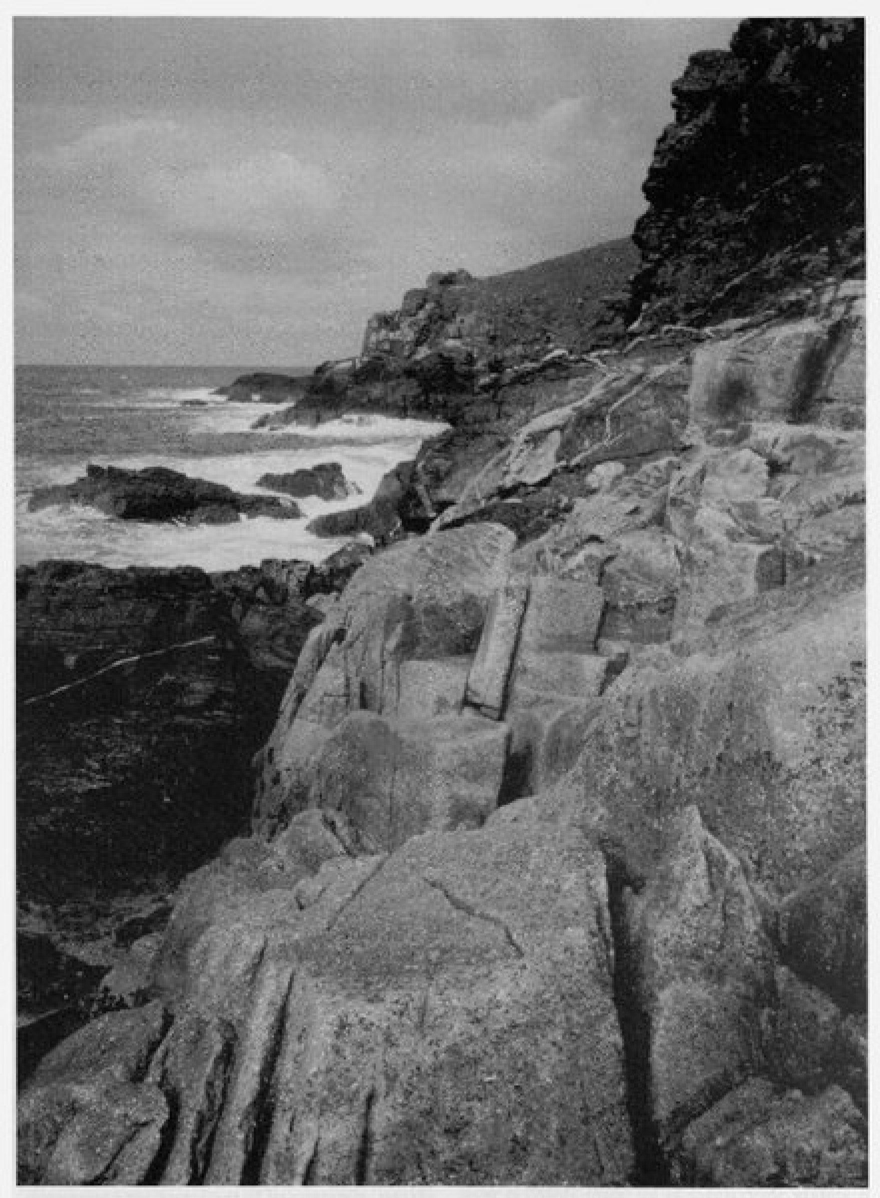

(Figure 5.15) Small granite cupola emplaced in pelitic hornfelses of the Mylor Slate Formation. Porthmeor Cove, Cornwall. (Photo: K.A. Cottle.)

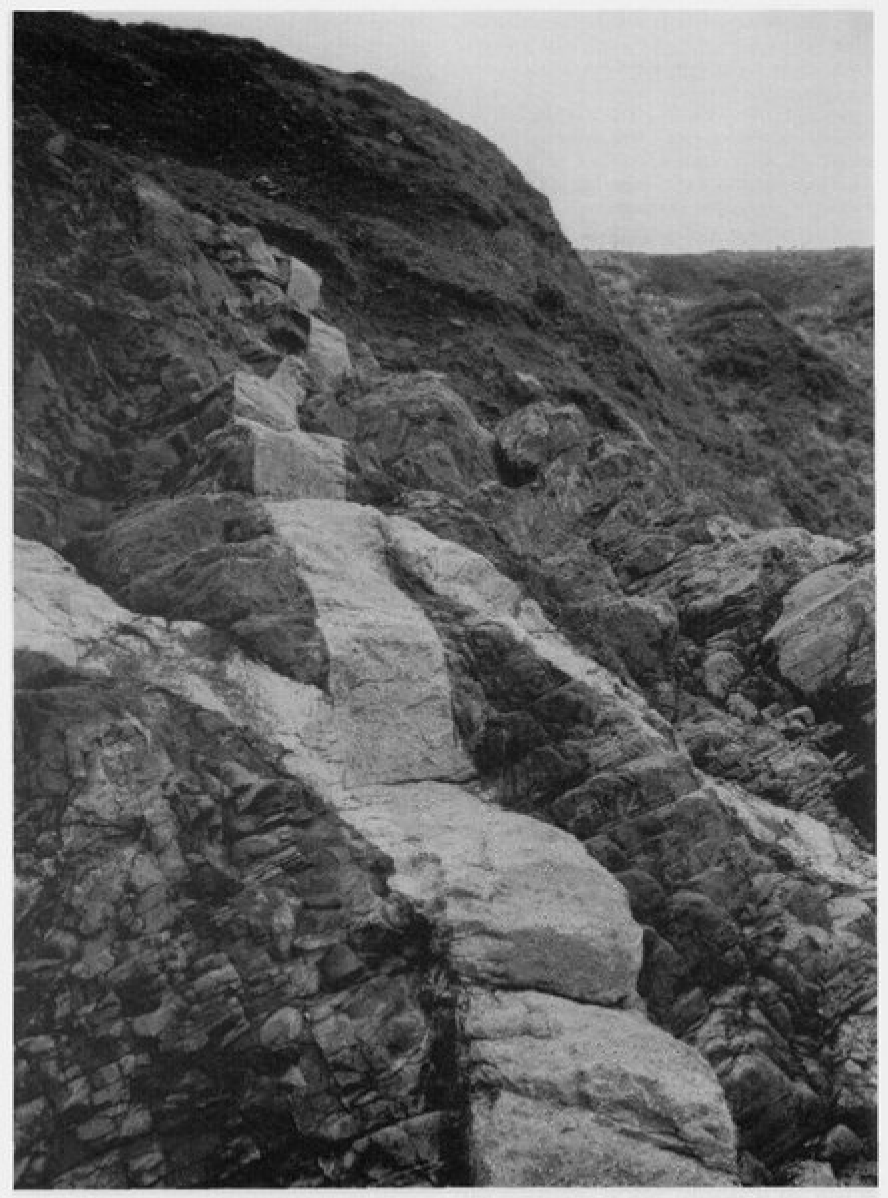

(Figure 5.16) Later dyke of megacrystic granite cutting and displacing an earlier leucogranite dyke. Porthmeor Cove, Cornwall. (Photo: R.A. Cottle.)

(Figure 5.17) The craggy outcrop of Roche Rock consists of quartz—tourmaline (schorl) rock. Roche Rock, Cornwall. (Photo: R.A. Cottle.)

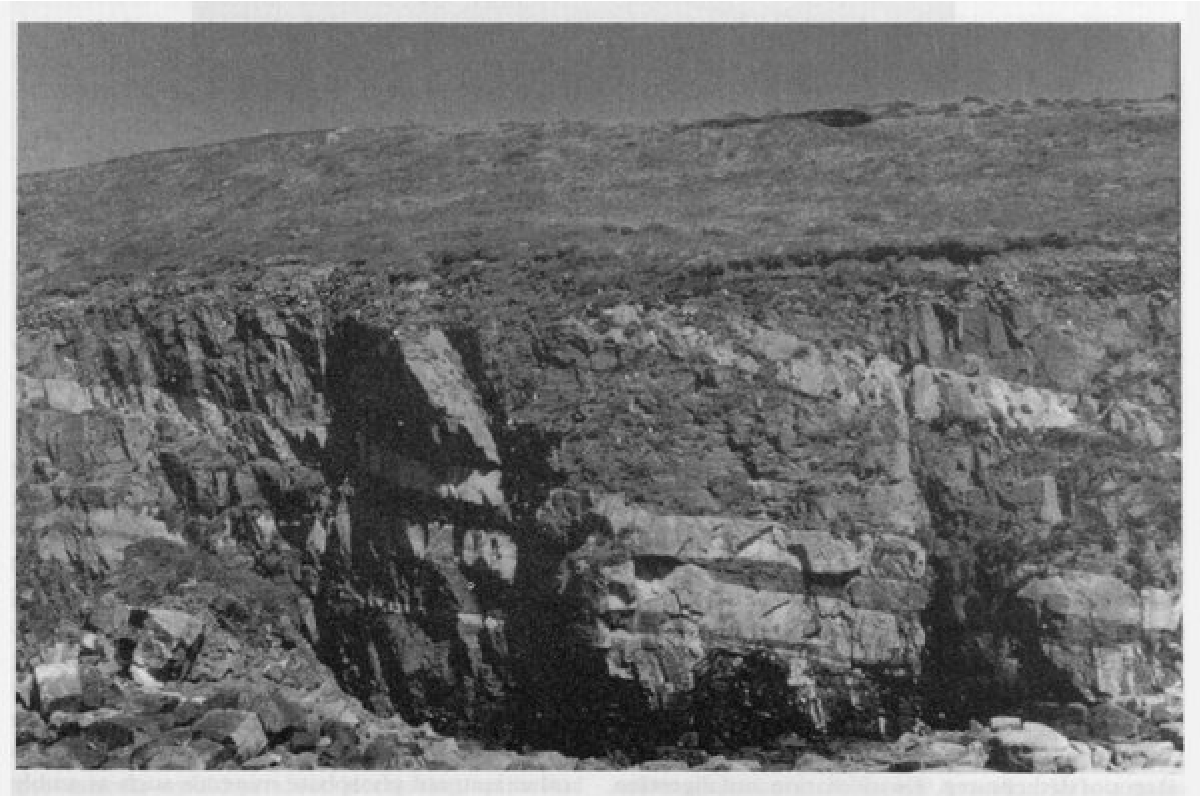

(Figure 5.18) Pegmatite—aplite—granite sheets cutting Mylor Slate Formation metasediments in the cliffs at Legereath Zawn, near Tremearne Par. Megiliggar Rocks, Cornwall. (Photo: C.S. Exley.)

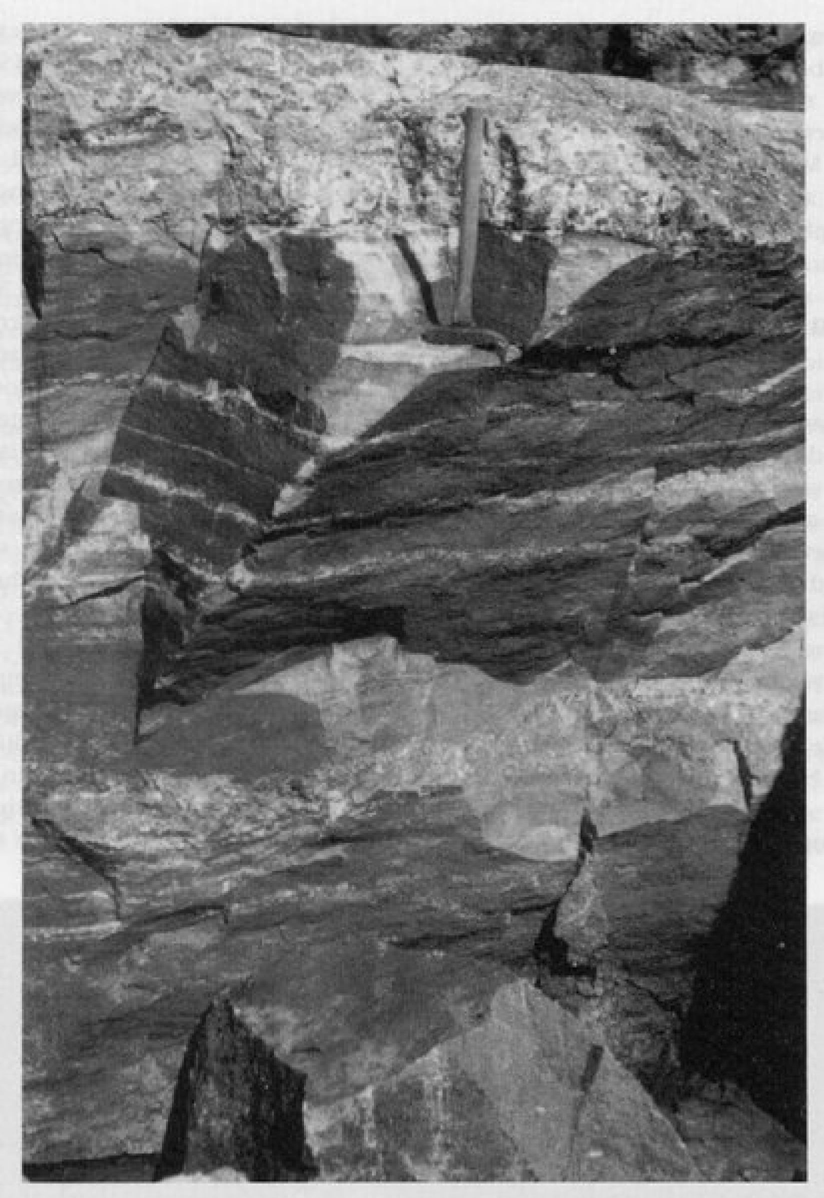

(Figure 5.19) Pegmatite—aplite—granite layering in one of the granitic sheets. Megiliggar Rocks, Cornwall. (Photo: C.S. Exley.)

(Figure 5.20) Pegmatite—aplite—granite boulder on Tremearne Beach, demonstrating the quasi-sedimentary character of the igneous layering. Megiliggar Rocks, Cornwall. (Photo: C.S. Exley.)

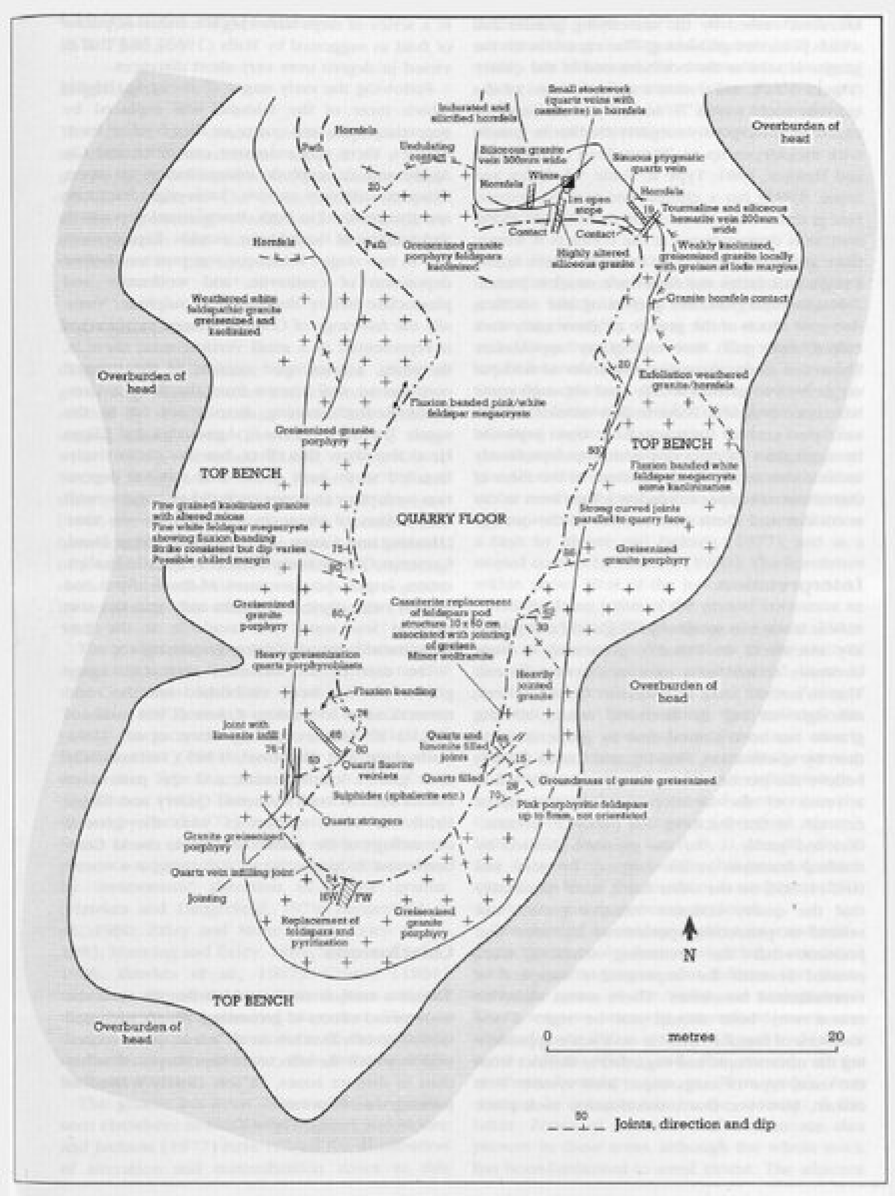

(Figure 5.21) (Opposite) Detailed map of Cameron Quarry (after Hosking and Camm, 1985).

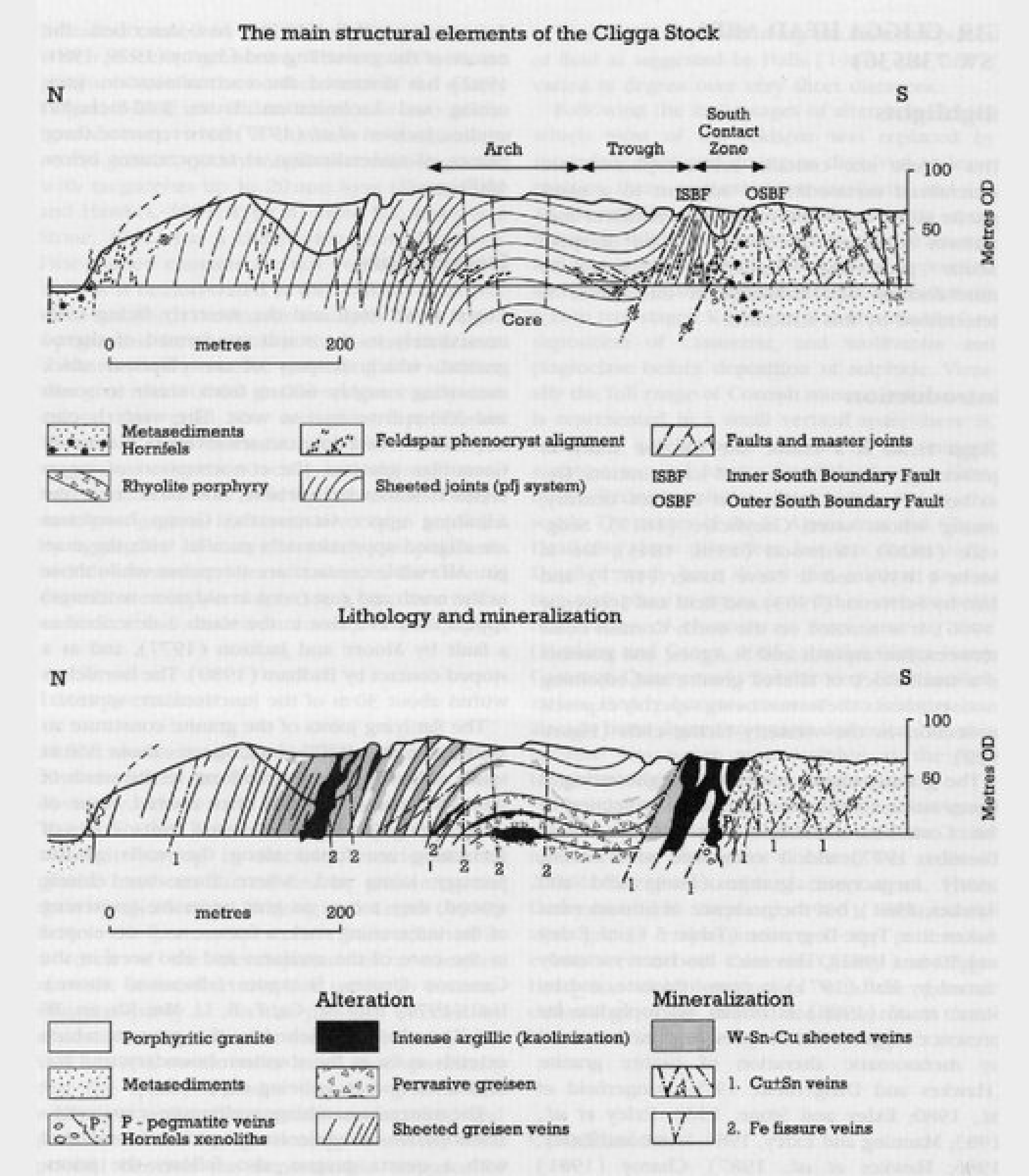

(Figure 5.22) Coastal section of the Cligga Head Granite, site C19 (after Moore and Jackson, 1977).

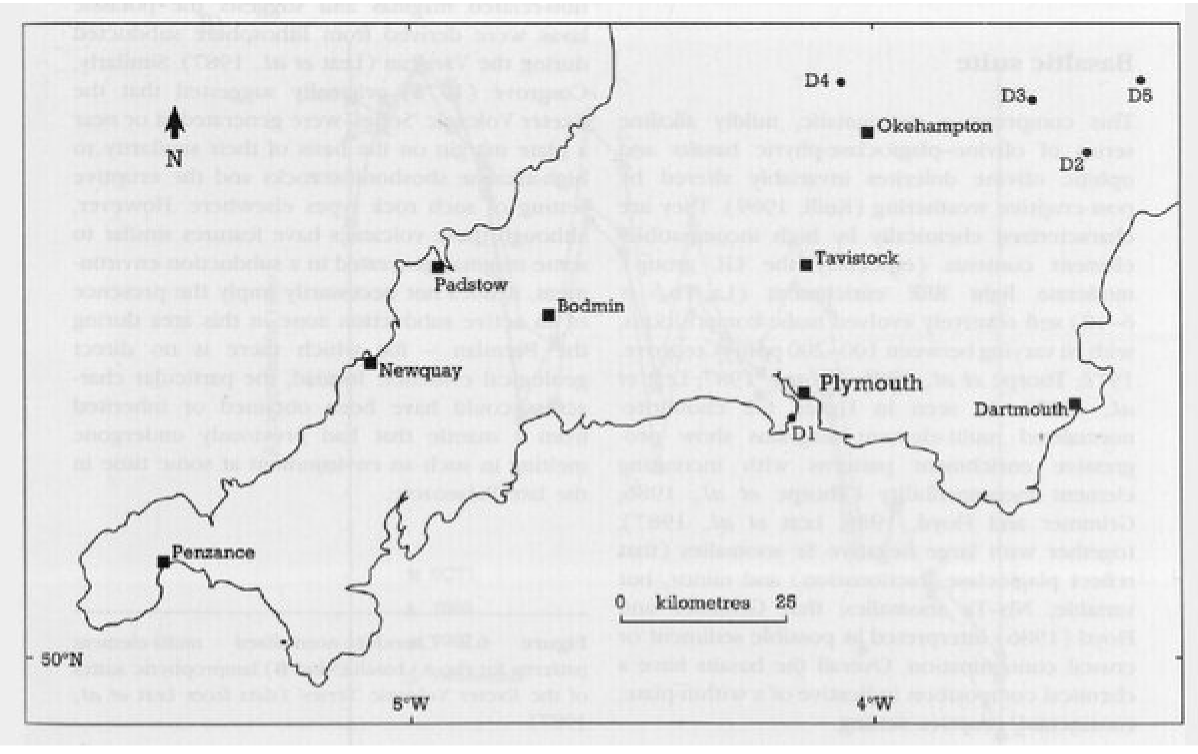

(Figure 6.1) Outline map of south-west England, showing the location of Group-D sites.

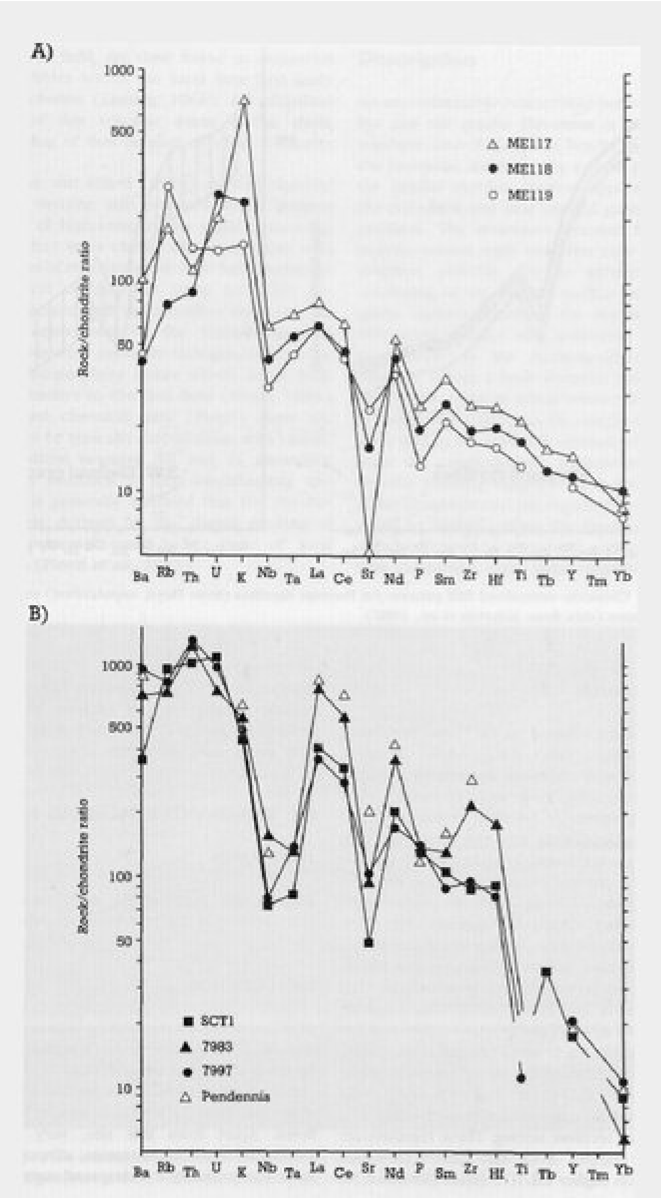

(Figure 6.2) Chondrite-normalized multi-element patterns for the A) basaltic and B) lamprophyric suites of the Exeter Volcanic 'Series' (data from Leat et al., 1987).

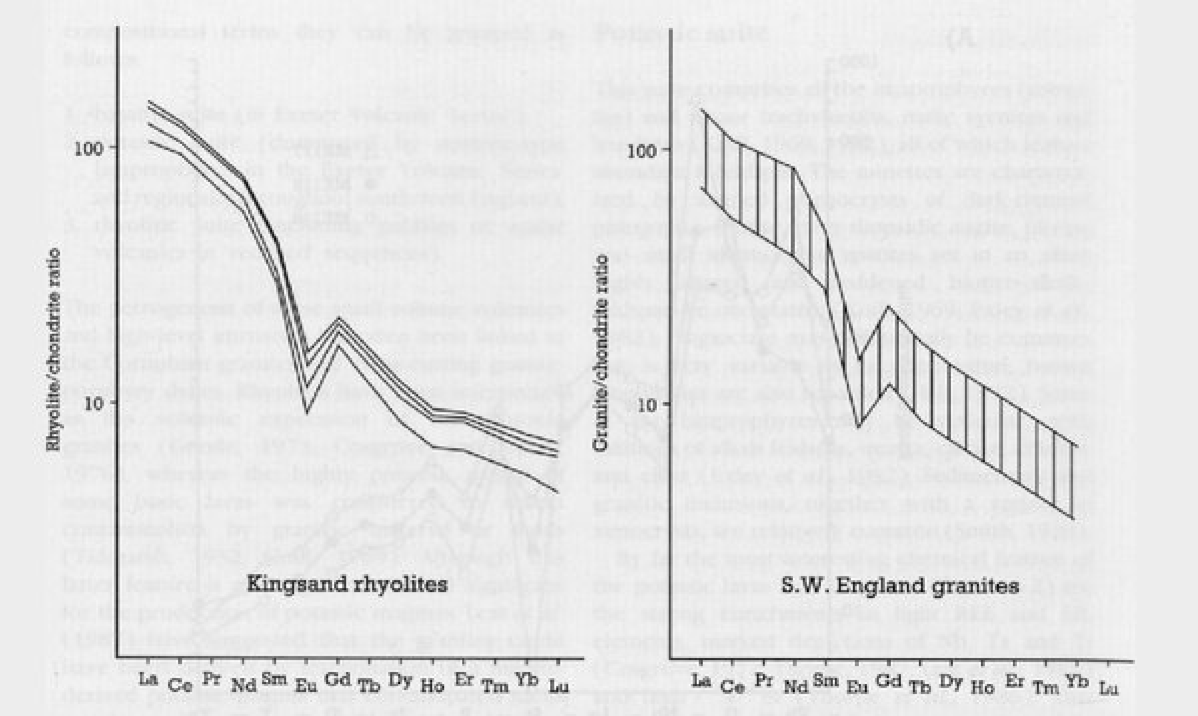

(Figure 6.3) Chondrite-normalized REE patterns for Permian rhyolites (from Floyd, unpublished) and south-west England granites (data from Alderton et al., 1980).

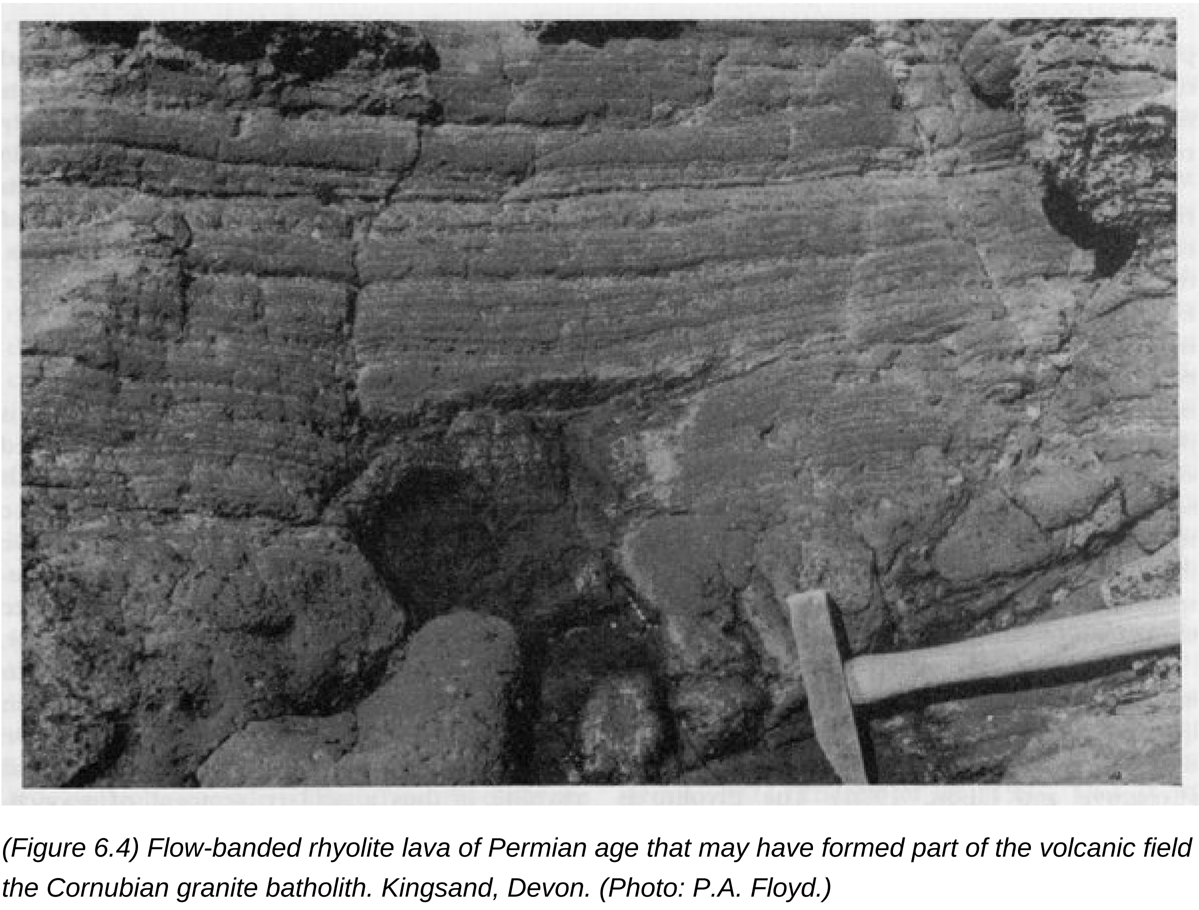

(Figure 6.4) Flow-banded rhyolite lava of Permian age that may have formed part of the volcanic field developed above the Cornubian granite batholith. Kingsand, Devon. (Photo: P.A. Floyd.)

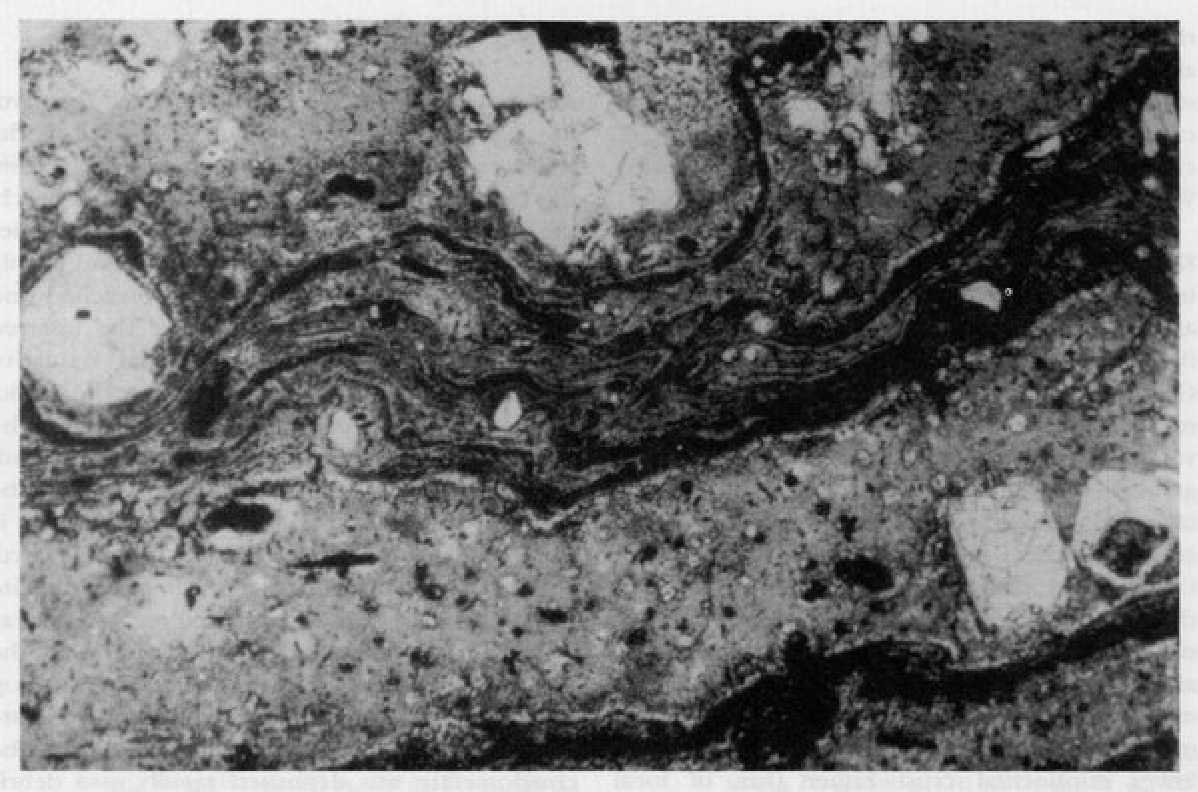

(Figure 6.5) Silica phenocrysts in the flow-banded, partly devitrified matrix of the Permian rhyolite lava. Kingsand, Devon. (Photo: P.A. Floyd.)

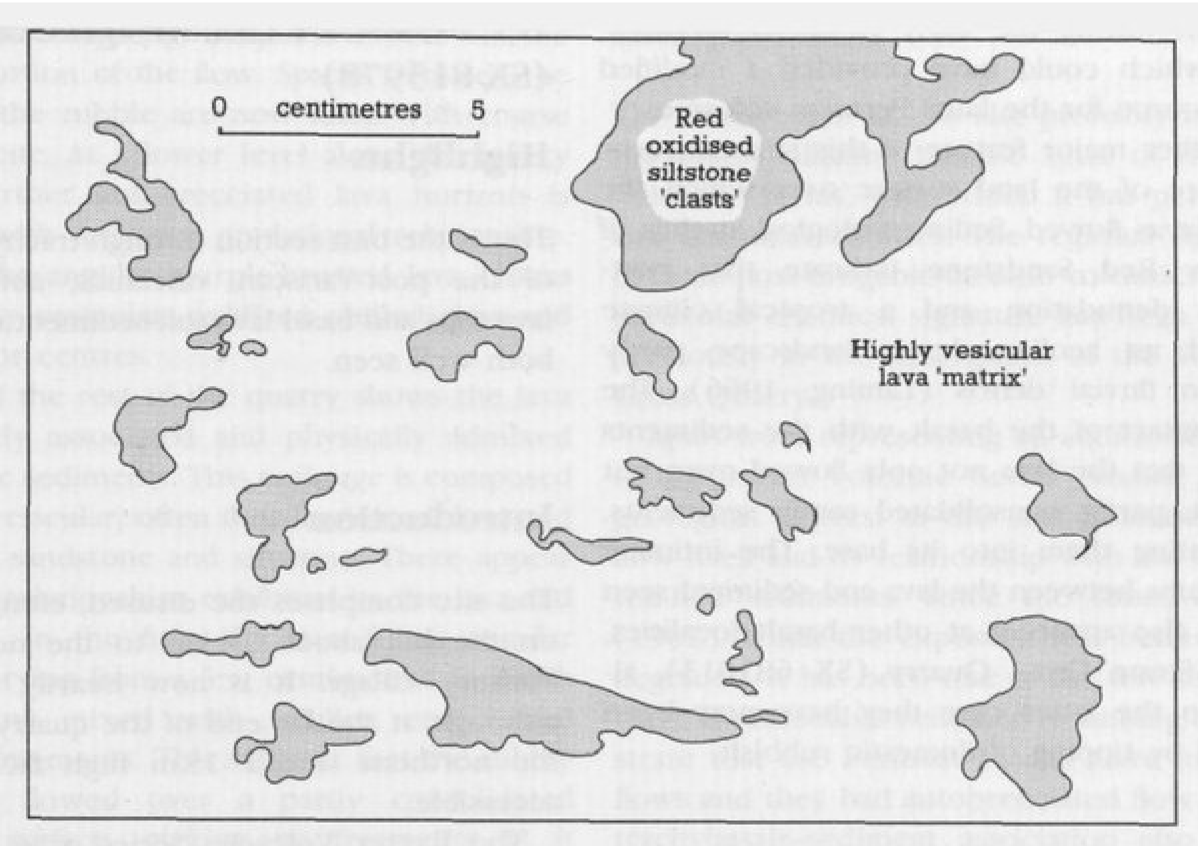

(Figure 6.6) Sketch of the lava—sediment relationship at the base of a late Stephanian basalt lava flow of the Exeter Volcanic 'Series', Webberton Cross Quarry, near Exeter.

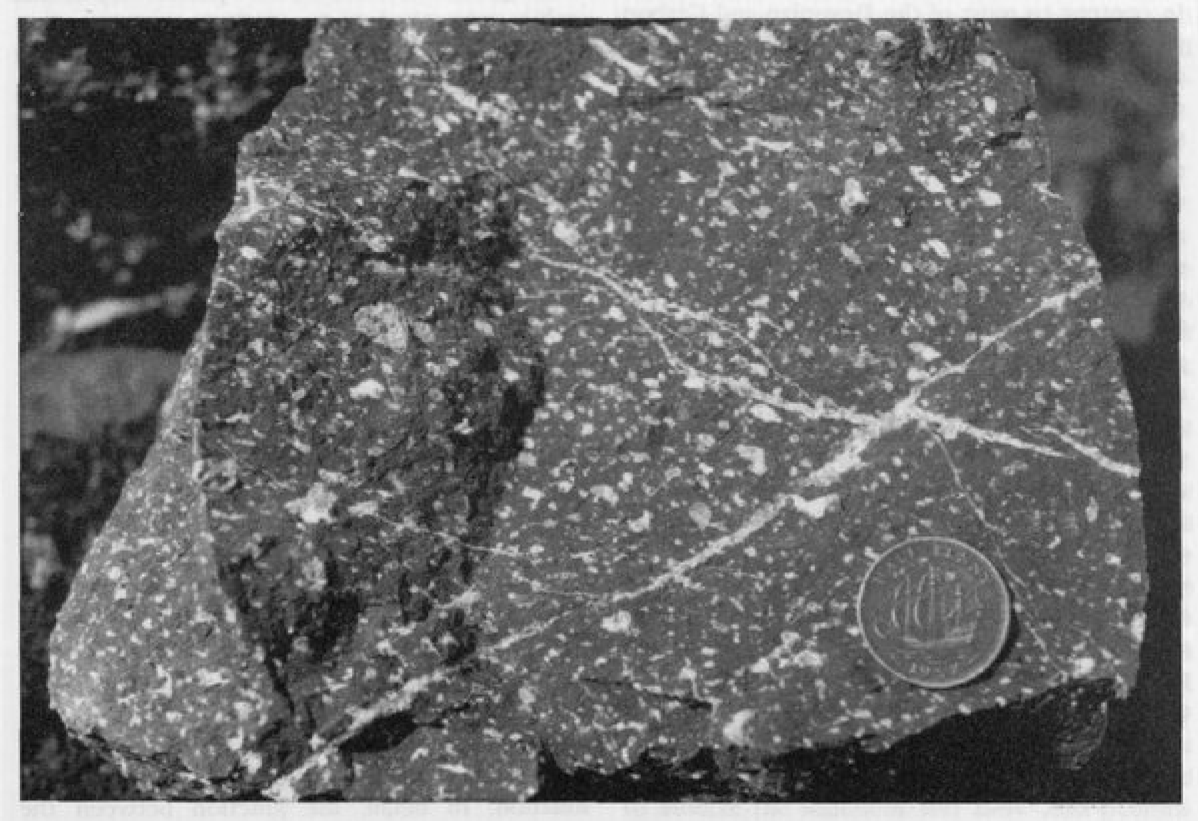

(Figure 6.7) Highly amygdaloidal (vesicles infilled with white zeolites and/or clays) and oxidized subaerial basalt lava flow. Webberton Cross Quarry, Devon. (Photo: P.A. Floyd.)

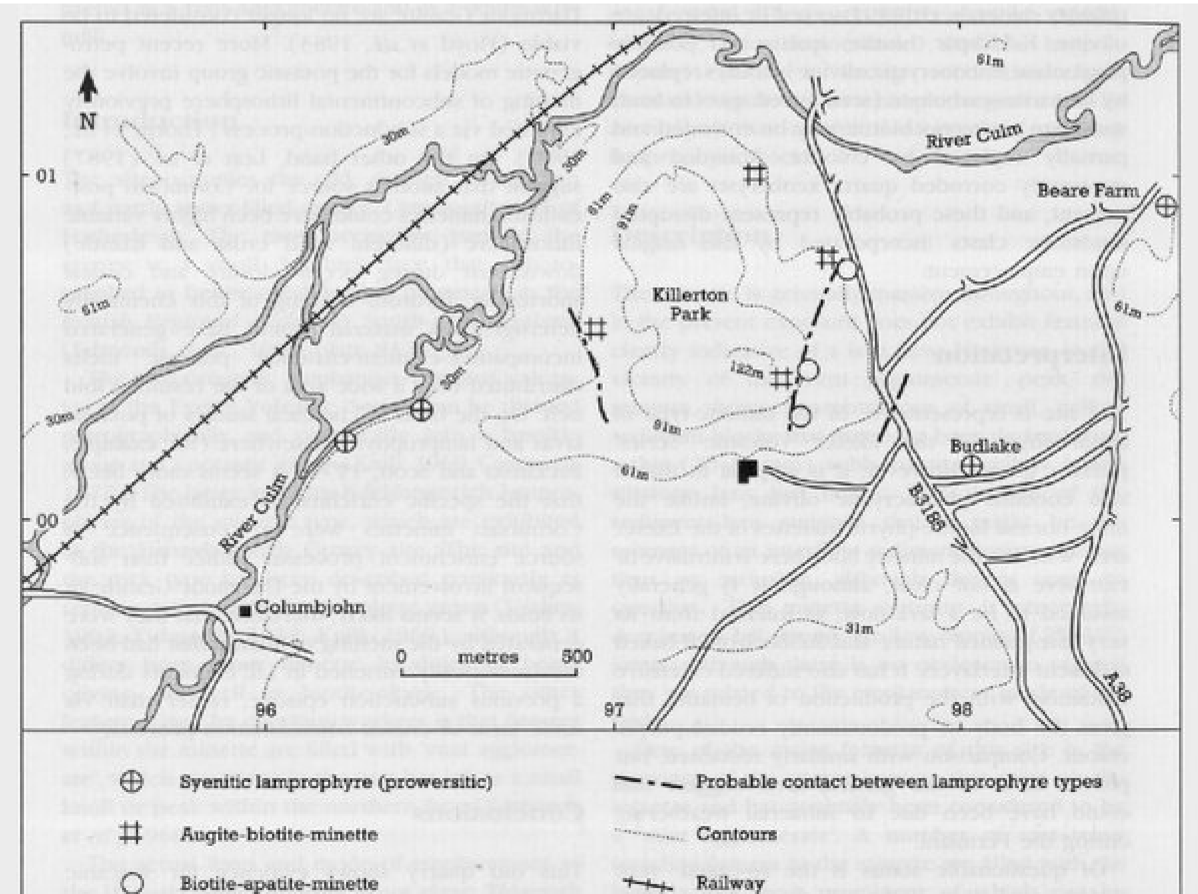

Intrusive phase	Outcrop and granite type		Rb-Sr age (Ma)	Initial $^{87}Sr/^{86}Sr$ ratio	Comments
Major	Dartmoor	(B)	280 ± 1	0.7101 ± 0.0004	-
	Bodmin Moor	(B)	287 ± 2	0.7140 ± 0.0002	Mineral age
	St Austell	(B)	285 ± 4	0.7095 ± 0.0009	-
	Carnmenellis	(B)	290 ± 2	0.7130 ± 0.0020	Mineral age
	Tregonning	(E)	280 ± 4	0.71498 ± 0.00381	Highly evolved, lithium-rich
	Land's End	(B)	268 ± 2	0.7133 ± 0.0006	Mineralization re-set age
Minor	Hemerdon Ball		304 ± 23	0.70719 ± 0.01025	Heavily mineralized
	Kit Hill		290 ± 7	0.70936 ± 0.00228	-
	Hingston Down		282 ± 8	0.71050 ± 0.00119	
	Castle-an-Dinas		270 ± 2	0.71358 ± 0.00122	Later intrusion re-set age
	Carn Marth		298 ± 6	0.70693 ± 0.00207	-
Dykes	Meldon 'Aplite'		279 ± 2	0.7098 ± 0.0017	-
	Brannel Elvan		270 ± 9	0.7149 ± 0.0031	Re-analysed
	Wherry Elvan		282 ± 6	0.7120 ± 0.0025	Re-analysed
Mineral veins	South Crofty		269 ± 4	-	
	Geevor		270 ± 15	0.7122 ± 0.0012	

(Table 2.1) Ages and initial Sr isotopic ratios of granitic rocks from the Cornubian batholith (data from Darbyshire and Shepherd, 1985, 1987)

Stage	Process	Age (millions of years) *	Depth (km)	Temperature (°C)	Salinity of fluids	Source of heat	Direction of least stress	Main changes in mineralogy: Feldspar	Main changes in mineralogy: Quartz	Main changes in mineralogy: Mica	Associated metalliferous mineralization	Comments
I	Emplacement of biotite granite, forming main batholith	290-285	? 3	500-600	-	Magmatic	Variscan (E-W)	-	-	-	-	Biotite granite which now forms eastern part of the St Austell granite
II	First phase of post-magmatic alteration and mineralization	285-275	2-3	500-?200	Moderate	Magmatic	Initially E - W, then N - S	Limited greisenization alongside veins	-	-	Sn, W	Early greisenization and mineralization e.g. Castle-an-Dinas (W)
IIIa	Emplacement of evolved lithium-rich granites and biotite granites in western part of St Austell granite	275-270	2-3	500-600	-	Magmatic	N - S	-	-	-	-	Granites belonging to this phase may underlie much of the batholith. Granites hydraulically fractured
IIIb	First part of second phase of post-magmatic alteration and mineralization	275-270	? 2	450-380	Moderate	Mainly magmatic, some radiogenic	N - S or NW - SE	Greisenization: converted to quartz, mica and topaz by F-rich fluids, mica of gilbertite type. Tourmalinization: replaced by tourmaline	Repeatedly fractured and fractures annealed by fresh growths of quartz	Some re-crystallization, biotite loses iron which is taken up by tourmaline growth	Sn, W, Cu	Main phase of metalliferous mineralization
IIIc	Emplacement of felsitic elvan dykes	275-270	? 2	400-500	Moderate	Magmatic	N - S	-	-	-	Sn, W, Cu	Further input of magmatic heat
IV	First phase of argillic alteration and NW-SE or N-S quartz-hematite veins and faulting	270-260	? 1-2	350-300	Moderate to high	Mainly radiogenic, possibly some magmatic or mantle heat	E - W	Na feldspar: altered to smectite/illite assemblage, little kaolinite K feldspar: altered to illite, maybe some smectite	Free silica released by argillation, forms overgrowths on quartz and now iron-stained non-tourmaline bearing lodes (NW - SE and N - S)	Much iron liberated from biotite which is carried out of the granite to form iron lodes. Some mica hydrated to gilbertite	Fe/U/Pb/Zn	Note: Salinity, lack of kaolinite and change in stress direction. Low temperature metalliferous mineralization
	Quiescent period?											
V	Second phase of argillic alteration. Main period of kaolinization ?Deep Mesozoic supergene alteration?	260 to present	0.2-1.5	50-150	Low	Radiogenic	Variable E - W or N - S, later becoming vertical	Na feldspar: altered readily to kaolinite K feldspar: altered less readily to kaolinite Smectite: altered readily to kaolinite	Free silica released by argillation, forms overgrowths on quartz and some minor quartz veins	Some iron liberated from biotite, not carried out of granite so colours matrix. In areas of intense kaolinization mica/illite altered to kaolinite	Fe/U (minor)	Note: Fresh water and main episode of kaolin formation. Isostatic uplift may have played a part
VI	Early Tertiary chemical weathering (also Mesozoic?)	25-60	0.0-0.2	20-50	Low	High surface temperature	Vertical	Altered kaolinite, is b-axis disordered in Eocene/Oligocene weathering	Some solution of silica from quartz grains	Some iron liberated from biotite, not carried out of the granite so colours matrix. In areas of intense kaolinization mica/illite altered to kaolinite	-	Tertiary weathering mantle is source of material for ball clays and associated sediments

* Radiometric dates from Bray (1980), and Darbyshire and Shepherd (1985, 1987)

(Table 2.2) Main evolution and alteration stages of the St Austell Granite (after Bristow et al., in press)

	Type B			Type C		Type D		Type E	Type F	Granite porphyry	Microgranite
	Bodmin Moor	Carnmenellis	Geevor Mine	Geevor Mine	Bodmin Moor	St Austell*	Cligga Head	Tregonning -Godolphin	St Austell*	Tregonning -Godolphin	Meldon micro -granite dyke, NW Dartmoor †
	(N = 10)	(N = 12)	(N = 7)	(N = 1)	(N = 3)	(N = 8)	(N = 2)	(N = 10)	(N = 6)	(N = 2)	(N = 1)
SiO_2	72.43	72.60	71.30	73.70	74.08	73.01	72.73	71.10	74.20	72.80	72.80
TiO_2	0.21	0.28	0.35	0.06	0.07	0.14	0.13	0.06	0.07	0.20	0.04
Al_2O_3	15.03	14.65	14.20	14.10	14.78	14.72	14.85	16.11	15.81	14.50	16.40
Fe_2O_3	0.32	0.50	0.80	0.60	0.19	0.47	0.34	0.36	0.08	1.88	0.84
FeO	1.48	1.24	1.38	0.44	0.88	0.74	0.94	0.81	0.17	1.21	
MnO	0.04	0.06	0.03	0.03	0.03	0.03	0.03	0.07	0.01	0.06	0.09
MgO	0.44	0.48	0.60	0.05	0.18	0.14	0.33	0.09	0.08	0.26	0.06
CaO	0.84	1.12	1.12	0.56	0.44	0.44	0.41	0.59	1.31	0.28	1.28
Na_2O	3.11	3.11	2.82	2.86	2.74	3.42	3.21	3.73	4.06	0.12	2.77
K_2O	5.06	4.36	5.11	4.77	5.73	5.36	5.03	4.84	4.66	7.66	3.96
Li_2O	0.06	0.07	0.06	0.07	0.04	0.18	0.11	0.27	0.01	0.03	0.94
P_2O_5	0.25	0.18	0.24	0.32	0.25	0.33	0.15	0.50	0.46	0.26	0.48
B_2O_3	-	-	0.41	0.47	-	-	0.27	0.14	-	-	-
F	-	-	-	-	-	(0.38)	0.36	1.22	(1.36)	-	1.40
H_2O	1.01	-	0.73	1.38	0.88	-	1.13	-	-	-	-
Nb	-	17	30	40	-	57	-	93	81	21	67
Zr	121	137	185	40	34	(50)	65	46	(11)	94	38
Y	41	48	30	20	40	-	-	10	-	18	-
Sr	94	93	98	22	43	41	178	61	64	34	47
Rb	419	462	480	760	444	982	695	1218	615	814	2293
Ba	196	397	230	15	102	(83)	150	204	(43)	699	197
La	31	16	-	-	12	8	-	~3	-	14	15
Ce	38	-	-	-	2	34	95	36	19	68	27
U	-	-	-	-	-	-	-	19	-	20	24
Th	-	-	-	-	-	-	-	22	-	31	-
Pb	46	47	18	10	42	-	-	16	-	6	5
Ga	-	40	30	30	-	-	40	40	-	20	35
Zn	62	72	45	35	48	-	103	48	-	45	31
Ge	-	-	-	-	-	-	-	11	-	4	11
Sn	23	14	19	17	29	-	40	36	-	71	14
Cs	28	34	-	-	48	-	-	127	-	33	223
K/Rb	100	78	88	52	107	45	60	33	63	78	14

* Values in parentheses from the work of Exley (1959)

† Total Fe as Fe_2O_3

Oxide values in weight %

Trace element values in ppm

(Table 5.2) Average analyses of granites from the Cornubian batholith (after Exley et al. 1983)

	Ti	Al	Fe^{III}	Fe^{II}	Mn	Mg	Ca	Na	K	P
Si	-0.33	-0.61	-0.28	-0.36	-0.26	-0.29	-0.26	-0.05	+0.11	-0.45
Ti		-0.35	+0.40	+0.77*	-0.27	+0.90*	+0.75*	-0.21	+0.07	-0.48
Al			-0.16	-0.23	+0.43	-0.33	-0.24	+0.33	-0.28	+0.72*
Fe^{III}				+0.21	-0.16	+0.34	-0.13	-0.69*	+0.61*	-0.20
Fe^{II}					-0.04	+0.76*	+0.60*	-0.01	-0.04	-0.09
Mn						-0.34	-0.20	+0.23	-0.29	+0.61*
Mg							+0.67*	-0.11	+0.02	-0.46
Ca								+0.24	-0.37	-0.40
Na									-0.92	+0.33
K										-0.21

* Based upon 26 'average' analyses used and described in Stone and Exley (1978). Highly significant correlations have asterisks: these are values for which the Null hypothesis is rejected at the 0.01 significance level. Boxed values are those belonging to the femic element association.

*(Table 5.3) Pearson product moment correlation coefficients for major and minor elements (after Exley and Stone, 1982, Table 23.1) * Based upon 26 average analyses used and described in Stone and Exley (1978). Highly significant correlations have asterisks: these are values for which the Null hypothesis is rejected at the 0.01 significance level. Boxed values are those belonging to the ferric element association.*